THE IONIC BASIS OF FREQUENCY SELECTIVITY IN HAIR CELLS OF THE BULLFROG'S SACCULUS

Thesis by

Richard Sheridan Lewis

In Partial Fulfillment of the Requirements

For the Degree of

Doctor of Philosophy

California Institute of Technology

Pasadena, California

1985

(Submitted July 2, 1984)

ACKNOWLEDGMENTS

The direction of my research interests and much of what I have managed to learn as a graduate student are largely due to the advice, instruction, and opportunities given me by various friends and colleagues. I thank Jim Hudspeth, my advisor, for teaching me by example not to be afraid to try difficult experiments or to develop new techniques. He and David Corey first suggested to me the study of isolated hair cells, and I thank Jim for his participation in early stages of the work. Dick Horn and the other initiators of the Internal Perfusion Workshop were the first to show me the excitement of ionic currents in cells, and pointed me in the direction of the gigohm seal. I am indebted to David Corey for his patient and enthusiastic instruction, at all hours, on topics ranging from electronic design to ion channels, as well as for giving me the chance to participate in the summer (patch) camp at Cold Spring Harbor. I thank John Maunsell and Herman Gordon for their early help in learning the ways of computers, and members of the Stevens lab at Yale for a variety of BASIC programs. I am grateful to Tom Holton for his thoughtful critiques of scientific arguments and manuscripts. I thank Richard "Jake" Jacobs for expert advice on construction techniques, and for showing me that things really can be done right the first time. I'm still trying. I also appreciate his meticulous help with plotting the figures. The members of my committee, Jim, Howard Berg, Dick Horn, Mary Kennedy, and Henry Lester, all have my thanks for their efforts on my behalf.

More than half the fun was getting there, and for that I owe a great deal to the community of Beckman Labs. In particular, Ruth Anne

Eatock enlivened the lunch table with her humor and energy, and I am grateful for her friendship and many late-night discussions in the lab. I would like to specially acknowledge Larry Katz, with whom I shared a house, several cats, and four years of thrills, from prairie fires to Battle Zone. He introduced me to that all-too-often overlooked side of graduate-student life: sports cars and private planes.

Lastly, I would like to thank Sandy Shotwell, whose understanding, support, and bad jokes kept me from flaming out in these last difficult months of writing.

I gratefully acknowledge the financial support given by NIH grants NS13154 and GM07737, by the System Development Foundation, and by the California Institute of Technology. The Jean Weigle Fund partially covered the cost of making copies of this thesis.

ABSTRACT

Hair cells from the bullfrog's sacculus, a vestibular organ responding to substrate-borne vibration, possess electrically resonant membrane properties which maximize the sensitivity of each cell to a particular frequency of mechanical input. The electrical resonance of these cells and its underlying ionic basis were studied by applying gigohm-seal recording techniques to solitary hair cells enzymatically dissociated from the sacculus. The contribution of electrical resonance to frequency selectivity was assessed from microelectrode recordings from hair cells in an excised preparation of the sacculus.

Electrical resonance in the hair cell is demonstrated by damped membrane-potential oscillations in response to extrinsic current pulses applied through the recording pipette. This response is analyzed as that of a damped harmonic oscillator. Oscillation frequency rises with membrane depolarization, from 80-160 Hz at resting potential to asymptotic values of 200-250 Hz. The sharpness of electrical tuning, denoted by the electrical quality factor, Q_e, is a bell-shaped function of membrane voltage, reaching a maximum value around eight at a membrane potential slightly positive to the resting potential.

In whole cells, three time-variant ionic currents are activated at voltages more positive than -60 to -50 mV; these are identified as a voltage-dependent, non-inactivating Ca current (I_{Ca}), a voltage-dependent, transient K current (I_A), and a Ca-dependent K current (I_C). The C channel is identified in excised, inside-out membrane patches on the basis of its large conductance (130-200 pS), its selective permeability to K over Na or Cl, and its activation by internal Ca

ions and membrane depolarization. Analysis of open- and closed-lifetime distributions suggests that the C channel can assume at least two open and three closed kinetic states.

Exposing hair cells to external solutions that inhibit the Ca or C conductances degrades the electrical resonance properties measured under current-clamp conditions, while blocking the A conductance has no significant effect, providing evidence that only the Ca and C conductances participate in the resonance mechanism. To test the sufficiency of these two conductances to account for electrical resonance, a mathematical model is developed that describes I_{Ca}, I_C, and intracellular Ca concentration during voltage-clamp steps. I_{Ca} activation is approximated by a third-order Hodgkin-Huxley kinetic scheme. Ca entering the cell is assumed to be confined to a small submembrane compartment which contains an excess of Ca buffer; Ca leaves this space with first-order kinetics. The Ca- and voltage-dependent activation of C channels is described by a five-state kinetic scheme suggested by the results of single-channel observations. Parameter values in the model are adjusted to fit the waveforms of I_{Ca} and I_C evoked by a series of voltage-clamp steps in a single cell. Having been thus constrained, the model correctly predicts the character of voltage oscillations produced by current-clamp steps, including the dependencies of oscillation frequency and Q_e on membrane voltage. The model shows quantitatively how the Ca and C conductances interact, via changes in intracellular Ca concentration, to produce electrical resonance in a vertebrate hair cell.

Table of Contents

INTRODUCTION

Much of our ability to discriminate between sounds in the environment, from the notes of a musical chord to the formants of human speech, derives from the highly developed frequency selectivity of the peripheral auditory system. A great deal of work (and controversy) over the years has been devoted to attempts to identify the physical processes responsible for this selectivity (for reviews, see Dallos, 1981; Rhode, 1984). The first basis for this endeavor was established by the classic experiments of von Békésy (1960), which demonstrated that the energy of sound impinging on the eardrum, after being transmitted via the middle-ear ossicles to the inner ear, produces a "traveling wave" of basilar-membrane motion which propagates along the length of the cochlea. This motion is transduced by the mechanoreceptive hair cells resting on the basilar membrane into electrical signals which, via synaptic interactions, affect the activity of afferent fibers of the auditory nerve. Von Békésy also discovered that the vibration of the basilar membrane is tonotopic, i.e., that positions on the basilar membrane from the basal to the apical end respond best to progressively lower frequencies of sound. He proposed that the frequency information carried by an auditory nerve fiber therefore depends on the portion of the cochlea that it innervates. The spectral tuning provided by the traveling wave was, however, much too broad to account for the degree of frequency resolution inferred from psychophysical measurements. Later comparisons between basilar-membrane motion and the tuning of auditory nerve fibers innervating the mammalian cochlea (Geisler et al., 1974; Evans & Wilson,

1975) reemphasized this discrepancy and supported the notion of a "second filter," a process postulated to act subsequent to motion of the basilar membrane to enhance the tuning provided by the traveling wave (Evans & Wilson, 1973). Studies of the guinea pig's cochlea demonstrating tuning of individual hair cells (Russell & Sellick, 1978) about as sharp as that of auditory nerve fibers (Evans, 1972) suggested a location for the second filter between basilar-membrane motion and the mechanical input to the hair cell or within the hair cell itself.

Over the past several years, increasingly refined measurements of basilar-membrane motion in mammalian cochleas (Khanna & Leonard, 1982; Sellick et al., 1982) have shown that the basilar membrane can be as sharply tuned as the auditory nerve fibers innervating it, forcing a reevaluation of the "second filter" concept. These studies have also shown that the mechanical tuning of the basilar membrane is particularly vulnerable to physiological insult (Sellick et al., 1982), thus providing an explanation for the low degree of tuning found initially by von Békésy (who experimented on dead cochleas), and later by investigators who unknowingly damaged living cochleas during the course of various invasive measurements. Theoretical models of the cochlea's mechanical properties indicate that passive characteristics of the basilar membrane and surrounding structures are insufficient to account for the high sharpness of basilar-membrane tuning; instead, the search is now directed towards identifying an *active mechanical process* in the mammalian cochlea that enhances vibrations of the basilar membrane at various frequencies along its length (Neely & Kim, 1983). A source of mechanical energy in the cochlea is demonstrated most dramatically by the emission of acoustic tones from the ear, either spontaneously (Zurek, 1981) or in

response to a brief sound stimulus (Kemp, 1978).

Recent studies of non-mammalian cochleas have indicated frequency tuning mechanisms fundamentally different from those of mammals, further confounding attempts to establish a common basis for frequency tuning among species. In these animals, properties intrinsic to the hair cells themselves act to produce frequency selectivity. For example, the responses of auditory nerve fibers and cochlear hair cells of the alligator lizard (Holton & Weiss, 1983) are sharply tuned even in the absence of a traveling wave or sharp mechanical tuning of the basilar membrane (Weiss et al., 1978). In this cochlea, frequency tuning is enhanced by the *mechanically resonant* properties of each hair cell's hair bundle; short hair bundles move maximally in response to high frequencies of mechanical input, while long hair bundles move preferentially in response to low frequencies (Frishkopf et al., 1982; Holton & Hudspeth, 1983). The monotonic variation in hair-bundle length with cell position along the organ and the corresponding frequency-dependence of hair-bundle motion can account for the cochlea's tonotopic organization. In the cochlea of the red-eared turtle, where the short basilar membrane is also unlikely to support a traveling wave, hair cells use a different strategy to achieve frequency selectivity. Each cell in this organ has unique *electrically resonant* membrane properties which specifically enhance its response to sound at the resonant frequency (Crawford & Fettiplace 1981a). The resonance is revealed by damped oscillations in membrane potential in response to small current pulses delivered through an intracellular micropipette, or by spontaneous voltage oscillations in the absence of applied current. Hair-cell and nerve-fiber responses in this organ are tonotopically organized over a frequency range of below

100 Hz to 700 Hz, and the variation of electrical resonance frequency closely parallels that of the acoustical tuning frequency measured for different hair cells along the length of the cochlea. Using an electrical equivalent circuit to describe the resonance of the hair cell's membrane, Crawford and Fettiplace showed that each cell's frequency-tuning properties can be viewed as the result of broad filtering of incoming acoustic stimuli by a common mechanism (such as middle-ear mechanics) followed by frequency-specific enhancement of the receptor potential by each cell's "private" electrical filter. The possible involvement of ionic channels, particularly a voltage-sensitive K channel, in generating electrical resonance was inferred from the inhibition of oscillatory behavior by K-channel blockers or by hyperpolarization to the estimated K Nernst potential. However, a lack of information about the types of ionic conductances present in these cells precluded a more complete understanding of the resonance mechanism.

This thesis describes investigations of the electrical behavior of hair cells from the bullfrog's sacculus, a vestibular organ sensitive to substrate-borne vibration (Lewis et al., 1982), aimed at identifying the ionic mechanism of electrical resonance and frequency selectivity in these cells. By applying gigohm-seal recording techniques to solitary hair cells enzymatically dissociated from the sacculus, I have identified three ionic conductances that are active in the voltage range encompassing electrically resonant behavior. These include a voltage-dependent Ca conductance, a voltage-dependent transient K conductance, and a Ca-dependent K conductance, which are characterized in Chapter 1. Chapter 2 presents a model, based on whole-cell and single-channel voltage-clamp data, which is able to reconstruct accu-

rately the membrane-potential oscillations produced by extrinsic current injections. The results of modeling the electrical behavior of the cell in terms of Ca and Ca-dependent K conductances establish these conductances as the ionic basis of electrical resonance in these hair cells. The contribution of electrical resonance to the cell's selectivity for particular frequencies of mechanical input is described in the Appendix.

CHAPTER ONE

VOLTAGE- AND ION-DEPENDENT CONDUCTANCES IN SOLITARY VERTEBRATE HAIR CELLS

Voltage- and Ion-dependent Conductances in Solitary Vertebrate Hair Cells[1]

An important function of the peripheral auditory system is the resolution of complex sounds into their constituent frequency components. It is well established that each mechanoreceptive hair cell of the cochlea is maximally sensitive to a particular frequency of sound (Russell & Sellick, 1978; Dallos et al., 1982), but the mechanisms by which this sharp frequency selectivity is achieved are still controversial (Dallos, 1981). The complex mechanical and hydrodynamic properties of the receptor organs and of the hair cells themselves are certainly involved (Dallos, 1981). However, in at least one auditory organ, the turtle cochlea, frequency tuning is greatly enhanced by the electrical properties of the hair-cell membrane; each cell in this organ behaves as an electrical resonator tuned to a narrow band of frequencies (Crawford & Fettiplace, 1981a). Using the 'Gigaseal', whole-cell recording technique (Hamill et al., 1981), we have investigated the biophysical basis of similar resonant behavior in enzymatically isolated hair cells from the bullfrog sacculus. We report here the identification of three voltage- and ion-dependent conductances which may contribute to the electrical tuning mechanism: a non-inactivating calcium conductance, an A-type K conductance, and a Ca-activated K conductance (Lewis, 1982).

Hair cells were dissociated from the excised sacculus of the bullfrog and whole-cell recording was performed as described in Fig. 1

[1]Lewis, R. S. & Hudspeth, A. J., Nature, Vol. 304, No. 5926, pp. 538-541, August 11, 1983.

legend. Damped oscillations in membrane potential can be evoked in isolated cells by the injection of a square step of depolarizing current (Fig. 2). As for hair cells in the turtle cochlea (Crawford & Fettiplace, 1981a), the oscillation frequency is a function of the sign and magnitude of the injected current, increasing with depolarization. However, the oscillation frequency at resting potential, after the termination of the current step, is relatively independent of the value of the preceding current injection (Crawford & Fettiplace, 1981a). All 20 cells we stimulated in this way oscillated at frequencies ranging from 80 to 160 Hz at resting potentials of -58 to -65 mV. This resonant behavior does not require the presence of the hair bundle, as occasional cells that had lost their hair bundles during the isolation procedure showed similar oscillations. In addition, oscillations of similar frequency were found using conventional microelectrode recording techniques on undissociated cells with or without hair bundles; the oscillations are therefore not an artifact of the cell isolation procedure.

Depolarization of hair cells in voltage-clamp experiments elicited several specific ionic currents. Some currents were not characterized because they could be activated only outside the voltage range of oscillations or in only a small proportion (less than 10%) of the cells. However, one inward and two outward currents were observed at voltages near the resting potential in more than 90% of the cells studied. These three currents were isolated and are described below.

The substitution of Cs for K inside the pipette blocked most of the depolarization-induced outward current, leaving a sustained inward current (Figure 3a). We have identified this as a Ca current based on the characteristics that it has in common with the Ca currents of other pre-

Figure 1. Differential-interference-contrast light micrograph of a hair cell, isolated from the bullfrog sacculus, in contact with a recording pipette. Sacculi were dissected from the animal and treated with 0.5 mg ml^{-1} papain (Calbiochem), in a solution containing (in mM) Na 120, K 2, Ca 0.1, L-cysteine 2.5, Cl 120, D-glucose 3, and HEPES 5 (pH 7.2), for 25 minutes at 22 °C. The organs were then washed with a similar solution lacking papain and cysteine and containing 0.5 mg ml^{-1} bovine serum albumin, and were scraped gently with a sharpened tungsten needle to free individual hair cells. After isolation, single cells readily formed seals of 1-20 GΩ shunt resistance with the tips of flint-glass pipettes containing (in mM) 126 K or Cs, Ca 1, Mg 2, aspartate 120, Cl 6, D-glucose 3, EGTA 2, and HEPES 5 (pH 7.2), with 10^{-7} M free Ca. Slight suction was applied to rupture the patch of membrane under the pipette, and the cells were current- or voltage-clamped through the pipette (Hamill et al., 1981) . The external solution normally used during recording contained (in mM) Na 120, K 2, Ca 4, Cl 128, D-glucose 3, and HEPES 5 (pH 7.2). In some experiments, tetraethylammonium chloride (TEA) or 4-aminopyridine (4-AP) was substituted for an equal amount of external NaCl, or different divalent cations were substituted for external Ca. External solutions were changed rapidly by lifting cells from the bottom of the chamber and passing them sequentially through different solutions flowing continuously from four 0.5-mm diameter tubes (Yellen, 1982). All experiments were done at 20-22 °C. The scale bar represents 10 μm.

Figure 2. Voltage oscillations in an isolated hair cell. The upper trace is a voltage record obtained by clamping the cell's membrane current to the value shown in the lower trace. Data were digitized at an interval of 256 μsec per point with a PDP 11/34 computer. During the current step the frequency of voltage oscillations was about 180 Hz, while at the resting potential (-55 mV) it was about 90 Hz. The latter value was measured by averaging the cell's responses to eight stimuli of different sizes, then taking the mean frequency of the first five averaged oscillations after the current step. A single response is shown.

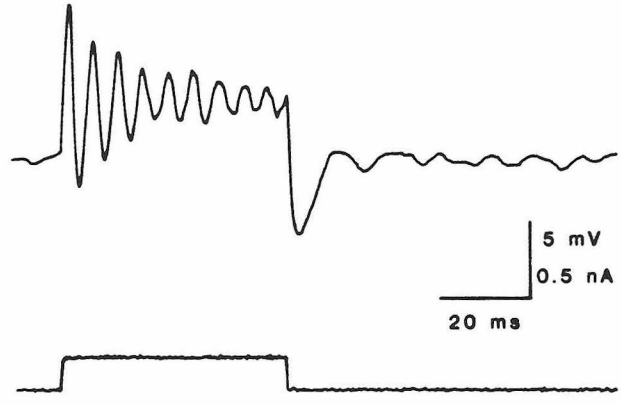
5 mV
0.5 nA
20 ms

parations (Hagiwara & Byerly, 1981). It is carried (in order of decreasing effectiveness) by Ba, Sr, and Ca. Also, it is blocked (in order of decreasing effectiveness) by Cd and Ni, and is abolished by removal of external Ca with or without Mg substitution.

The Ca current is activated at potentials more positive than -60 to -55 mV. At -30 mV, the time course of its activation is approximated well by a third-order Hodgkin-Huxley kinetic scheme (Hodgkin & Huxley, 1952) with a time constant of 0.4 msec. A contaminating outward current, insensitive to internal Cs and external tetraethylammonium ion (TEA), 4-aminopyridine (4-AP), or Ba, precluded kinetic analysis above -30 mV. Our initial observations of the hair cell's Ca current suggested that, unlike those in other preparations (Hagiwara & Byerly, 1981), it does not show inactivation (see Figure 3a). In order not to obscure any possible Ca-dependent inactivation (Eckert & Tillotson, 1981), we measured the inward current using an internal solution that contained Ca buffered to 10^{-8} M with 0.1 mM EGTA, a level of buffer that should not significantly affect the cell's endogenous Ca buffering capacity. In three cells tested, the inward currents produced during 1-sec voltage steps ranging from -50 to -42 mV did not decline from their maximal values of -20 to -90 pA. Thus, at least at these levels of activation, the hair cell's Ca conductance is capable of sustained activity.

Two outward K currents are produced by depolarization of hair cells dialysed with K internal solution. We consider one of these, a transient K current, to be an A-type K current based on similarities to the A currents described in molluscan neurons (Connor & Stevens, 1971a; Neher, 1971). Two of these properties, steady-state voltage-dependent inactivation and TEA insensitivity, were used in the experiment of Figure 3b to

isolate the hair cell's A current from the Ca and Ca-activated K currents. This transient current is the only one we have observed routinely in hair cells that shows voltage-dependent inactivation. It reverses at -90 mV, close to the calculated K Nernst potential of -104 mV. The A current was never observed when Cs was substituted for internal K. Like that of molluscan neurons, the hair cell's A current is relatively insensitive to external TEA (Thompson, 1977), but is blocked in a voltage-dependent manner by 20 mM 4-AP (Thompson, 1982). In contrast to the Ca-activated K current, it is not abolished by divalent cations that block the Ca current (Thompson, 1977). It becomes activated at voltages more positive than about -50 mV, and its kinetics can be fitted well by a Hodgkin-Huxley m^3h scheme (Hodgkin & Huxley, 1952) in which the time constant of activation is 10 msec and that of inactivation is 80 msec at -40 mV.

The largest current produced by depolarization of the hair cell is a Ca-activated K current (Figure 3c). It was isolated by using its sensitivity to TEA, which specifically blocks the Ca-dependent outward current in these cells with a 50% blocking concentration of 1 mM. The data in Figure 3c were obtained by subtracting the responses to voltage steps in the presence of 20 mM TEA from those in its absence. The resultant difference current reverses at -82 mV and is blocked by internal Cs. The following observations suggest that this current is Ca-dependent. First, all of the TEA-blockable outward current in single cells is abolished by external agents or conditions that block the hair cell's Ca current: Ni, Cd, replacement of Ca by Mg, or removal of external Ca without substitution. Like the Ca-activated K currents of other preparations (Meech, 1978), it can also be eliminated by Ba (but not Sr) substitution for

Figure 3. Voltage-clamp recordings from isolated hair cells, showing the three ionic currents. In each panel the upper set of traces shows membrane current and the lower set represents command voltage. To the right of each current trace is the corresponding command voltage in mV; the holding potential in mV is to the left of the voltage command traces in each panel. For *A* and *C*, voltage steps were presented every 400 msec, and the responses were sampled at an interval of 64 μsec/point and averaged; for *B*, the values were 1 sec and 256 μsec/point, respectively. Data were corrected for capacitive and leakage currents by subtracting from each current trace an appropriate multiple of the passive current elicited by a small depolarizing voltage step. The series resistance contributed by the pipettes was typically about 4 megohms after cell rupture; this was determined under current-clamp conditions by measuring the nearly instantaneous voltage change produced by a step of current. The voltage error introduced in voltage-clamp experiments by current flowing across the series resistance was compensated for by adding to the command voltage a correction signal proportional to membrane current. The data shown here were obtained from three different cells. *A*, Ca current. In this experiment 126 mM Cs replaced all K in the pipette. These data were recorded after a steady-state block of outward current by internal Cs was obtained, about 30 seconds after the membrane patch under the pipette was ruptured. Averages of five presentations. *B*, Transient K current (A current). These data were obtained by the following subtraction method. With 20 mM external TEA blocking the Ca-activated K current, a series of voltage steps was applied to the cell from holding potentials of -65 or -105 mV. At -65 mV, about 95% of the A current is inactivated, and the voltage steps elicited primarily Ca current. At

-105 mV the A current's inactivation is removed, and the voltage steps elicited the sum of Ca and A currents. Subtracting the former set of currents from the latter isolated the A current from the Ca current. Similar but noisier results were obtained without TEA. Averages of four presentations. *C*, Ca-activated K current. The responses shown were obtained by subtracting the currents produced by voltage steps in the presence of 20 mM TEA (a fully blocking dose) from those produced in its absence. Averages of two presentations.

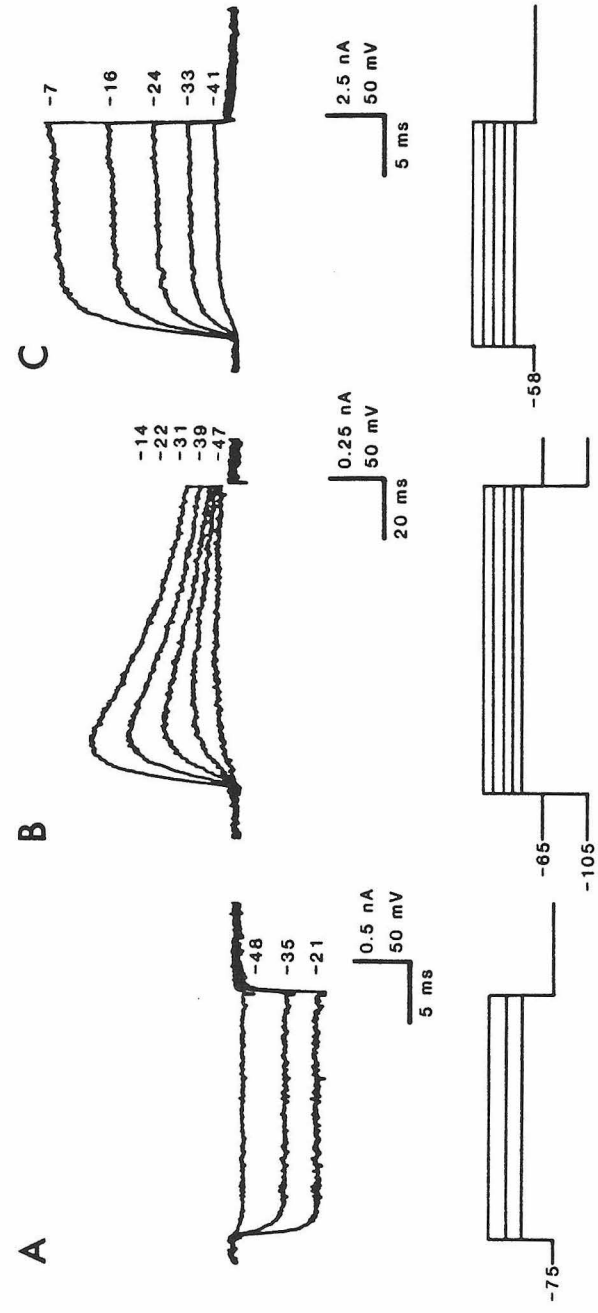
A
B
C
-48
-35
-21
-14
-22
-31
-39
-47
-7
-16
-24
-33
-41
0.5 nA
50 mV
5 ms
0.25 nA
50 mV
20 ms
2.5 nA
50 mV
5 ms
-75
-65
-105
-58

external Ca but is relatively insensitive to 4-AP (20 mM blocks <5% of the current). Lowering external Ca from 4 to 0.5 mM (with Mg substitution) slows the kinetics and lowers the steady-state magnitude of this current. Finally, the cell's current-voltage relationship measured 20 msec after the start of a voltage-clamp step peaks at +30 to +40 mV, producing an "N"-shaped curve similar to that found for other preparations having a Ca-activated K conductance (Meech, 1978). The hair cell's Ca-activated K current is activated at potentials above -60 to -45 mV; its kinetic behavior cannot be fit well by a Hodgkin-Huxley scheme (Hodgkin & Huxley, 1952) of any order.

The currents identified in this study account for some of the previously reported physiological properties of hair cells. The Ca conductance we have observed is probably involved in the Ca-dependent (Furukawa & Matsuura, 1978) release of transmitter from hair cells onto afferent nerve fibers: its activation at voltages close to the resting potential and its failure to be significantly inactivated are consistent with a role in the tonic release of transmitter by hair cells at rest (Sand et al.,1975). The A current and particularly the large Ca-activated K current are most likely responsible for the striking outward rectification observed in hair cells of the bullfrog sacculus (Corey & Hudspeth, 1979) and the turtle cochlea (Crawford & Fettiplace, 1981b).

Which of the ionic currents in the hair cell contribute(s) to membrane-potential oscillations? Because oscillations persist in isolated cells lacking hair bundles and efferent nerve terminals, modulation of either the transduction (Corey & Hudspeth, 1979) or the postsynaptic efferent (Art et al., 1982) conductances is not essential for the oscilla-

tion phenomenon. Similarly, as the A current is largely inactivated at resting potential, it may not be significantly involved. The best candidates for currents underlying the hair cell's electrical resonance are the Ca and Ca-activated K currents. Aside from those discussed above, these two currents are the only ones we have routinely observed that are active in the voltage range in which oscillations occur. Moreover, TEA, a rather specific blocker of the hair cell's Ca-activated K current, effectively reduces or abolishes oscillations, a result also obtained with turtle hair cells (Crawford & Fettiplace, 1981a,b).

It has been shown in several preparations that electrical resonance can be produced by the interactions of relatively fast, voltage-dependent conductances (Mauro et al., 1970; Morris & Lecar, 1981; Plant, 1978). In those and other cell types, the Ca-activated K current typically shows rather slow kinetic behavior, and is thought to modulate membrane potential slowly, leading in some cases to "bursting" patterns of activity (Meech, 1978; Morris & Lecar, 1981; Plant, 1978). In this regard, it is interesting that the Ca-activated K conductance in hair cells is activated 10-100 times more rapidly for a given range of depolarizations than any that have been reported previously (but see Adams et al., 1982). This rapid kinetic behavior may enable the hair cell's Ca-activated K channel to participate in electrical processes usually reserved for fast, voltage-dependent channels.

CHAPTER TWO

THE IONIC BASIS OF ELECTRICAL RESONANCE IN THE HAIR CELL

INTRODUCTION

The property of electrical resonance, while highly developed in some types of hair cells and electroreceptors, is present to a greater or lesser extent in a large variety of electrically excitable cells. The study of this phenomenon dates back to some of the earliest investigations of excitable membranes; resonance characteristics of the squid giant axon were first revealed by the dependence of membrane impedance on the frequency of small applied sinusoidal currents (Cole and Baker, 1941), and by damped subthreshold voltage oscillations induced by small current pulses (Cole & Curtis, 1941). In terms of an electrical equivalent circuit, the membrane behaved as a capacitance in parallel with the series combination of a resistance and an inductance (Cole & Baker, 1941). The physical bases of membrane resistance and capacitance were relatively easily explained as the respective manifestations of membrane ionic permeability and dielectric properties. However, the biological counterpart of inductance was at the time unclear; in electrical terms, inductance arises from the storage of energy in a magnetic field, and it seemed impossible for a biological membrane to generate a magnetic field of sufficient strength to account for its inductance (Cole, 1941). Later it was shown that inductance has no direct physical counterpart in the membrane, but rather is a "phenomenological" property arising under certain conditions from time-variant ionic conductances (Hodgkin & Huxley, 1952; Mauro et al., 1970); inductive properties can arise from an outward ionic current that turns on with membrane depolarization, or from an inward current that turns off with depolarization (for a derivation, see Detwiler et al., 1980). With their mathematical

description of electrical excitability in the squid axon, Hodgkin and Huxley (1952) determined that the membrane inductance at voltages close to resting potential resulted from K current activation and Na current inactivation, with the former being somewhat more important.

Ionic conductances give rise to electrical resonance in a large number of cell types, extending across the boundaries of phyla and tissue. Voltage-dependent Ca and K conductances underlie a large variety of oscillatory voltage behavior in barnacle muscle fibers (Morris & Lecar, 1981). Extremely slow spontaneous membrane potential oscillations occur in neuron R15 of *Aplysia* in the presence of tetrodotoxin and low external Ca (Junge & Stephens, 1973); in this and other molluscan "bursting" neurons the oscillations result from the activation of a Ca conductance which leads to intracellular Ca accumulation and the subsequent activation of a Ca-dependent K conductance (Gorman et al., 1982; in *Tritonia*, Smith, 1978). The resonance phenomenon even extends to cells outside the nervous system; β-cells of the pancreas, when stimulated with glucose, show a slow pattern of bursting activity the phasic nature of which has been attributed to a similar interaction of Ca and Ca-activated K conductances via changes in internal Ca concentration (Atwater et al., 1980; Chay & Keizer, 1983).

In all of the examples cited above, electrical resonance acts to control patterns of electrical activity. For membranes that are not spontaneously active, such as those of squid axon and barnacle muscle, electrical resonance determines the firing frequency in response to a maintained current stimulus. In "bursting" cells a more complex pattern of activity is generated in which periods of repetitive spiking alternate with long periods of quiescence.

Electrical resonance serves a different function in non-spiking sensory cells of the visual and the acousticolateralis systems, where it is involved in the processing of incoming sensory information. Light-induced hyperpolarization of rod photoreceptors in the retina of vertebrates elicits a Cs-sensitive inward current (Fain et al., 1978; Bader et al., 1982) which mimics a membrane inductance. The combined effect of this inductance and of electrical coupling between rods allows the electrical response to an absorbed photon to spread out over a large area of retina initially, and restricts it to an ever decreasing area at later times. Thus, a bipolar cell that spatially integrates the output of many rods may achieve good temporal resolution, while one that integrates rod output over time maximizes spatial resolution (Detwiler et al., 1980). In electroreceptors and hair cells, electrically resonant properties are highly developed and form the basis of a sharply tuned electrical filter. Electroreceptors, located in modified lateral line organs and used for electrolocation and communication by weakly electric fish, respond to a step change in the external electric field with damped oscillations of membrane potential (Bennett, 1971); the resonance indicated by this response is thought to allow the receptor cell to respond selectively to alternating electric fields at the frequency of the individual's own electric organ discharge in the presence of high levels of background noise (Hopkins, 1976). Although the ionic mechanism of the electrical filter in this cell has not yet been established, the results of pharmacological experiments suggest the participation of Ca and K conductances (Clusin & Bennett, 1979; H. Zakon, manuscript in preparation).

In hair cells from the auditory and vestibular organs of several

species, electrically resonant properties serve in an analogous manner to enhance sensitivity to particular frequencies of sound or vibration. In an elegant series of studies, Fettiplace and Crawford described the electrical characteristics of resonance in cochlear hair cells of the turtle, *Pseudemys scripta elegans*, and defined their contribution to the hair cell's frequency selectivity for acoustic stimulation (Crawford & Fettiplace, 1980, 1981a,b). Subsequently, similar resonance properties were reported for saccular hair cells from the bullfrog, *Rana catesbeiana* (Lewis & Hudspeth, 1983a), and the leopard frog, *Rana pipiens* (Ashmore, 1983); in these cells also, electrical resonance enhances the responses to particular frequencies of mechanical stimuli (Lewis & Hudspeth, 1983b; Ashmore, 1983). Fettiplace and Crawford modeled the membrane properties of turtle hair cells in terms of an equivalent circuit consisting of a capacitance in parallel with the series combination of a resistance and an inductance, similar to the one applied to the squid giant axon. While this empirical description of the electrical filtering properties of the membrane made it possible to assess the contribution of electrical resonance to acoustic tuning (Crawford & Fettiplace, 1981a), it could provide only limited insight into the biophysical basis of the resonance mechanism. The participation of a voltage-sensitive K conductance was suggested by the blockage of oscillatory behavior by TEA and 4-AP, and by the disappearance of oscillations near or below the estimated K Nernst potential, E_K (Crawford & Fettiplace, 1981a,b); by analogy to the squid giant axon, the membrane's inductance at voltages above E_K could be accounted for by an outward K current activated by depolarization. However, in an attempt to present a consistent basis for frequency tuning in hair cells from alligator

lizard and turtle, Weiss (1982) has shown theoretically that resonant characteristics can arise from bidirectional coupling between purely passive membrane properties and voltage-dependent mechanical properties of the transduction apparatus. A suggestion has also been made that electrical resonance involves activation of the hair cell's postsynaptic efferent conductance (Ashmore, 1983). Unfortunately, attempts to identify and study the ionic conductances of turtle hair cells under voltage clamp have been thwarted by the small size of the cells, which makes two-microelectrode impalement difficult, and by restricted access to the basal surface of the cells *in situ*, which precludes rapid solution changes.

These difficulties were largely overcome in voltage-clamp studies of enzymatically dissociated hair cells from the bullfrog's sacculus using the gigohm-seal recording technique (Lewis & Hudspeth, 1983a). In these experiments the presence of resonant behavior in solitary cells lacking efferent input, and, in some cases, hair bundles, clearly showed that neither the efferent nor the transduction conductances is a necessary part of the resonance mechanism, thereby ruling out the explanations proposed earlier by Ashmore (1983) and Weiss (1982). Of three time-variant ionic currents that were shown to be active in the voltage range in which oscillations occur, only the voltage-dependent Ca current (I_{Ca}) and the Ca-activated K current (C current, or I_C) were thought to be involved in generating the resonance, because only conditions that inhibited these currents unequivocally altered the cell's oscillatory behavior under current clamp (Lewis & Hudspeth, 1983b). Although the pharmacological evidence supported the idea that I_{Ca} and I_C are involved in producing the hair cell's electrical resonance, it did not establish

the *sufficiency* of these currents in doing the same. One could imagine, for example, that resonance is produced primarily by an unrelated internal process and is only modulated by the activity of the Ca and Ca-activated K conductances.

The sufficiency of a particular ionic mechanism to account for a given electrical behavior can be tested through modeling. Hodgkin and Huxley used this approach to establish the ionic basis of the action potential; by developing an explicit mathematical description of the time- and voltage-dependent behavior of axonal Na and K conductances under voltage clamp, they were able to predict accurately the voltage trajectory of the axon under current clamp conditions in which voltage is free to vary. Subsequent modeling based on voltage-clamp data has provided an understanding of the biophysical mechanisms underlying a variety of activity patterns in different cell types, including repetitive firing in molluscan neurons (Connor & Stevens, 1971b) and cardiac Purkinje fibers (McAllister et al., 1975), and "bursting" activity in molluscan neurons (Plant, 1978; Smith, 1978).

In this chapter I present the results of modeling the hair cell's electrical behavior in terms of Ca and C conductances as a test of the sufficiency of these conductances to account for the observed electrical resonance. The model's description of the hair cell differs in one important respect from the Hodgkin-Huxley model of the squid giant axon: whereas all of the conductances in the squid axon could be described as functions of voltage and time, activation of the hair cell's C conductance also depends on the intracellular Ca concentration, which adds a considerable amount of complexity to a description of the system. I_{c_∞} and I_c were measured under voltage clamp conditions in the same cell,

and parameter values in the model were varied to provide the best approximations to the time courses of both currents. After having been thus constrained by voltage-clamp data, the model predicts voltage oscillations closely resembling those observed experimentally in response to extrinsic current pulses. In this way, the results of modeling establish the sufficiency of the Ca and C conductances to generate electrical resonance in the hair cell.

METHODS

Hair cell dissociation

Sacculi were dissected from adult bullfrogs and treated for 25 minutes at 20-22°C with 0.3 to 0.5 mg/ml papain (Calbiochem) dissolved in a saline solution containing (in mM) 120 Na, 2 K, 0.1 Ca, 2.5 cysteine, 130 Cl, 3 D-glucose, and 5 HEPES (pH 7.2). This mild treatment loosens connections among cells to the extent that hair cells can be dissociated from the sacculus by gently scraping the epithelium with a tungsten needle about 8 μm in tip diameter. The commercial source of the enzyme is an important factor in determining the success of dissociation: papain of higher purity, obtained from Worthington Biochemical Products or Sigma Chemical Co., is ineffective at comparable concentrations at loosening hair cells from the epithelium, even though these samples express higher levels of papain activity than the Calbiochem enzyme (assayed by hydrolysis of benzoyl-arginine-ethyl ester). Thus, a contaminating enzyme in Calbiochem papain is likely to be the active dissociating agent.

Internal and external solutions

Whole-cell and single-channel recording (Hamill et al., 1981) were performed on solitary hair cells at 20-22°C, using the internal (intracellular) and external (extracellular) solutions whose compositions are listed in Table 1. Pipettes contained internal solution for whole-cell recording and external solution for single-channel recording from

TABLE 1. Composition of solutions (mM).

V_{JP} denotes junction potential in mV between the listed solution and standard saline. pH of all solutions was 7.2.

External solutions

Solution	Na	K	Ca	Mg	TEA	4-AP	Cl	D-glu	HEPES	V_{JP}
Standard saline	120	2	4	-	-	-	128	3	5	0
TEA saline	100	2	4	-	20	-	128	3	5	0
4-AP saline	110	2	4	-	-	10	128	3	5	0
TEA/4-AP saline	90	2	4	-	20	10	128	3	5	0.6
Low-Ca saline	120	2	0.5	3.5	-	-	128	3	5	0
1 mM TEA saline	119	2	4	-	1	-	128	3	5	0
KCl saline	-	122	4	-	-	-	128	3	5	-4

Internal solutions

Solution	K	Cs	Na	Ca	Mg	Asp	Cl	EGTA	D-glu	HEPES	V_{JP}
K aspartate	124	-	-	.134	2	120	4.3	2	3	5	-13
Cs aspartate	-	124	-	.134	2	120	4.3	2	3	5	-13
KCl +1 μM Ca	122	-	3	.875	2	-	128	1	3	5	-4
10 " "	122	-	3	.010	2	-	127	-	3	5	-4
100	122	-	3	.100	2	-	127	-	3	5	-4
K aspartate											
+ 1 μM Ca	127	-	-	2.00	2	120	8	2	3	5	-13
8 " "	128	-	-	2.32	2	120	8.6	2	3	5	-13
26 " "	128	-	-	2.40	2	120	8.8	2	3	5	-13
100 " "	128	-	-	2.71	2	120	9.4	2	3	5	-13
167 " "	128	-	-	3.00	2	120	10	2	3	5	-13

inside-out membrane patches.

Slow, time-dependent changes in ion channel properties can cause difficulties in both whole-cell and excised-patch recordings. In many preparations, the voltage-dependent Ca current (I_{Ca}) deteriorates with time during whole-cell voltage-clamp experiments (Byerly & Hagiwara, 1982; Fenwick et al., 1982). This is thought to result from the slow exchange of pipette solution for the cell's soluble cytoplasm, resulting in the removal of some as yet unidentified cellular component(s) essential for normal Ca channel function (Byerly & Hagiwara, 1982). The slow deterioration of I_{Ca} is especially pronounced in the hair cells I have studied; I_{Ca} induced by brief voltage steps typically starts to decline less than five minutes after the whole-cell recording configuration is established. The rundown of I_{Ca} may account for the decrease in activation rate and steady-state magnitude of the Ca-activated K current (C current, or I_C) observed during a similar time period. Thus, slow changes in both I_{Ca} and I_C in hair cells limit the period for whole-cell recordings of these currents to less than five minutes. In contrast, the hair cell's transient K current, I_A, persists long after I_{Ca} and I_C have disappeared entirely, and even after the cell has lost its normal cylindrical shape. In addition, slow shifts in the Ca- and voltage-dependent gating of single Ca-activated K channels have been reported (Methfessel & Boheim, 1982; Moczydlowski & Latorre, 1983). Because of the lability of I_{Ca} and I_C, a continuous-stream perfusion system (Fig. 1; Yellen, 1982) was used to allow rapid changes of external solutions (whole-cell recording) or internal solutions (single-channel recording). Different solutions were pumped through the inlet tubes with a peristaltic pump (Gilson) and were removed from the chamber with a

Figure 1. Schematic diagram of the recording configuration. After formation of a gigohm seal between a solitary hair cell and pipette, the cell was lifted from the bottom of the chamber. Thereafter, either slight suction was applied to rupture the membrane under the pipette (for whole-cell recording), or the pipette was moved suddenly to excise a membrane patch (for single-channel recording). Membrane voltage or current was clamped by means of a virtual ground-type patch-clamp circuit, shown schematically at the right, which made contact with the pipette interior via an Ag/AgCl wire. The bath was grounded with an Ag/AgCl wire, either bare, or, in later experiments, in an agar bridge containing standard saline. Continuous streams of various solutions entered the chamber from four 0.5-mm-diameter glass tubes shown at top. Effects of different external solutions (whole-cell recording) or internal solutions (single-channel recording) were assayed by placing a cell or patch sequentially within the mouths of these tubes while recording. The perfusion solutions were removed from the chamber by a suction tube located near the perfusion inlets.

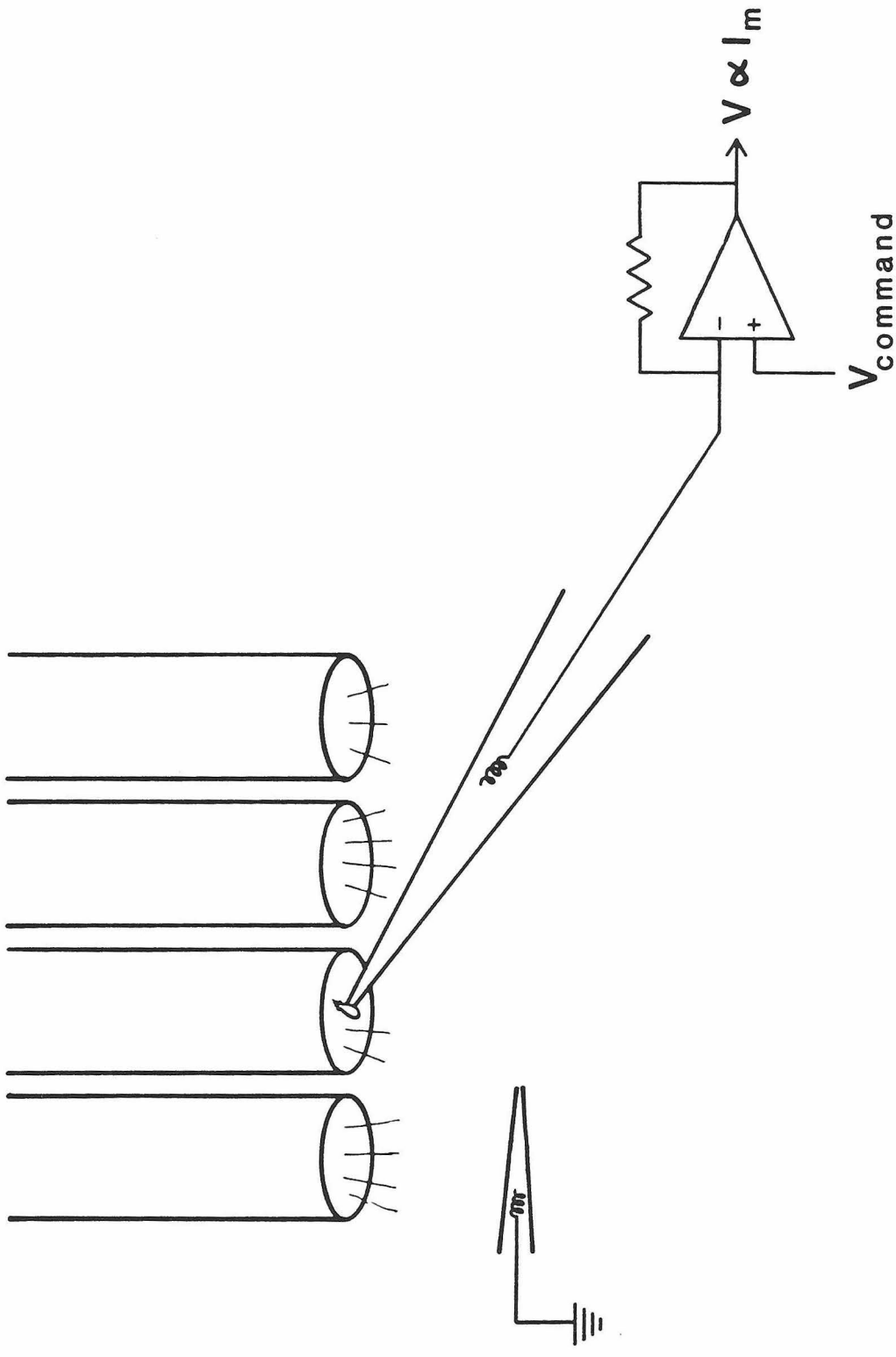
V ∝ I m
V command
- +

suction tube located nearby. Cells or patches were placed within the openings of perfusion tubes to ensure complete exchange of the surrounding solutions. Exchange was essentially complete within 1 second, as judged by the time required for a TEA-containing stream to block whole-cell C current.

Whole-cell recording

Solitary hair cells were voltage- or current-clamped with a whole-cell clamp based on the Yale Mark V (designed by D. P. Corey). Pipettes were fabricated from flint glass capillaries (Garner Glass Co.), were coated near their tips with Sylgard® (Dow Corning Corp.) to reduce stray capacitance between pipette and bath, and were heat-polished to give internal tip diameters of 2-3 μm. The pipettes had axial resistances of 1-3 MΩ when filled with K aspartate internal solution. After formation of a gigohm seal between pipette and cell, the residual capacitance of the pipette was nulled electronically. Slight suction was then applied to the pipette to rupture the patch of membrane under the pipette and attain the whole-cell recording conformation.

Series resistance compensation. After rupture, a significant series resistance (R_s) exists between the clamp's connection to the pipette and the cell's interior. For each cell, R_s was assessed by analyzing the average current response to a small voltage clamp step (ΔV = 10 mV; Hamill et al., 1981). The capacitive transient at the start of the step was integrated to give the total charge displacement (Q); membrane capacitance (C_m) was calculated according to $C_m = Q/\Delta V$. The decay of the transient was fitted by eye with an exponential function which was filtered

by the time constant of the clamp (about 40 μsec). R_s was calculated from the relation $\tau = R_s \cdot C_m$, where τ is the time constant of decay of the capacitive transient. R_s ranged from 2 to 6 MΩ, with an average value of 4.4 MΩ (n=35). Any currents flowing across R_s causes membrane voltage to differ from the desired command voltage by an amount $\Delta V = I \cdot R_s$); the command potential of the voltage clamp was therefore changed by an amount proportional to clamp current to compensate for the voltage drop across R_s. Although up to 90% of R_s could be compensated in this way, this often caused large oscillations in current at the start and end of voltage clamp steps, which obscured active membrane currents for 100-300 μsec. To avoid this I used an average of 50% compensation; this leads to membrane voltage errors of less than 2 mV during ionic currents of less than 1 nA amplitude, which was typical in the experiments reported here. Incomplete R_s compensation caused greater errors during the large capacitive currents elicited at the start and end of voltage steps, but in most cases this was not a significant problem. During these times, membrane voltage exponentially approaches the command voltage level with an approximate time constant of $R_s \cdot C_m$, where C_m is cell membrane capacitance (Horn & Brodwick, 1980). For the hair cell, the approach is quite fast; with an average C_m = 15 pF, 2 MΩ of uncompensated R_s gives a time constant of 30 μsec.

Liquid junction potentials. A substantial potential can appear across the tip of the recording pipette, or between a perfusion stream and bath, caused by differences between the mobilities of ions in the pipette or stream and those in the bath. These potentials were measured in the following way. Using a 3M KCl-filled electrode in the bath as reference, a pipette containing a given internal solution was placed in

a bath containing the same solution. In current-clamp mode the current through the pipette was clamped to zero; under these conditions, the pipette voltage indicated by the clamp was the junction potential between the Ag/AgCl wire in the pipette and the internal solution, and was canceled electronically. The bath solution was then changed to standard saline; now the voltage reading of the clamp was equal to the liquid junction potential set up across the tip of the pipette, between standard saline and the pipette solution. Results are listed in Table 1. The liquid junction potential was present before but not after establishing the gigohm seal; accordingly, this voltage was added to the command voltages applied to the pipette in voltage-clamp experiments, so that pipette current could be zeroed in the standard saline bath solution immediately before seal formation.

Stimulation and recording. Command voltages were supplied by a PDP 11/23 computer (Digital Equipment Corporation) via a 12-bit D/A converter (Analog Devices) in a computer interface (Cheshire Data). All stimulation and recording programs were written in BASIC-23. Data were sampled synchronously with a 12-bit A/D converter (Data Translation). In some experiments transients were shaped and subtracted from the output of the voltage clamp to null the capacitive currents at the start and end of voltage steps. This procedure allowed small ionic currents to be recorded at high gain without saturating the A/D converter with the cell's capacitive currents. The subtraction transients were sampled at lower gain and added back to the digitized current traces if desired. This procedure offered two additional advantages: by calibrating the circuit that generates the transients, one could quickly estimate R_s during an experiment, and being able to view the membrane current

without transients enabled one to detect small changes in R_s during the course of a recording. Increases in R_s were less likely when constant suction (-20 to -40 cm H_2O) was applied to the pipette.

Families of current or voltage steps were given sequentially from the most negative to the most positive values, at repetition intervals noted in the figure legends. In voltage-clamp experiments, leakage and capacitive currents were removed by averaging the response to eight small (±10 to ±20 mV) voltage steps presented immediately prior to each family of test voltage steps and subtracting the appropriate multiples of this average from the test responses. Collection of leakage current data prior to each family of test steps avoided errors in leak correction that can result from slow changes in leakage conductance during the course of a recording.

Ensemble variance analysis. Ensemble variance analysis of macroscopic C currents was performed as originally described by Sigworth (1980) to provide estimates of the open-state probability of the Ca-activated K channel in whole-cell recordings and of the amplitude of the single-channel current underlying the macroscopic C current. Assuming the cell has a single, homogeneous population of C channels that exhibit only one nonzero conductance level and are gated independently of each other, the following relationships can be applied:

(1) $$I(t) = N \cdot i \cdot p(t)$$

(2) $$\sigma_I^2(t) = N \cdot i^2 \cdot p(t) \cdot (1-p(t))$$

where I(t) is total current at time t, N is the total number of activatable channels, p(t) is the open-state probability at time t, i is the single channel current amplitude, and $\sigma_I^2(t)$ is the current variance at time t. Equations (1) and (2) can be combined to give

(3) $$\sigma_I^2(t) = i \cdot I(t) - (1/N) \cdot I^2(t).$$

These three relations express the idea that the fluctuations in current resulting from the stochastic gating of ion channels approach zero when none or all of the channels are activated (p=0 or p=1), and are largest when half are open (p=0.5).

The following stimulation protocol was applied to hair cells bathed in standard saline. First, a set of 16 10-mV or -20-mV voltage-clamp steps was delivered from a holding potential of -70 or -55 mV, respectively, to record leakage current. Immediately thereafter, a group of eight test steps to -30 mV was applied with an interpulse interval of 0.5 sec. This basic pattern was then repeated. At these holding potentials and repetition rates, most of the A current is inactivated and does not contribute significantly to the response. The average leakage current was scaled and subtracted from the immediately following set of eight test responses. "Local" mean macroscopic currents and variances around the mean were computed for each group of eight responses. Since I_c deteriorated slowly during the recording, grand averages were made from the local means during the period when local mean I_c was at least 90% of its starting value. For responses showing an early inward Ca current, a third-order Hodgkin-Huxley waveform with a time constant of 0.4 ms (corresponding to the average kinetic behavior of I_{Ca} at this voltage) was scaled and subtracted to exactly negate the inward current. This was done rather than recording I_{Ca} from the same cell for subtraction because cells generally did not remain stable over a long enough period to permit collection of the required data for both I_{Ca} and I_c. The grand average for variance was plotted point-for-point against that of the macroscopic current, and a parabola described by equation (3) was

fitted to the plot by a least-squares method.

Three possible sources of error arise in the interpretation of the ensemble variance data. First, the method of removing the contribution of I_{Ca} to the macroscopic current is not based on actual measurement of I_{Ca} in the same cell, but on subtraction of an idealized waveform fitted to I_{Ca} in other cells. The possible error accruing from this source is probably small, however, as the kinetic behavior of I_{Ca} is quite similar among hair cells. Second, although an estimate of macrosopic I_{Ca} is subtracted, the microsopic fluctuations due to Ca channel gating are not, and still contribute to the overall variance. However, the following arguments suggest that this error is also negligible. Assuming that Ca channels satisfy the same criteria as the C channel given above, equations (1) and (2) can be used to estimate the Ca current variance at -30 mV. Using ensemble fluctuation analysis, the current through single Ca channels in chromaffin cells, with 5 mM external Ca and -30 mV membrane potential, has been estimated at -0.12 pA (Fenwick et al., 1982). For hair cells, $p = 0.36$ and $I=-200$ pA at -30 mV (on average); with these values for I, i, and p, equation (2) estimates the Ca current variance at -30 mV to be 15 pA^2, or less than 2% of the total observed variance. Another observation suggesting that Ca current variance is minimal is that no significant increase in the variance was ever seen between the starting time of the voltage-clamp step and the time at which I_c started to appear. Because I_{Ca} is activated before I_c (see Fig. 10), any variance due to I_{Ca} should be visible in that time period. A third possible source of error stems from thermal noise associated with the overall membrane conductance. However, these fluctuations would only be significant at voltages near the reversal potential for K current, at which

ionic current through the channel is small (Sigworth, 1980). Since the test steps were over 50 mV above reversal potential for I_c, thermal noise is probably not a significant source of error.

Single channel experiments

All single-channel experiments were performed on Ca-activated K channels in excised, inside-out membrane patches (Hamill et al., 1981). Borosilicate glass pipettes (Drummond Microcaps) were coated with Sylgard® and were heat-polished to give resistances of about 5 to 10 MΩ when filled with standard saline. After the formation of gigohm seals, patches were excised by lifting the hair cell off the bottom of the chamber and flicking the Leitz micromanipulator joystick. In over 90% of the cases, this flings the cell from the pipette, leaving an intact membrane patch spanning the pipette tip. Liquid junction potentials of the pipette and external perfusion solutions relative to the bath were corrected in the same way as in whole-cell recordings. A List EPC-5 patch clamp was used, and its output was low-pass filtered with an 8-pole Bessel filter (Frequency Devices, Inc.). "Intracellular" solutions were supplied by the continuous perfusion streams described above and are listed in Table 1. Most internal solutions contained 2 mM EGTA; $CaCl_2$ was added to these to provide the desired levels of free Ca, given an effective dissociation constant for Ca of $1.46 \cdot 10^{-7}$ M at pH 7.20, measured by the method of Bers (1982). Final adjustments of free Ca concentration were made using a calibrated Ca electrode (Orion Research Inc.).

Data for histogram analysis were recorded on an FM tape recorder (Hewlett-Packard) having a bandwidth of 5 kHz. For computer analysis,

these data were played back later and digitized at a rate of 5 times the Bessel cutoff frequency. The amplitude of single-channel currents was estimated either by fitting amplitude histograms of sampled data with a Gaussian curve, or, if satisfactory histograms were not obtainable, by visually fitting lines to "square" current events.

For the construction of channel lifetime histograms, data were digitized as described above and interpolated using a cubic spline algorithm (Colquhoun & Sigworth, 1983), resulting in an interpoint time interval of 25 μsec. Transitions between open- and closed-channel current levels were detected using a threshold criterion of 50% of the open-channel current magnitude, after the baseline current was fitted by eye. Short event durations were corrected for the risetime of the recording apparatus (which was always dominated by the Bessel filter cutoff frequency) as described by Colquhoun and Sigworth (1983). Single- or double-exponential conditional probability density functions of the form

$$f(t) = \sum_i \frac{a_i/\tau_i \cdot \exp(-t/\tau_i)}{P(t>t_{min})} \qquad (4)$$

were fitted to the durations data; f(t) is the probability density of an event of duration t given that it is longer than the minimum detectable duration, t_{min}, and a_i is the area of and τ_i the time constant of the ith exponential component of the probability density function. $P(t>t_{min})$ is the probability that the event is longer than t_{min}. A maximum likelihood method (Colquhoun & Sigworth, 1983; program generously provided by R. Horn and K. Lange) was used to fit the probability density function to the data. This method was chosen because it allows sensible estimates of error for the fitted parameters and because it is not affected by the size of histogram bins, since it uses the measured durations of events

rather than binned data.

The current-voltage relation for open C channels was obtained by the ramp-clamp method (Yellen, 1982). Repetitive voltage ramps were applied to a patch, and open-channel segments were identified to the computer. These segments were then averaged point by point for each voltage. The same was done for the closed-channel segments. The closed-channel average was subtracted from the open average to give the I/V relation through a single open C channel.

Voltage-dependent relaxations of the C channel's open-state probability were also studied in the presence of constant levels of internal Ca. Repetitive voltage steps were applied to the patch and closed-channel segments identified and averaged as in ramp clamp experiments. This closed-channel average, comprising a small leakage current and residual capacitive transients, was subtracted from the average of all responses.

Description of models

Here I will present the features of two models that I used to describe a mechanism for electrical resonance in the hair cell. The two models differ only in the formalism used to describe the Ca-activated K conductance.

I. Ca current (I_{Ca})

Voltage-dependent I_{Ca} activation is described by a third-order Hodgkin-Huxley kinetic scheme (Hodgkin & Huxley, 1952):

(5) $$I_{Ca}(t) = \overline{G}_{Ca} \cdot m^3(t) \cdot (V_m(t)-E_{Ca})$$

where $\bar{G}_{Ca}$ is the Ca conductance with all Ca channels open, m(t) is the activation-parameter value (0 to 1) at time t, $V_m(t)$ is membrane potential, and E_{Ca} is the Ca Nernst potential. This formulation assumes that current through open Ca channels is ohmic, which is certainly not the case at potentials approaching E_{Ca}, but is a reasonable approximation at the negative potentials considered in this study (Hagiwara & Byerly, 1981). There is no inactivation term, since the Ca current in hair cells does not inactivate at these potentials (Lewis & Hudspeth, 1983a). The time-dependent behavior of the activation parameter, m, is described by

(6) $$dm/dt = \beta_m \cdot (1-m(t)) - \alpha_m \cdot m(t)$$

where α_m and β_m are the closing and opening rate constants, respectively. Equation (6) can be solved for m, yielding

(7) $$m(t) = m_0 + (m_{inf}-m_0) \cdot [1-\exp(-t/\tau_m)]$$

where m_0 is the initial value of m before a voltage change, and τ_m is the time constant of m's exponential approach to its equilibrium value at the new voltage, m_{inf}. Given that $m_0=0$ at holding potentials below -60 mV, τ_m and m_{inf} can be expressed in terms of α_m and β_m by

(8) $$\tau_m = 1/(\alpha_m+\beta_m)$$

(9) $$m_{inf} = \beta_m/(\alpha_m+\beta_m)$$

α_m and β_m are, in turn, empirically described as functions of voltage:

(10) $$\alpha_m = \alpha_0 \cdot \exp(-(V_m+V_0)/V_A) + K_A$$

(11) $$\beta_m = \beta_0 \cdot \exp((V_m+V_0)/V_B) + K_B$$

where α_0, K_A, β_0, and K_B are rates and V_0, V_A, and V_B are voltages to be experimentally determined. This description of the Ca current is not intended to imply any particular mechanism for Ca channel gating, but simply to provide a means of predicting I_{Ca} as a function of time and voltage.

II. Dynamic regulation of submembrane Ca concentration

The processes that determine the time course of Ca concentration at the inside surface of the membrane are of obvious importance in a system such as the hair cell, in which a Ca-activated conductance plays a major role in determining the cell's electrical behavior. Work on other preparations, such as mammalian nerve terminals, the squid giant axon, and other molluscan neurons, has identified at least five processes that may regulate the concentration of free Ca next to the inner membrane surface following its influx through Ca channels. These processes include Na/Ca exchange (Blaustein, 1974), sequestration and uptake by mitochondria (Brinley et al., 1978) and endoplasmic reticulum (Blaustein et al., 1978), an ATP-dependent Ca pump in the plasma membrane (Schatzmann, 1975), several classes of cytoplasmic Ca buffers (Brinley, 1978), and diffusion (Smith, 1978; Barish & Thompson, 1983). Available evidence indicates that these various mechanisms are active in different ranges of internal Ca concentration and operate at different rates, so that a complete description of the dynamic regulation of Ca in any given cell is likely to be quite complex; furthermore, essentially nothing is known about Ca regulation in the hair cell. For these reasons, I adopted a relatively simple model for Ca regulation, which has been successfully used to model Ca current inactivation caused by Ca accumulation in insect skeletal muscle fibers (Standen & Stanfield, 1982).

This Ca regulation model makes three assumptions. (1) Ca entering the cell through Ca channels is confined to a small submembrane compartment, occupying a small fraction σ of the cell's total volume. This compartment is not meant to correspond to any specific physical structure, but merely to reflect the action of Ca buffering on the diffusion rate;

a lower diffusion rate tends to concentrate incoming Ca close to the membrane. (2) The concentration of endogenous buffer is in great excess to the amount of Ca that enters, such that a constant fraction, U, of Ca remains free. U is given a value of 0.02, corresponding to an estimate of the proportion of free Ca in molluscan neurons (Gorman & Thomas, 1980). (3) Ca leaves the compartment at a rate proportional to its concentration. The rate constant for this process is K_s, and reflects contributions of Ca pumping, sequestration, and diffusion. This model predicts that, in response to a transmembrane Ca current, the Ca concentration [Ca] subadjacent to the plasma membrane changes at a rate given by

(12) $$d[Ca]/dt = U \cdot I_{Ca}(t)/(zFC_{vol}\sigma) - K_s \cdot [Ca](t)$$

where z is the valence of Ca, F is the Faraday, C_{vol} is the total cell volume (calculated for a cylinder of 8 μm diameter and 25μm length to be 1.25 pliter), and [Ca](t) is the submembrane Ca concentration at time t. Note that a change in U can be compensated by a change in σ; in fitting the model to hair cell data I left U constant and changed σ.

III. Ca-activated K current (I_c)

Model I ("Michaelis-Menten model"). According to this scheme transitions of the Ca-activated K channel among open and closed states are assumed to be much faster than the time course of changing Ca concentration, so that the Ca-activated K conductance, G_c, is always in equilibrium with the level of free Ca in the cell. Also, G_c is solely a function of the concentration of Ca and is independent of membrane potential. With these assumptions, C conductance can be expressed in terms of a Michaelis-Menten-type relationship:

(13) $$G_c(t) = \bar{G}_c/(1+K_d/Ca^n(t))$$

where $\bar{G}_c$ is the C conductance with all C channels open, K_d is the dissociation constant for the C channel's Ca binding site, and n is an integer representing the number of identical Ca binding sites which must be occupied to open the channel. I chose this description of C current activation because of its simplicity and its successful use in modeling the effects of I_c on repetitive activity in a variety of preparations (in *Aplysia*, Plant, 1978; in *Tritonia*, Smith, 1978; in mammalian C nerve fiber, Scriven, 1981; in pancreatic β-cell, Chay & Keizer, 1983).

Model II ("Five-state model"). According to this scheme, transitions among states of the C channel occur at rates that are comparable to that of Ca concentration change and are functions of Ca and voltage. I have adopted a linear five-state model, similar to those used to describe C channel activation in rat myotubes (Magleby & Pallotta, 1983), in which two Ca ions must bind to the channel to open it, and a third Ca can then bind to prolong the opening:

(S1) $$C \underset{k_{-1}}{\overset{k_1}{\rightleftharpoons}} CaC \underset{k_{-2}}{\overset{k_2}{\rightleftharpoons}} Ca_2C \underset{\alpha_c}{\overset{\beta_c}{\rightleftharpoons}} Ca_2O \underset{k_{-3}}{\overset{k_3}{\rightleftharpoons}} Ca_3O$$

state: 1 2 3 4 5

C, CaC, Ca_2C represent closed channel states with 0, 1, or 2 Ca bound, while Ca_2O and Ca_3O are open states with 2 or 3 Ca bound. Each transition, other than the open-closed transition, is characterized by a Ca dissociation constant, K_i. The voltage dependence of these transitions derives from the assumption that Ca binds to a site within the transmembrane electric field (Moczydlowski & Latorre, 1983; Gorman & Thomas, 1980), making the effective dissociation constant a function of membrane

voltage:

(14) $$K_i(V) = K_i(0)\cdot\exp(\delta_i zFV_m/RT)$$

$K_i(0)$ is the dissociation constant of the ith binding site at 0 transmembrane voltage, δ_i is the fraction of the electric field "felt" by Ca at the ith binding site, and z, F, R, and T have their usual meanings. These dissociation constants are related to the forward and reverse rate constants k_i and k_{-i} by

(15) $$K_i\cdot[Ca] = k_{-i}/k_i$$

The closing rate constant, α_c, is also expressed as a function of voltage:

(16) $$\alpha_c = \alpha_c(0)\cdot\exp(-V_m/V_a)$$

$\alpha_c(0)$ is the closing rate constant at 0 mV membrane potential, V_m is membrane potential, and V_a is a voltage used to express the voltage dependence of α_c.

The change in occupancy of each state with time is described by a differential equation, assuming mass-action kinetics:

(17a) $$dP_1/dt = k_{-1}P_2(t)-k_1P_1(t)$$

(17b) $$dP_2/dt = k_1P_1(t)+k_{-2}P_3(t)-(k_{-1}+k_2)P_2(t)$$

(17c) $$dP_3/dt = k_2P_2(t)+\alpha_cP_4(t)-(k_{-2}+\beta_c)P_3(t)$$

(17d) $$dP_4/dt = \beta_cP_3(t)+k_{-3}P_5(t)-(\alpha_c+k_3)P_4(t)$$

(17e) $$dP_5/dt = k_3P_4(t)-k_{-3}P_5(t)$$

where $P_i(t)$ is the probability that the channel is in state i at time t. The summed occupancy of the two open states at any given time t gives the probability that the channel is open. Therefore

(18) $$G_c(t) = \widetilde{G}_c\cdot(P_4(t)+P_5(t))$$

For both models I and II, current through open C channels is assumed to be ohmic, yielding

(19) $$I_c(t) = G_c(t) \cdot (V_m(t) - E_c)$$

where E_c is the equilibrium potential for C current.

IV. Leakage conductance

Leakage conductance is assumed to be independent of voltage and time:

(20) $$I_L(t) = G_L \cdot (V_m(t) - E_L)$$

where G_L is leakage conductance and E_L is the leakage current's equilibrium potential.

Model predictions of ionic currents under voltage clamp

The values of parameters in models I and II were varied to provide the best fits to I_{Ca} and I_c recorded in the same cell at voltages of -60 to -30 mV.

Model I. Equations used in model I predictions are listed below for reference:

(7) $$m(t) = m_{inf} \cdot (1 - \exp(-t/\tau_m))$$

(5) $$I_{Ca}(t) = \bar{G}_{Ca} \cdot m^3(t) \cdot (V_m - E_{Ca})$$

(12) $$d[Ca]/dt = U \cdot I_{Ca}(t)/(zFC_{vol}\sigma) - K_s \cdot [Ca](t)$$

(13) $$G_c(t) = \bar{G}_c/(1 + K_d/[Ca]^n)$$

(19) $$I_c(t) = G_c(t) \cdot (V_m - E_c)$$

First m_{inf} and τ_m were varied to fit I_{Ca} at each voltage. Using values of the I_{Ca} fit at each time point, equation (12) was integrated numerically with a fourth-order Runge-Kutta method (step size of 0.1 msec) to provide the value of [Ca] at each time point for equation (13). σ, K_s, G_c, K_d, and n were varied to provide the best description of I_c at -30

mV. These values were then used to predict I_c at the other voltages.

Model II. Equations used in Model II are identical to those of Model I, except in the form of $G_c(t)$; equation (13) is replaced by:

(17a) $$dP_1/dt = k_{-1}P_2(t)-k_1P_1(t)$$

(17b) $$dP_2/dt = k_1P_1(t)+k_{-2}P_3(t)-(k_{-1}+k_2)P_2(t)$$

(17c) $$dP_3/dt = k_2P_2(t)+\alpha_cP_4(t)-(k_{-2}+\beta_c)P_3(t)$$

(17d) $$dP_4/dt = \beta_cP_3(t)+k_{-3}P_5(t)-(\alpha_c+k_3)P_4(t)$$

(17e) $$dP_5/dt = k_3P_4(t)-k_{-3}P_5(t)$$

(18) $$G_c(t) = \bar{G}_c \cdot (P_4(t)+P_5(t))$$

I_{ca} was fit at all voltages as for model I, but equations (8) and (9) were used to compute α_m and β_m at each voltage; these values were used to calculate m as a function of time, using

(6) $$dm/dt = \beta_m \cdot (1-m(t)) - \alpha_m \cdot m(t)$$

This system of seven differential equations was solved numerically with a FORTRAN subroutine, MODDEQ, written by Kiku Matsumoto at Caltech. This subroutine uses a Runge-Kutta-Gill method to compute starting values and an Adams-Moulton method for integration. A step size of 10 μsec was used, as further decreases in step size caused no change in the solution. Procedures used to fit I_c are described in the text.

Model predictions of membrane potential under current clamp

Assuming that the hair cell is isopotential, the total membrane current must equal the sum of capacitive and ionic currents:

(22) $$I_m(t) = C_m \cdot dV_m/dt+G_{ca}(t) \cdot (V_m-E_{ca})+G_c(t) \cdot (V_m-E_c)+G_L \cdot (V_m-E_L)$$

where I_m is total membrane current, C_m is membrane capacitance, and all other terms are as previously described. Under current clamp conditions

I_m is simply equal to the applied clamp current, I_{app}. Substitution and rearrangement of equation (21) yields

(23) $$dV_m/dt = -1/C_m \cdot [G_{ca}(t) \cdot (V_m - E_{ca}) + G_c(t) \cdot (V_m - E_c) + G_L \cdot (V_m - E_L) - I_{app}]$$

Equation (23) was added to the system of differential equations (6,12,and 17a-e), equations (10), (11), and (16) were included to provide values of α_m, β_m, and α_c at each value of voltage, and the entire system solved with MODDEQ as described above.

RESULTS

The results will be presented in three parts. Part One is a characterization of voltage oscillations in current- clamped hair cells and of whole-cell Ca and Ca-activated K currents under voltage clamp. Part One ends with an attempt to describe I_c using model I (the "Michaelis-Menten model"). In Part Two, experimental data on the activation of Ca-activated K channels in excised patches are presented which support the five-state C-channel gating scheme of model II. Part Three summarizes the data used to constrain the values for the parameters of model II and describes the adjustment of values for the remaining free parameters to fit whole-cell C currents under voltage clamp. The model's predictions of voltage oscillations under current-clamp conditions are then compared with the experimental results of Part One to test the sufficiency of I_{Ca}, I_c, and I_L in producing electrical resonance in the hair cell.

Part One: Whole-cell experiments

Nature of electrical resonance in hair cells

As was demonstrated in Chapter 1, electrical resonance in the hair cell is revealed by damped membrane-potential oscillations upon application of depolarizing current steps. The oscillatory response to this simple current-step stimulus is a convenient indicator of the properties characterizing the cell's tuned resonance, namely, frequency and damp-

ing. The frequency and damping of the oscillations vary with the magnitude of the applied current; this dependence is illustrated in the experiment of Figs. 2 and 3, which show the oscillatory responses of a cell to a series of current clamp steps from 125 to 1000 pA. Depolarization increased the oscillation frequency in this cell from about 93 Hz at the resting potential of -49 mV, to 240 Hz at -41 mV (Fig. 3A). The frequency at resting potential, following the current step, is largely independent of the size of the preceding current step; it indicates the cell's "natural" resonant frequency (Crawford & Fettiplace, 1981a). For small current steps the frequency is a steep function of membrane potential (f/V slope = 39 Hz/mV), but at higher current it levels off to a value approaching 250 Hz. This asymptotic behavior was consistently observed in all cells that were examined.

Damping of the voltage oscillations leads to an exponential decay of their amplitude with time (Fig. 2B). In their analysis of similar phenomena in hair cells from the turtle's cochlea, Crawford and Fettiplace (1981a) recognized this type of electrical response as that of a damped harmonic oscillator. Using this analogy one can express the sharpness of electrical tuning in terms of a "quality factor," Q_e. For a harmonic oscillator, Q is a measure of the energy stored vs. energy dissipated, per cycle; a high Q denotes high sharpness of tuning. I will express tuning in terms of a Q value rather than a damping factor, since this facilitates comparisons of the tuning properties of bullfrog hair cells with those of hair cells and nerve fibers in other preparations, for which Q's are often used. I refer to the quality factor as Q_e, or electrical quality factor, to distinguish it from acoustical tuning sharpness, which is also often expressed in terms of a Q value. Q_e can

Figure 2. Electrical resonance in a solitary hair cell. *A*, Voltage responses to a series of 50-msec depolarizing current-clamp steps (holding current = 0 pA, resting potential = -49 mV). The values of the current steps are shown to the right of each trace. Note that oscillation frequency during the current step increases with depolarization. The frequency at resting potential, following the current step, is independent of the value of current during the step. For this cell, the frequency at resting potential, termed the natural resonant frequency, was 93 Hz. The damping of the oscillations increased with depolarization for current steps higher than 125 pA in this cell. *B*, Response to a 375-pA step (from *A*) showing the method used to measure steady-state voltage (V_{s-s}), oscillation frequency (f), and electrical quality factor (Q_e). A line is fit by eye to the midpoint of the oscillations to indicate V_{s-s}. Next, cursors are positioned an integral number of oscillation cycles apart, and the average frequency between them is calculated to give f. Finally, a curve decaying exponentially from the first cursor to V_{s-s} is fit by eye to the oscillation peaks. Q_e is calculated from f and the time constant of this exponential (τ_e) by equation (23). Cell 60; repetition interval = 1 sec; sampling interval = 0.4 ms; Internal = K aspartate; External = standard saline. Averages of 3 responses.

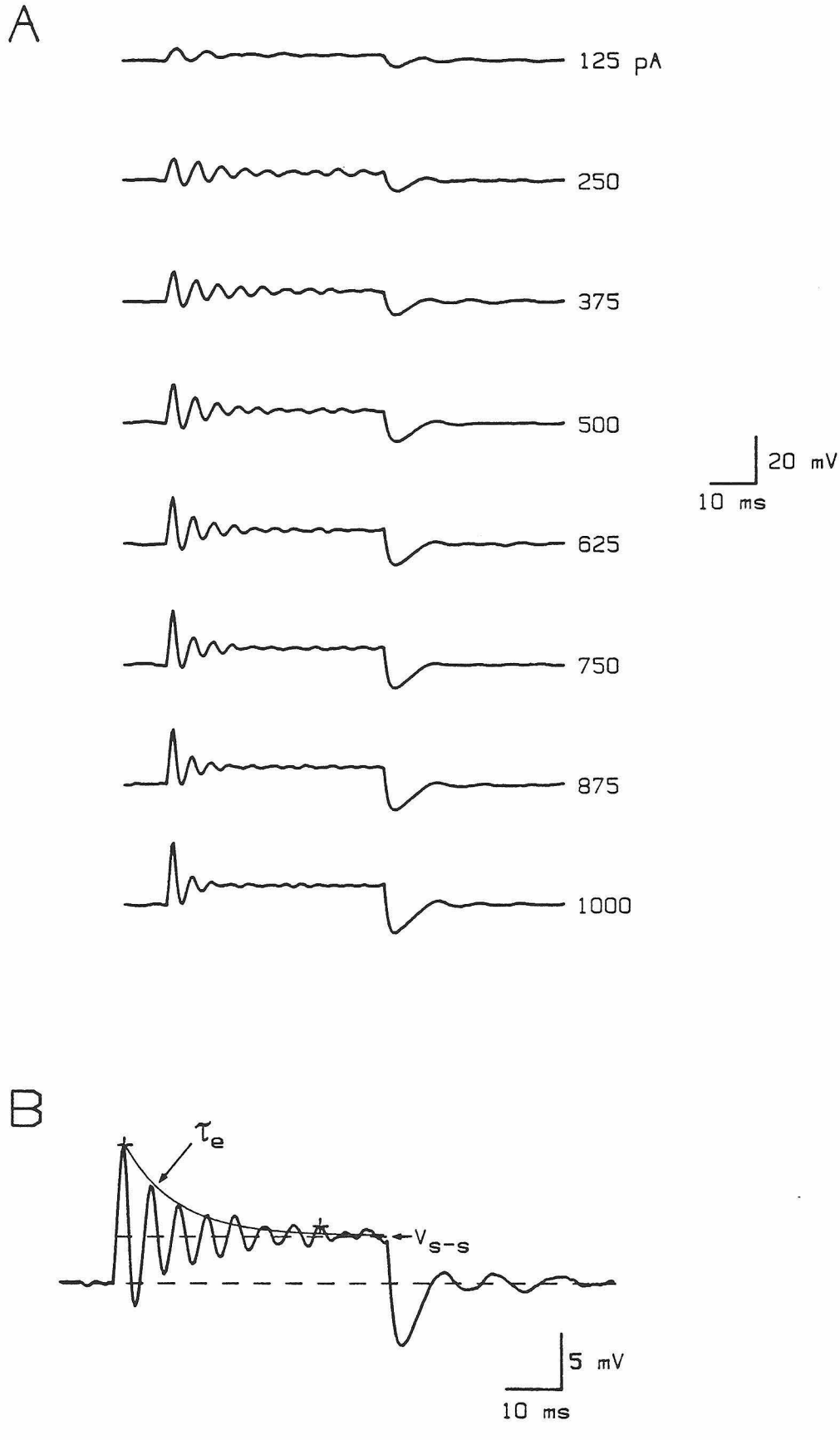
A
125 pA
250
375
500
625
750
875
1000
20 mV
10 ms
B
τ_e
V_{s-s}
5 mV
10 ms

Figure 3. Change in electrical resonance properties with depolarization. These data were derived from Fig. 2 using the method of analysis outlined in the caption of Fig. 2B. Values of membrane potential refer to steady-state voltage measure during the current step. *A*, Oscillation frequency increases with depolarization from resting potential. An exponential function, $f = 250-212 \cdot \exp(-(V+50)/3.57)$, has been superimposed on the data. Near the resting potential the frequency was a steep function of voltage (f/V slope = 39.1 Hz/mV), but at higher voltages it approached an asymptotic value of about 250 Hz. *B*, The sharpness of tuning, represented by the quality factor Q_e, reached its highest value at a voltage about 3 mV positive to the resting potential. The decrease in Q_e above this voltage was due to an increase in oscillation damping.

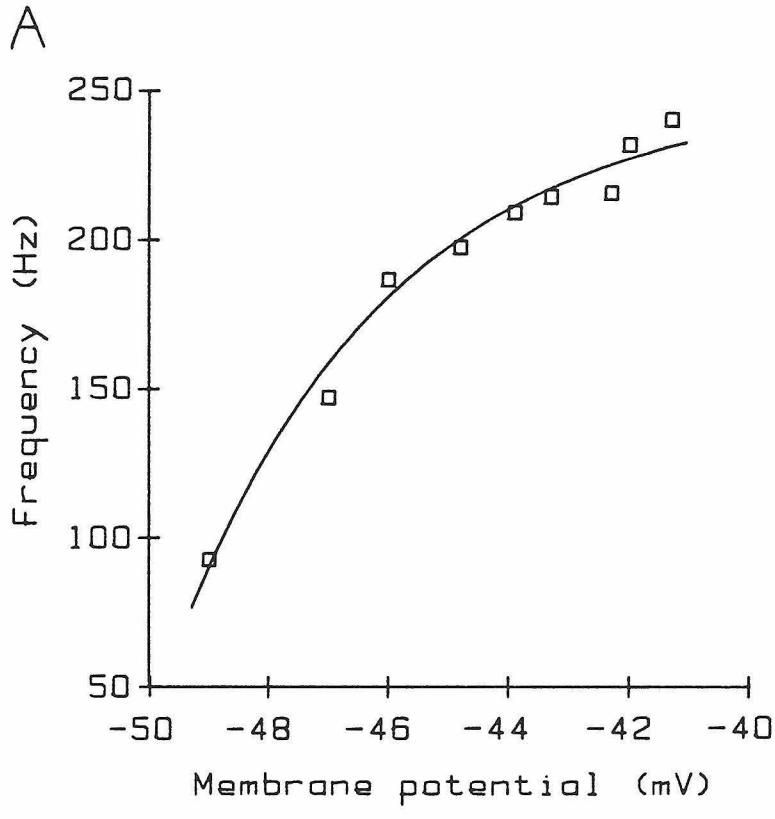
A
250
200
150
100
50
Frequency (Hz)
-50
-48
-46
-44
-42
-40
Membrane potential (mV)

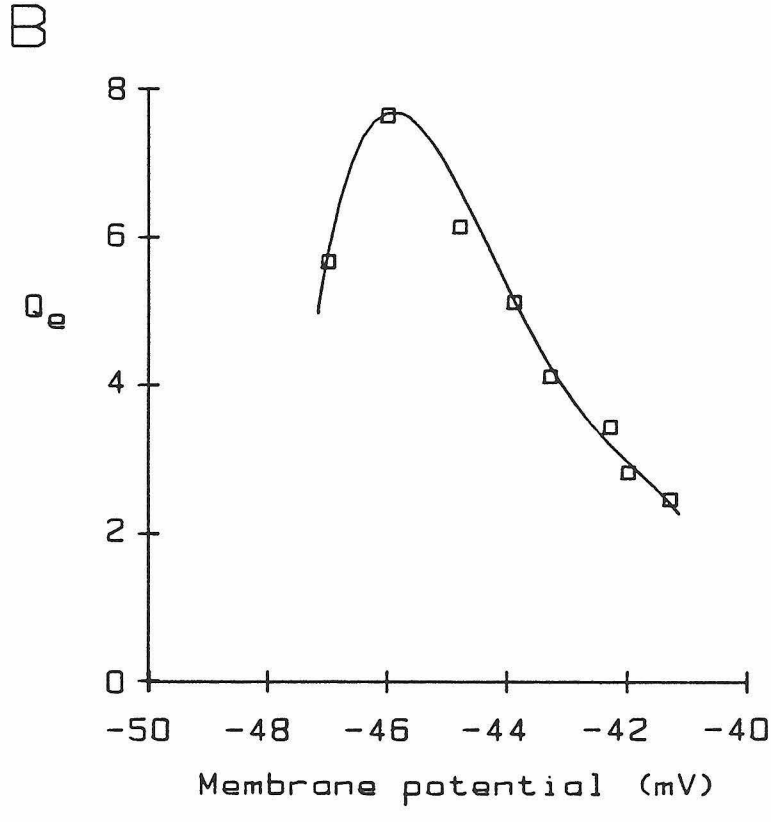
B
8
6
4
2
0
Q_e
-50
-48
-46
-44
-42
-40
Membrane potential (mV)

be calculated from measurements of the frequency and damping of current-induced oscillations by the expression

(24) $$Q_e = [(\pi f \tau_e)^2 + 0.25]^{1/2}$$

where f is the oscillation frequency and τ_e is the time constant of the exponential decay of oscillations induced by a small step of current (Crawford & Fettiplace, 1981a). The methods used to measure f and τ_e are described in the legend to Fig. 2. Oscillation damping appears to increase with depolarization (Fig. 2A); in terms of Q_e, the sharpness of tuning is a bell-shaped function of voltage, reaching a maximum value at potentials slightly positive to resting potential (Fig. 3B). Peak Q_e values ranged from the unmeasurably small to greater than 10. To some extent, Q_e must reflect the intactness of a cell's membrane and its ionic conductances, for Q_e always decreased with time during whole-cell recordings, during which period the leakage conductance increased and both Ca and C conductances decreased under voltage clamp (see Methods).

To assess the possible involvement of Ca, C, and A conductances in generating electrical resonance, I analyzed oscillatory activity under conditions that interfere with one or more of these conductances. In the experiment illustrated in Fig. 4, a single hair cell was clamped to a series of 8 steps of depolarizing current and its voltage responses recorded as it was passed through four external solutions. A common difficulty with these solution exchange experiments was rundown of the resonance mechanism, i.e., a decrease in oscillation frequency and increase in oscillation damping with time; this particular experiment was chosen because the oscillations evoked after returning to standard saline at the end of the experiment (Fig. 4E) were similar to those at the start (Fig. 4A). In seven other cells I observed effects qualitatively similar

to the ones shown here, but rundown precluded quantitative analysis.

Exposure to 1 mM TEA, which blocks about 50% of the cell's C conductance, alters both its resting potential and electrical resonance properties. It depolarized the cell in Fig. 4 by 3 mV, indicating that C channels are partially activated at the normal resting potential. Depolarization is expected from the TEA-induced decrease in outward current through these channels; as the membrane depolarizes, I_{Ca} increases until intracellular Ca and membrane voltage are high enough to activate a higher level of I_C that balances the increased I_{Ca}. In this way the new resting potential is established. TEA inhibits electrical resonance behavior by decreasing the frequency and increasing the damping of the voltage oscillations. TEA's effect on frequency is achieved through lowering the dependence of oscillation frequency on voltage, without noticeably changing the natural resonant frequency observed at voltages close to resting potential. In Fig. 5A, 1mM TEA reduced the f/V slope near resting potential from 21 to 7 Hz/mV. In addition, the increased damping caused by TEA acts to reduce the sharpness of tuning (Fig. 5B). Q_e was decreased from its control range of 4 to 8, to a range of 2 to 4 for the series of applied currents. As in standard saline, however, Q_e reached a peak value several millivolts positive to the resting potential.

Lowering external Ca to 0.5 mM, with replacement by Mg, also affects both resting potential and electrical resonance properties. In voltage clamp experiments, this condition diminishes both the Ca and C conductances; at all test voltages, I_{Ca} is lowered to about 25% of its value in standard saline (4mM Ca), while I_C is decreased, and its activation slowed, by an amount dependent on the test voltage. The effects

Figure 4. Effects of TEA, low Ca, and 4-AP on membrane-potential oscillations. Each panel shows the responses to a series of eight depolarizing current clamp steps delivered from a holding current of 0 pA. The current step values are indicated to the right of traces in *E*. External solutions were changed in the order shown, from *A* to *E*. *A*, Standard saline (control). Resting potential (RP)=-64 mV. Depolarization evoked voltage oscillations similar to those shown in Fig. 2. *B*, 1 mM TEA saline (RP=-61 mV). This concentration of TEA blocks about 50% of the hair cell's C current in voltage-clamp experiments; here, under current clamp, it degraded the cell's resonance behavior by decreasing the frequency and increasing the damping of oscillations. *C*, 0.5 mM Ca saline (RP=-55 mV). Under voltage clamp, this condition lowers I_{Ca} to about 25% of its normal size, and decreases I_C amplitude and activation rate by an amount dependent on membrane potential. Oscillation frequency was relatively unaffected, but damping was increased. *D*, 10 mM 4-AP saline (RP=-62 mV). This concentration of 4-AP blocks the A current in hair cells but had no easily discernible effect on the oscillations. *E*, Return to standard saline (RP=-64 mV). The oscillation response returned to its original form recorded at the start of the experiment (in *A*).

Overall, conditions that interfere with either or both of I_C and I_{Ca} (TEA, low Ca) diminish the resonance, while the treatment that blocks I_A (4-AP) has little or no effect. Cell 3; repetition interval = 650 ms; sampling interval = 0.4 ms; Internal = K aspartate. Averages of two to four responses.

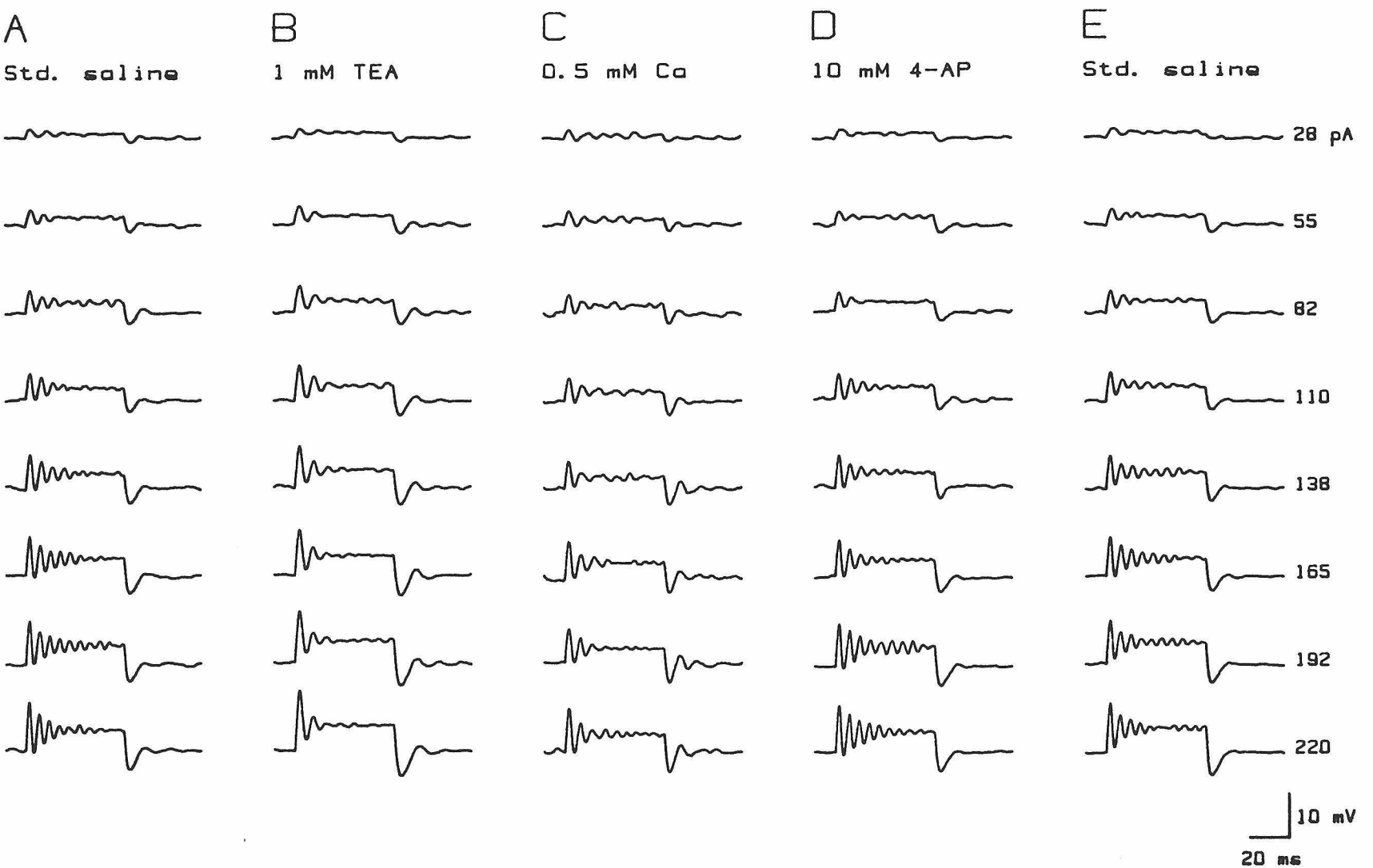
A
Std. saline
B
1 mM TEA
C
0.5 mM Ca
D
10 mM 4-AP
E
Std. saline
28 pA
55
82
110
138
165
192
220
10 mV
20 ms

Figure 5. Effects of TEA, low Ca, and 4-AP on electrical resonance properties. Experiment of Fig. 4; the data shown here are only from traces for which reliable estimates of f or Q_e could be made. External solutions: □: standard saline; ◇: 1 mM TEA saline; △: 0.5 mM Ca saline; ▽: 10 mM 4-AP saline; ■: return to standard saline. *A*, Effects of treatments on oscillation frequency measured at different steady-state voltages. In standard saline and 4-AP, oscillation frequency increased most rapidly for small depolarizations from resting potential (f/V slope = 20.5 Hz/mV) and appeared to approach a limiting value above 200 Hz at higher voltages. An exponential function, $f = 213-245 \cdot \exp(-(V+65)/2.04)$, has been superimposed on the standard saline data and is shifted along the V axis by 2.4 mV to fit the 4-AP results. In low Ca, frequency increased at a maximum rate of 31.7 Hz/mV and did not approach a limiting value for the range of current steps applied. TEA had the most dramatic effect on frequency, lowering its range by decreasing the sensitivity of frequency to voltage (f/V slope = 6.7 Hz/mV). *B*, Effects of treatments on the sharpness of electrical tuning at different steady-state voltages. In standard saline and 4-AP, electrical quality factor (Q_e) increased with depolarization, reaching a peak value about 4 mV positive to resting potential. In low Ca, Q_e also increased with depolarization but did not reach a maximum for this range of applied currents; at all but the highest current step level, low Ca decreased Q_e relative to its value in standard saline or 4-AP. TEA lowered the range of Q_e values dramatically; under this condition Q_e peaked about 3 mV positive to resting potential.

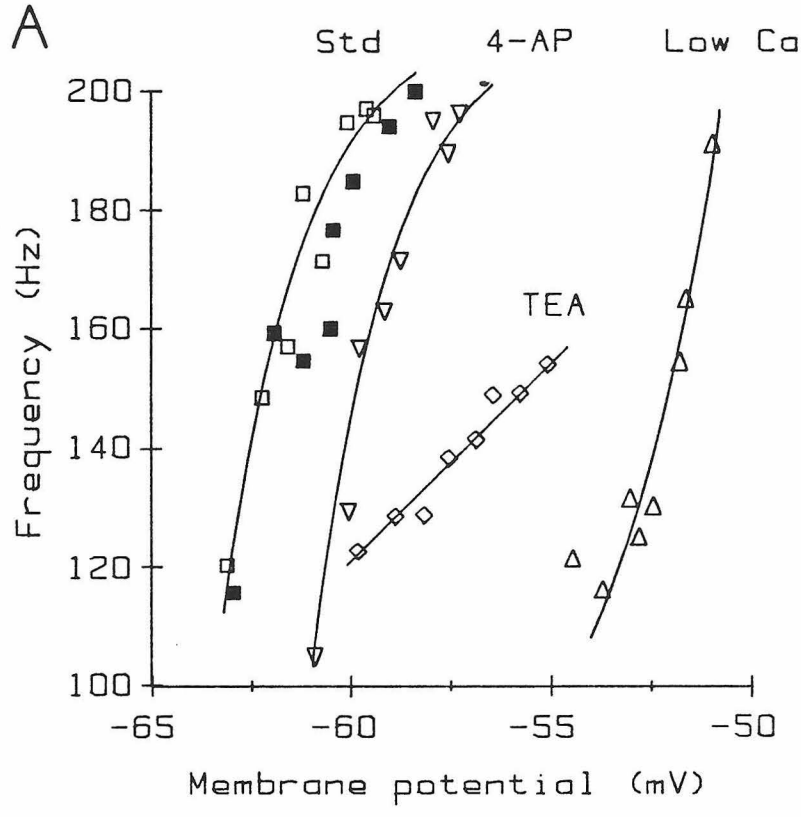
A
Std
4-AP
Low Ca
TEA
200
180
160
140
120
100
Frequency (Hz)
-65
-60
-55
-50
Membrane potential (mV)

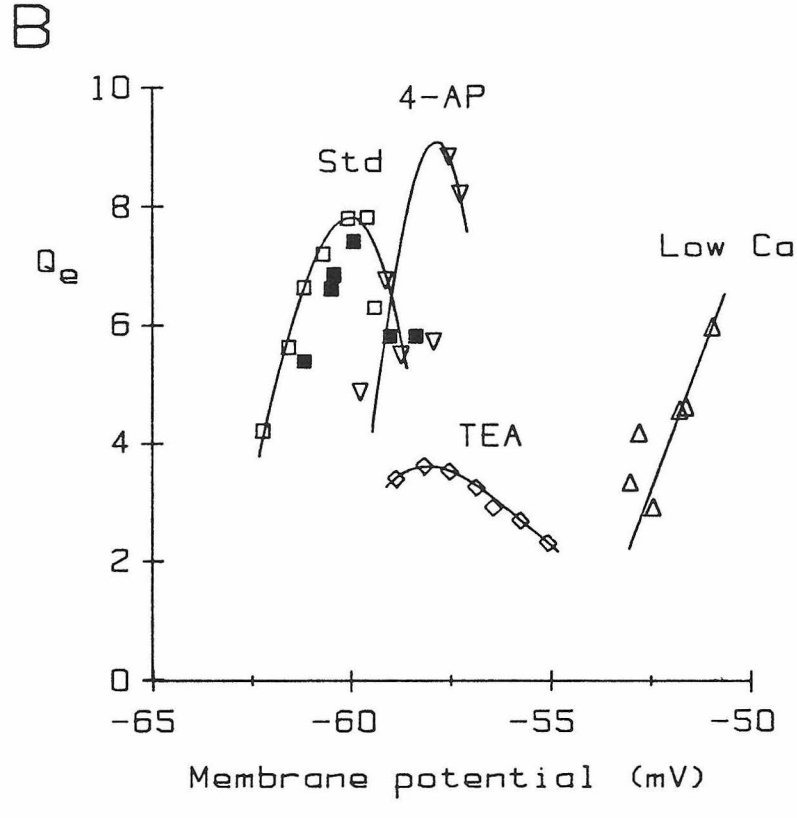
B
4-AP
Std
Low Ca
TEA
10
8
6
4
2
0
Qe
-65
-60
-55
-50
Membrane potential (mV)

on I_c are most extreme close to its threshold activation potential and diminish with depolarization. At -36 mV, the steady-state level of I_c is reduced to 38% of its control value, and its activation is greatly slowed; at resting potential, the fractional decrease in magnitude would be even greater. In the current-clamp experiment considered here, lowering Ca depolarized the cell by 9 mV, which suggests that some Ca channels are also open at resting potential. The depolarization at first seems paradoxical; lowering the inward current through open Ca channels by lowering external Ca might be expected to hyperpolarize the cell. This prediction would apply if the outward K current in these cells were solely voltage-dependent. However, because the cell's dominant K conductance, G_c, is activated by internal Ca as well as by voltage, a decrease in Ca influx causes a decrease in I_c, which acts to depolarize the cell. Net depolarization implies that the absolute decrease in I_c is greater than that of I_{ca}, such that a net inward current results; the cell depolarizes until I_c rises enough to balance the sum of inward currents I_{ca} and I_L, thereby reaching the new resting potential. Lowering external Ca also appeared to shift the oscillation frequency/voltage relation along the voltage axis by about +9 mV, with little change in the f/V slope (Fig. 5A). Low external Ca affected the resonance primarily by lowering the cell's Q_e values in the current range studied (Fig. 5B). Thus, the main effect of lowered Ca is a decrease in the hair cell's sharpness of tuning, without much change in the frequency to which it is tuned.

Addition of 10 mM 4-AP to the external medium caused a depolarizing shift of about 2 mV in resting potential and all features of the oscillations (Fig. 5). The source of the shift remains unexplained: it was probably not due to a block of the A current because at these poten-

tials, about 90% of the A conductance was inactivated, and measurable I_A activation occurs only at voltages more positive than -45 to -40 mV (results of eight cells). Also, since no measurable junction potential exists between the 4-AP saline and standard saline, the shift was not likely to be an artifact. One possible explanation (as yet untested) is that 10 mM 4-AP blocked I_{Ca} slightly, and the shift occurred by the mechanism proposed above for lowered external Ca.

In summary, treatments that interfere with the Ca or C conductances (TEA or low Ca) depolarize the hair cell, indicating that these two conductances help determine the cell's resting potential. Also, only these treatments, and not one which blocks I_A (4-AP), substantially affect the electrical resonance properties of the cell, suggesting that only the Ca and C conductances contribute to the resonance mechanism.

Separation of Ca and C currents under voltage clamp

When 4-AP is present to block I_A, depolarization of hair cells to potentials above -60 to -50 mV elicits a combination of inward Ca current and outward C current. Because TEA blocks I_C but not I_{Ca} (Lewis & Hudspeth, 1983a), this drug may be used to separate the two currents in a single cell, as illustrated in Fig. 6. In the presence of 10 mM 4-AP, depolarization to -30 mV elicited a combination of I_{Ca} and I_C (upper left trace). With 20 mM TEA added externally to block I_C, the same depolarization elicited only I_{Ca} (lower left trace). Subtracting the second response from the first removes the contribution of I_{Ca} to the total current, leaving only I_C (right trace). Ca and C currents produced by a series of seven depolarizing voltage steps in this cell were separated

Figure 6. Meaurement of Ca current and Ca-activated K current from a single cell. Pictured here are the ionic currents evoked by a voltage clamp step from -70 mV, the holding potential, to -30 mV, delivered in the presence of 4-AP saline (upper left) or in TEA/4-AP saline (lower left). The lowest trace shows the command voltage. In 4-AP saline, depolarization elicits an early inward current (I_{Ca}), followed by a larger outward current (I_C). Addition of TEA blocks I_C, leaving I_{Ca}. Subtracting the current elicited in the presence of TEA from that produced in its absence leaves only current that was blocked by TEA (in this case, I_C); this result is shown at the right. 4-AP was included in all solutions to block the portion of I_A that was not inactivated at these potentials, so that a reasonably pure Ca current could be measured in the presence of TEA. The dotted lines indicate the baseline current level. Cell 36; repetition interval = 0.6 sec; sampling interval = 100 μsec; internal = K aspartate. Averages of two responses.

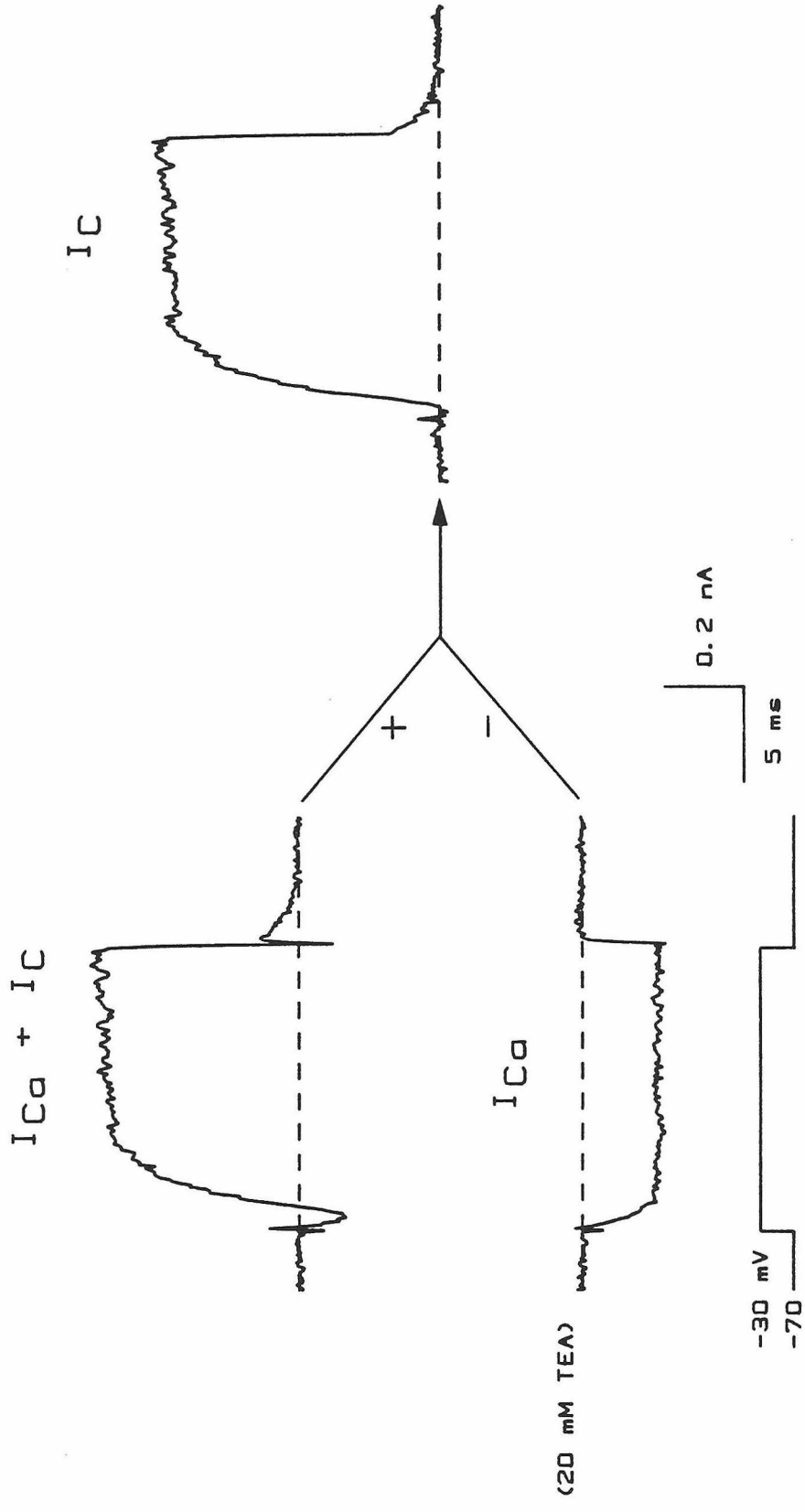
I_C
$I_{Ca} + I_C$
I_{Ca}
+
−
0.2 nA
5 ms
-30 mV
-70
(20 mM TEA)

from one another using the TEA-subtraction protocol, and the results are displayed in Figs. 7 (I_{Ca}) and 9 (I_C). These data are used in the remainder of this chapter to constrain the values for parameters in models I and II.

Kinetic description of whole-cell Ca current

The activation kinetics of the voltage-dependent Ca current in hair cells are well described by a third-order (m^3) Hodgkin-Huxley scheme with no inactivation (Hodgkin & Huxley, 1952; see Methods). In Fig. 7A, predictions of this kinetic scheme are superimposed on the observed Ca currents evoked by a series of depolarizing voltage-clamp steps. While the Hodgkin-Huxley model fits I_{Ca} activation quite well, the observed current appears to lag behind the model in returning to zero at the end of the voltage step. I have observed a similar lag in all of the hair cells I have examined; this is an experimental artifact which probably has several sources. First, the sampling interval in these experiments (100 μsec) was close to the time constant of Ca tail current decay, so that by the time the computer sampled the first data point after the voltage had returned to the holding potential, the tail current had decayed significantly. This explains why a fast increase in inward I_{Ca} is not seen immediately after repolarization, when the driving force on Ca is suddenly increased. Consistent with this interpretation, recordings of I_{Ca} at an increased time resolution of 40 μsec/point reveal tail currents that initially exceed the steady-state level of I_{Ca} and rapidly decay to zero. The major cause of the lag in I_{Ca} decay was probably caused by the effects of series resistance. The amount of series resis-

tance compensation used in this experiment caused current oscillations at the start and end of the voltage step that could not be cancelled perfectly by leakage subtraction. These residual transients obscured the initial part of the tail current. Also, about 2 MΩ of series resistance was uncompensated, which, given capacitive transients of -3 to -5 nA magnitude at the end of the step, caused a +6 to +10 mV error in membrane potential during the early part of the tail current. Since the closing rate of Ca channels is voltage dependent, the voltage error acted to slow the apparent time course of tail current decay. The Ca current in this cell became activated at potentials positive to -55 mV, as shown by the steady-state current-voltage plot in Fig. 7B.

The steady-state activation parameter, m_{inf}, and activation time constant, τ_m, corresponding to the fitted traces in Fig. 7A are shown at different voltages in Fig. 8A. To estimate m_{inf} at each voltage, the Ca conductance with all Ca channels open, G_{ca}, must be known; G_{ca} was not measured directly in this cell, but was estimated in the following way. First, m_{inf} at -30 mV was estimated from analysis of Ca tail currents in eight cells at higher time resolution (40 μsec/point). At voltages above +20 mV, the peak Ca tail current magnitude in these cells reached an asymptotic level (corresponding to full activation), and the peak tail current following a step to -30 mV was 42% ±6% of this value (indicating 42% activation, or $m_{inf}^3 = 0.42$). This estimate of m_{inf} at -30 mV fixes the magnitude of G_{ca} (see equation (5)). Values of m_{inf} and τ_m were used with equations (8) and (9) to provide estimates for α_m and β_m, the closing and opening rate constants of the m^3 scheme (Fig. 8B). α_m and β_m were approximated by exponential functions of voltage, as described in the legend to Fig. 8. Uncertainty in the estimate for G_{ca} will affect

Figure 7. Voltage-dependent activation of Ca current. *A*, Inward Ca currents evoked by depolarizing voltage steps delivered from a holding potential of -70 mV. The step command voltage in millivolts is indicated to the left of each trace. The bottom trace indicates the time course of the voltage steps. Superimposed on each data trace is the current predicted by a third-order Hodgkin-Huxley scheme which was fitted to each by eye. This kinetic scheme describes the current's activation time course quite well; the apparent lag between the predicted and actual tail currents may be due to the slow sampling rate and to series resistance compensation errors, as discussed in the text. Cell 36; repetition interval = 0.6 sec; sampling interval = 100 μsec; internal = K aspartate; external = TEA/4-AP saline. Averages of two responses. *B*, Steady-state current-voltage relation for the Ca current. Steady-state values of the Ca current from *A* are plotted against command voltage. The Ca current in this cell became significantly activated at potentials more positive than -55 mV.

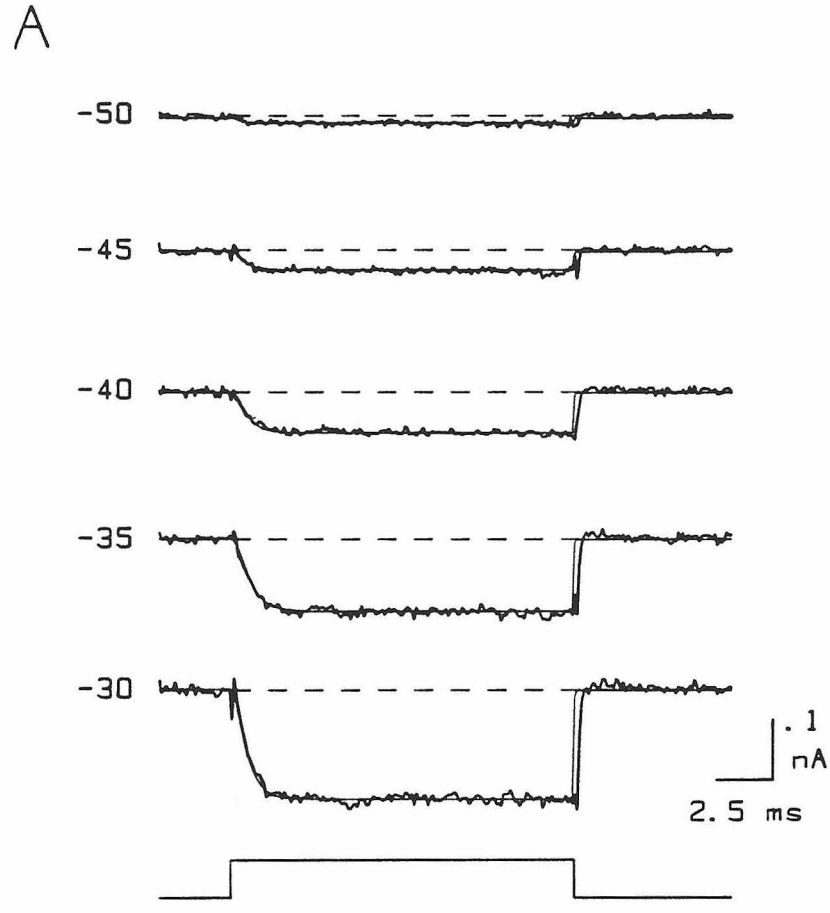
A
-50
-45
-40
-35
-30
.1
nA
2.5 ms

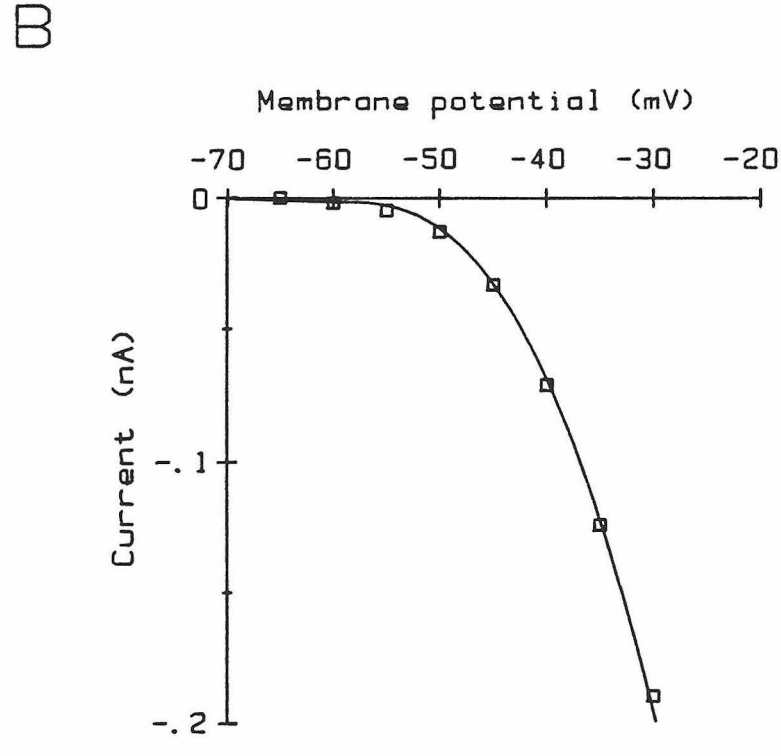
B
Membrane potential (mV)
-70
-60
-50
-40
-30
-20
0
-.1
-.2
Current (nA)

Figure 8. Kinetic description of the Ca current. Experiment of Fig. 7. *A*, Steady-state activation (m_{inf}) and time constant (τ_m) of Ca current as a function of voltage. Filled symbols represent m_{inf} and τ_m values corresponding to the Hodgkin-Huxley model fits shown in Fig. 7A. The level of activation at -30 mV (m_{inf}^3) was set at 0.36, based on the results of Ca tail current experiments; this value gave a maximal Ca conductance, G_{Ca}, of 4.1 nS for this cell. Open symbols are calculated values based on extrapolations of α_m and β_m shown in *B* (activation at these potentials was too slight to permit accurate measurement of m_{inf} or τ_m directly). *B*, Opening (β_m) and closing (α_m) Ca-channel rate constants as a function of voltage. The filled symbols were derived from m_{inf} and τ_m using equations (8) and (9). An exponential curve of the form $\beta_m = \beta_0 \cdot \exp((V_m+V_0)/V_B)+K_B$ was fitted by eye to the filled β_m points; β_0=0.97/sec, V_0=70 mV, V_B=6.2 mV, and K_B=940/sec. The open triangles represent β_m extrapolations using this function. The open symbol values for α_m were calculated from the extrapolated β_m values and m_{inf} measured at the corresponding voltages. An exponential function of the form $\alpha_m = \alpha_0 \cdot \exp(-(V_m+V_0)/V_A)+K_A$ was visually fitted to all of the α_m points; α_0=22800/sec, V_0=70 mV, V_A=8.0 mV, and K_A=510/sec.

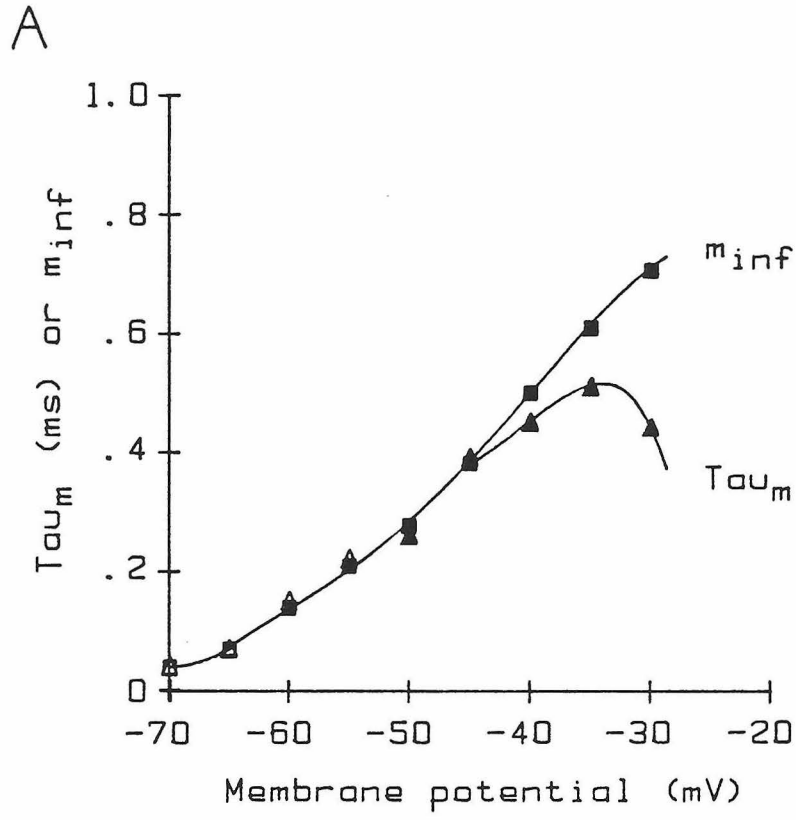
A
1.0
.8
.6
.4
.2
0
Tau$_m$ (ms) or m$_{inf}$
m$_{inf}$
Tau$_m$
-70
-60
-50
-40
-30
-20
Membrane potential (mV)

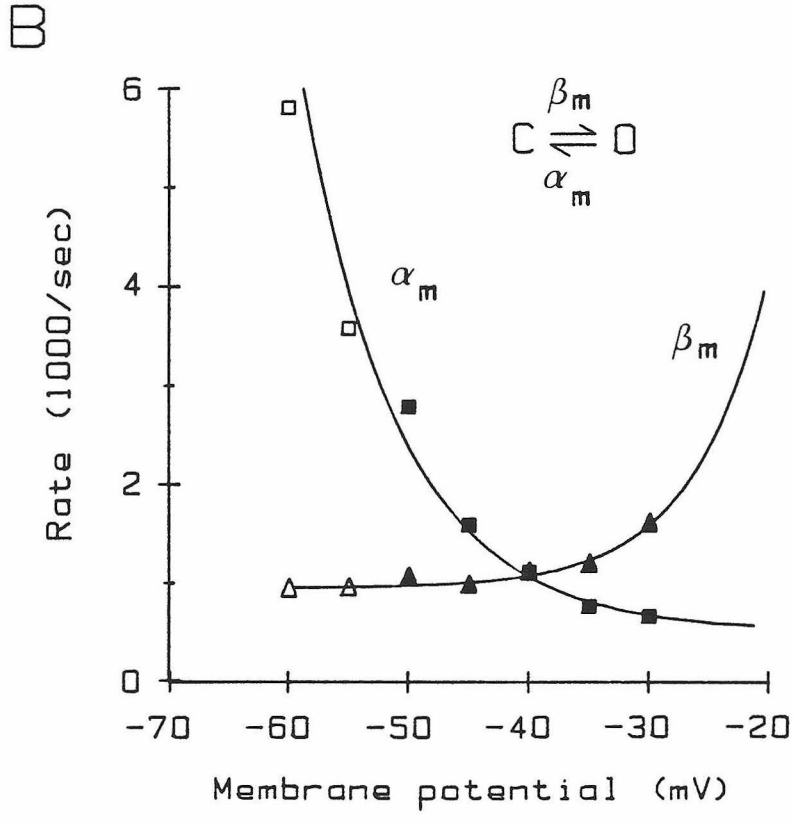
B
6
4
2
0
Rate (1000/sec)
β_m
C ⇌ O
α_m
α_m
β_m
-70
-60
-50
-40
-30
-20
Membrane potential (mV)

the calculated values of α_m and β_m but not their ability to correctly predict the waveform of I_{Ca} in the voltage range studied here. This source of error will only be significant for attempts to predict the behavior of I_{Ca} outside the voltage range of actual observation.

Kinetic description of whole-cell Ca-activated K current (C current)

Fig. 9A shows the C currents elicited by a series of depolarizing voltage clamp steps from -55 to -30 mV (same cell and test voltages as in Fig. 7). A plot of steady-state I_C vs. voltage illustrates that the C current was activated at voltages above -55 mV (Fig. 9B), close to the voltages at which I_{Ca} in the same cell started to become activated (see Fig. 7B). This result is consistent with the dependence of I_C on internal Ca. The C chord conductance, calculated from I_C using a reversal potential of -80 mV and assuming ohmic behavior, increased approximately linearly with voltage above -50 mV. As will be shown later, part of the apparent voltage dependence of G_C results from the intrinsic voltage dependence of C-channel gating, but the majority derives indirectly from the voltage dependence of I_{Ca}, which supplies Ca to activate G_C.

In response to any given voltage step, I_C starts to increase a substantial time following I_{Ca} activation, which is also consistent with the dependence of I_C on internal Ca accumulation. The difference in the onset latencies of I_{Ca} and I_C is illustrated in Fig. 10A, in which the early phases of the two currents have been plotted on an expanded time scale (same cells as Figs. 7 and 9). For each of the voltage steps, I_{Ca} developed first, following a short delay of 200-300 μsec. The activation of I_C occurred only after a comparatively long delay, the length of

Figure 9. Activation of the Ca-activated K current. *A*, Outward C currents (upper traces) elicited by a series of depolarizing voltage steps (lower traces), isolated by the TEA-subtraction protocol illustrated in Fig. 6. *B*, Steady-state and peak tail C currents as a function of step voltage. Steady-state current was measured for the records in *A* as the current level at the end of each voltage step. The C current in this cell was activated at potentials more positive than -50 mV. Peak tail current was estimated as the single exponential extrapolation of tail current back to the time the voltage step ended. Note that, while steady-state I_c was still increasing with depolarization at -30 mV, the tail current magnitude, which is proportional to C conductance, was near an asymptotic value. The Ca current in this cell still increased substantially with depolarization around -30 mV (see Fig. 7), which presumably produced an increasing concentration of intracellular Ca in this voltage range; therefore, the apparent saturation of the C tail current amplitude at voltages close to -30 mV suggests that almost all of the cell's C channels were activated at these voltages in the steady state.

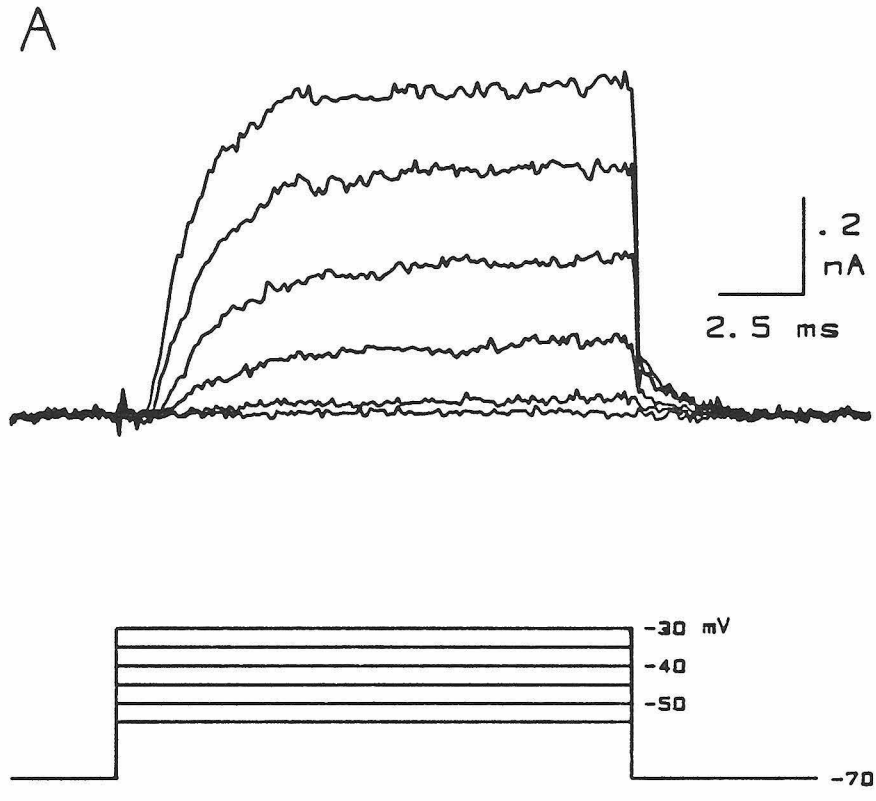
A
.2
nA
2.5 ms
-30 mV
-40
-50
-70

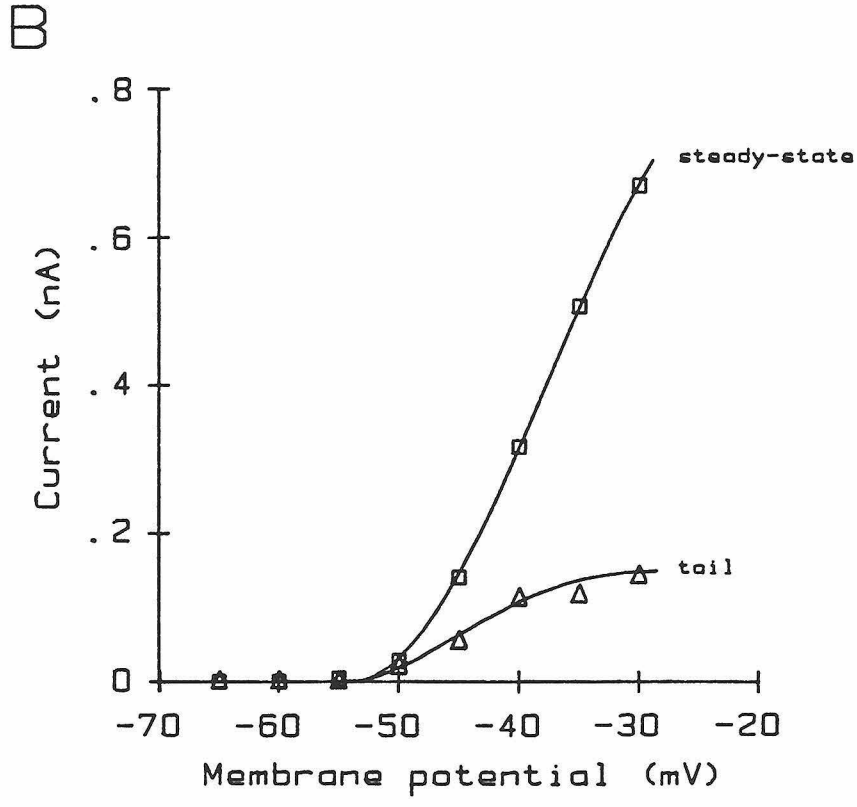
B
.8
.6
.4
.2
0
Current (nA)
steady-state
tail
-70
-60
-50
-40
-30
-20
Membrane potential (mV)

which decreased with increasing depolarization. The onset latencies for I_c in this cell ranged from 1.2 msec at -50 mV to 0.8 msec at -30 mV; these values were typical for all cells studied. After this long delay, I_c increased rapidly: at -30 mV, the current reached 50% of its steady-state value in an additional 0.9 msec. The fast activation kinetics of I_c in the hair cell stand in marked contrast to the sluggish kinetic behavior of C currents in most other preparations. In neurons from the marine molluscs *Tritonia* (Thompson, 1977) or *Aplysia* (Gorman and Thomas, 1980), I_c is still increasing at the end of a 300 msec voltage clamp step. Although the reason for this difference in kinetic behavior is not yet clear, it may be due to differences in the rates at which intracellular Ca loads dissipate (see Discussion). The fast kinetic behavior of the hair cell's C current is also reflected by the time course of C tail current decay. Upon repolarization to -70 mV, I_c decays approximately as a single exponential with a time constant of 1.0 msec (±0.3 msec, n=18), regardless of the size of the preceding depolarization (Fig. 10B). In contrast, the C tail current in molluscan neurons is orders of magnitude slower: in *Helix aspersa* this current decays exponentially with a time constant of 85 msec (Meech & Standen, 1975), while in nudibranchs it can persist up to 30 seconds (Barish & Thompson, 1983).

In a large number of preparations, recent single-channel experiments have shown that the Ca-activated K channel is gated by both membrane potential and intracellular Ca ions (Barrett et al., 1982; Marty, 1981; Wong et al., 1982; Maruyama et al., 1983). It is usually impossible to analyze this dual dependence of C-channel activity quantitatively in whole cells, since internal Ca concentration next to the membrane

Figure 10. Kinetic behavior of the Ca-activated K current. Data from Figs. 7 and 9. *A*, Activation of I_c and I_{ca} shown on an expanded time scale. Command voltages are indicated to the right of each trace; the dotted line indicates the baseline current level. Both I_c and I_{ca} turn on with a sigmoidal time course, but the latency between the start of the voltage step (indicated by the arrow) and a measurable ionic current response was much longer for I_c than for I_{ca} (0.8 to 1.3 ms for I_c; 0.2 ms for I_{ca}). Although I_c had a greater onset latency than I_{ca}, at each voltage the maximum rate of rise of I_c is much greater than that of I_{ca}; at -40 mV, I_c increases by 0.14 nA/ms, while I_{ca} changes by only -.08 nA/ms. Long latency followed by a rapid rise in activation is consistent with the passage of the C channel through multiple closed states before opening (as in scheme (S1)). The differences in activation rates and onset latencies for inward and outward currents are important factors in the generation of electrical resonance in these cells. *B*, Rapid exponential decay of C tail currents. C tail currents produced upon repolarization from -30, -35, -40, and -45 mV to -70 mV (from Fig. 9) are plotted here relative to the initial value of each tail current on a logarithmic scale against time. All of the currents decayed with roughly a single exponential time course (time constant = 1.0 msec), regardless of the level of C-current activation immediately preceding the return to holding potential. The initial rapid phase of the decline is probably an artifact of incomplete R_s compensation.

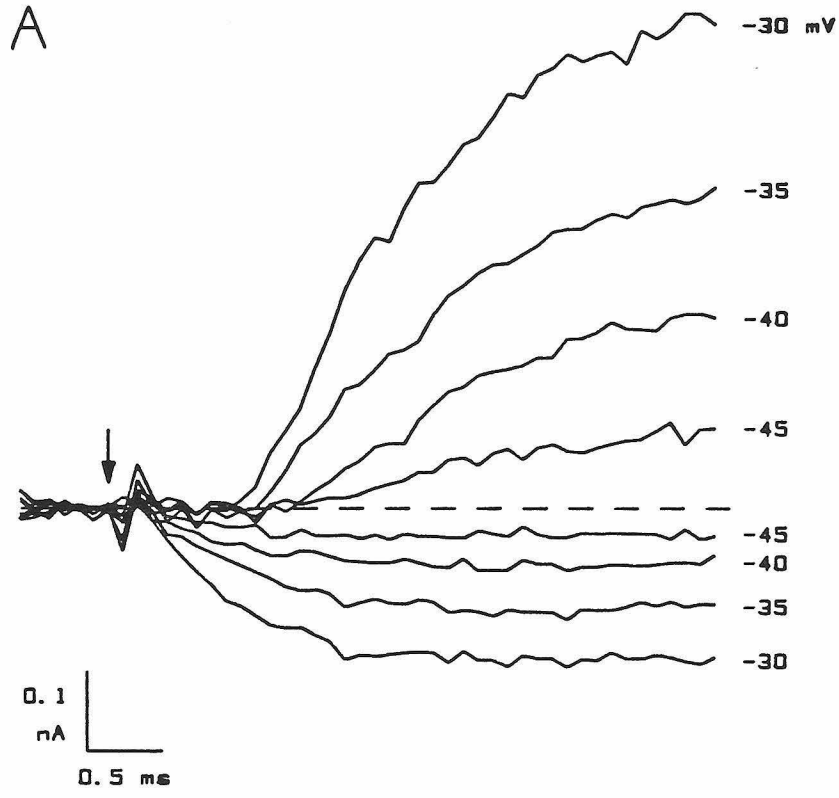
A
-30 mV
-35
-40
-45
-45
-40
-35
-30
0.1
nA
0.5 ms

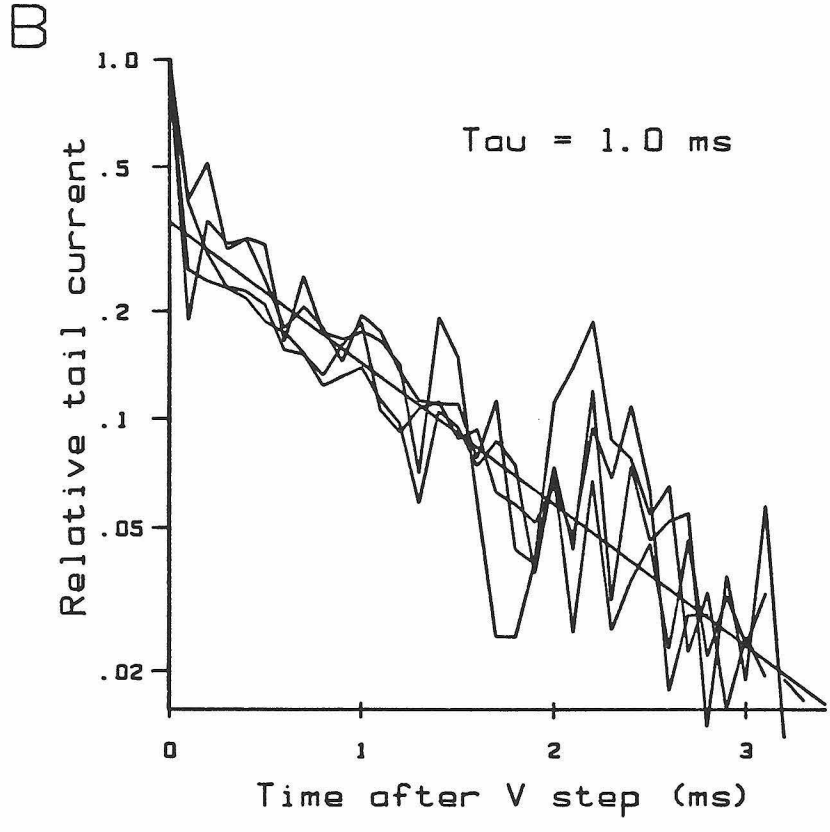
B
Tau = 1.0 ms
Relative tail current
1.0
.5
.2
.1
.05
.02
0
1
2
3
Time after V step (ms)

cannot be controlled or known with certainty. In neurons from *Aplysia* (Woolum & Gorman, 1981), *Helix* (Hermann & Hartung, 1982), and bullfrog sympathetic ganglia (Adams et al., 1982), the *voltage dependence* of I_c kinetic behavior has been investigated by voltage clamping the membrane to different potentials after intracellular Ca injection in the presence of Ca-channel blockers. I performed the converse experiment in hair cells to study the *Ca dependence* of whole-cell I_c kinetics, independently of voltage. These experiments measure the outward current elicited by a constant voltage step in the presence of varying levels of external Ca. Complete removal of external Ca, with or without substitution by Mg, abolishes both I_{Ca} and I_c (Lewis & Hudspeth, 1983a). However, less drastic reduction of external Ca, from 4 to 0.5 mM, lowers I_{Ca} to about 25% of its initial value; the decreased rate of Ca influx under these conditions lowers the rate of I_c activation and its steady-state magnitude (Fig. 11). The effects of Ca influx on I_c kinetics and amplitude are most extreme at voltages close to the potential at which I_c begins to turn on, and diminish with depolarization. For the cell in Fig. 11, the steady-state magnitude of I_c in 0.5 mM external Ca was 38% of its control value (in 4 mM Ca) at -36 mV, 63% at -23 mV, 83% at -9 mV, 86% at +4 mV, and 89% at +18 mV. Similar results are obtained if the influx of Ca is lowered by partially blocking I_{Ca} with 20-50 μm Cd, suggesting that the rate of Ca influx through Ca channels is a major determinant of the kinetic behavior and magnitude of I_c. The dependence of I_c magnitude on Ca influx is easily explained; a lower rate of Ca entry produces a lower level of internal Ca and hence opens a smaller number of C channels. The observed decrease in I_c activation rate, including the increased onset latency, could arise from two sources. First, the opening

Figure 11. Rate of Ca entry affects the time course and magnitude of the Ca-activated K current. This cell was clamped from a holding potential of -90 mV to -23 mV in a saline containing 4 mM or 0.5 mM Ca. Decreasing external Ca from 4 to 0.5 mM lowers I_{Ca} to about 25% of its initial value. As seen here, the decrease in I_{Ca} diminished the steady-state magnitude of I_C reached during the voltage step to 63% of its initial value. In addition, the activation rate of I_C was noticeably slowed; note the increased onset latency for the C current in the presence of low Ca. The decreases in both I_C magnitude and activation rate can be explained by the effect of lowered Ca entry rate on the concentration of internal Ca; in particular, the slowing of activation suggests that C current kinetics are partly controlled by Ca-dependent transition rates among multiple closed C-channel states. Cell 1; sampling interval = 64 μsec; internal = K aspartate; external = standard saline or 0.5 mM Ca saline. Single responses are shown.

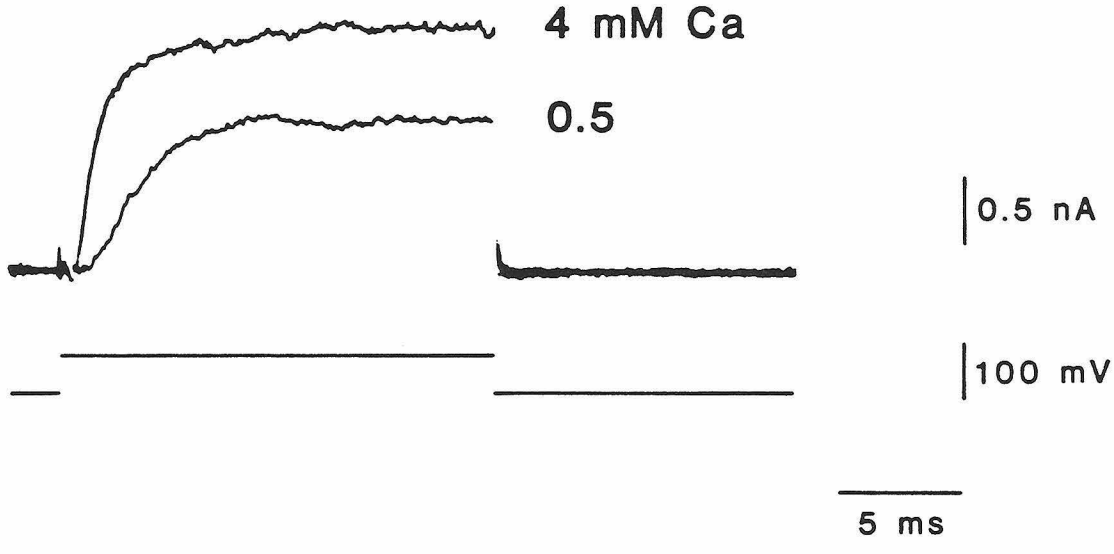
4 mM Ca
0.5
0.5 nA
100 mV
5 ms

of C channels by internal Ca may be cooperative, so that more than one Ca ion must bind to open the channel. Second, the transition rates between C-channel states may be functions of internal Ca concentration. Results of single-channel experiments on C channels in other preparations and in hair cells support both of these hypotheses and are presented in Part Two of the results.

An important constraint on any model which describes the activation of I_c is the fraction of the cell's C channels that are opened by a given voltage clamp step. This open-state probability was estimated by applying the method of ensemble variance analysis (Sigworth, 1980) to the fluctuations in C current observed during whole-cell depolarizations. Macroscopic C currents in response to repetitive voltage-clamp steps to -30 mV were recorded; the results of four such presentations from one cell are illustrated in Fig. 12A. At this amplification, small fluctuations in whole-cell C current are evident; subtracting the mean of eight such responses from these records "isolates" the fluctuations in C current around the mean, and these are shown at higher gain in Fig. 12B. A large increase in current noise is apparent during the voltage step and is presumably caused by the independent, stochastic activity of many C channels. The current variance for each response is simply equal to the square of the fluctuations about the mean. The mean current and variance for 32 depolarizations of this cell are displayed in Fig. 13A. The variance reached a maximum during the rising phase of the mean current. Since the variance should be greatest when half of the channels are open on average, this result indicates that the majority of the cell's C channels were open at -30 mV in the steady state. The variance also increased slowly during the later part of the step; this may have

Figure 12. Microscopic fluctuations in whole-cell C current. *A*, Whole-cell C currents evoked by voltage clamp steps to -30 mV delivered from a holding potential of -55 mV. Four responses of a group of eight consecutive presentations are shown; the bottom trace shows the voltage step. The mean of eight such records was subtracted from each trace to produce the traces shown at 16-fold higher gain in *B*. These data were not corrected for Ca current, as it was too small to contribute a measurable early inward current in this cell. *B*, Microscopic current fluctuations associated with the stochastic gating of C channels. Each trace corresponds to the fluctuations of the trace to its left, in *A*, around the mean. The increase in current fluctuations during the voltage step is evident, and presumably results from the independent, stochastic activity of many C channels. Cell 46; repetition interval = 0.5 sec; sampling interval = 100 μsec; internal = K aspartate; external = standard saline.

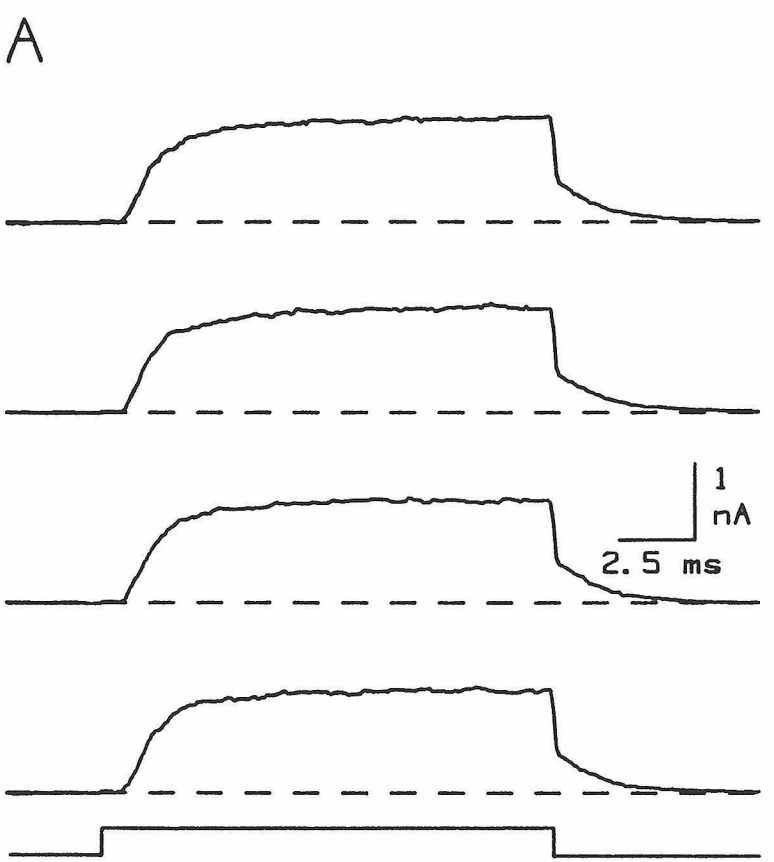
A
1
nA
2.5 ms

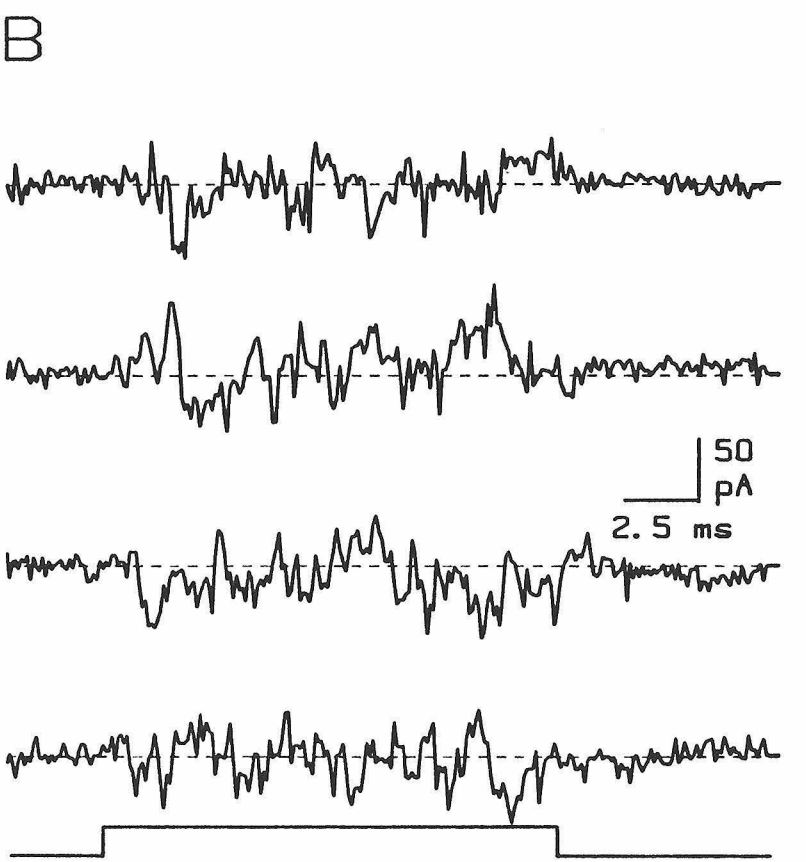
B
50
pA
2.5 ms

Figure 13. Ensemble variance analysis of whole-cell C current. Experiment of Fig. 12. *A*, Mean of 32 macroscopic C current records (top) and the corresponding current variance (bottom). The initial small rise in macroscopic current and variance marks the start of the voltage clamp step; note that the variance increased significantly only as I_c started to become activated, showing that the current fluctuations are due to the activity of C channels rather than Ca channels. The variance reached a peak value during the rising phase of I_c; this indicates that more than half of the cell's C channels were activated at -30 mV in the steady state. A slowly rising component of the fluctuations is evident during the later part of the step, and may have been caused by a small contaminating current. *B*, Current variance as a function of mean macroscopic current. This is a point-by-point plot of the lower trace against the upper trace of *A*. Only the points during the first third of the step have been plotted to exclude the slowly-rising variance component of the later part of the step. A parabola described by equation (3) was fit to the points using a least-squares method, and indicates a single-channel current amplitude of 2.6 pA and a total of 550 C channels in the cell. Dividing the steady-state average I_c by $N \cdot i$ gives the open-state probability at -30 mV in the steady state, or $P_o = 0.96$.

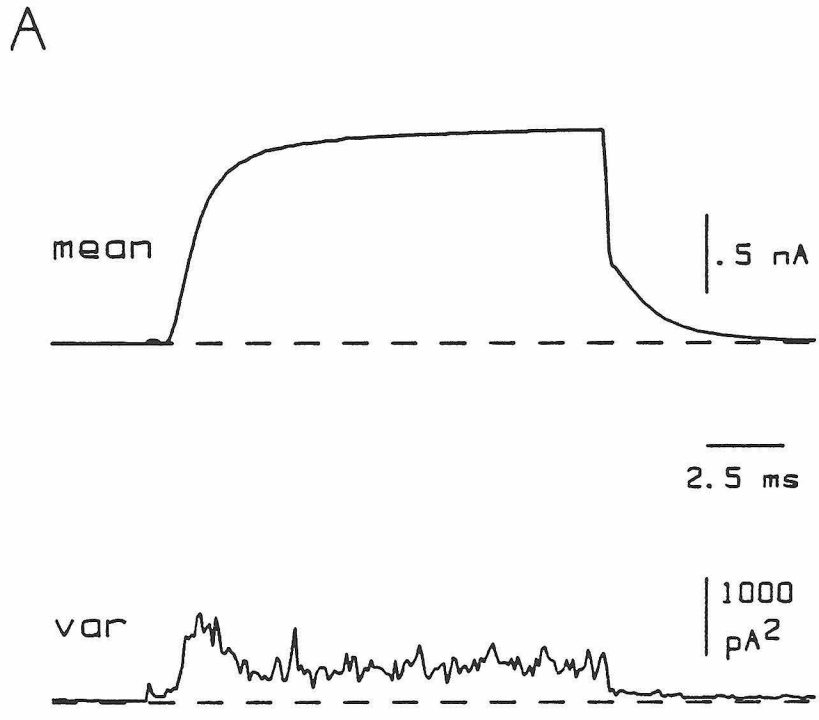
A
mean
.5 nA
2.5 ms
var
1000
pA2

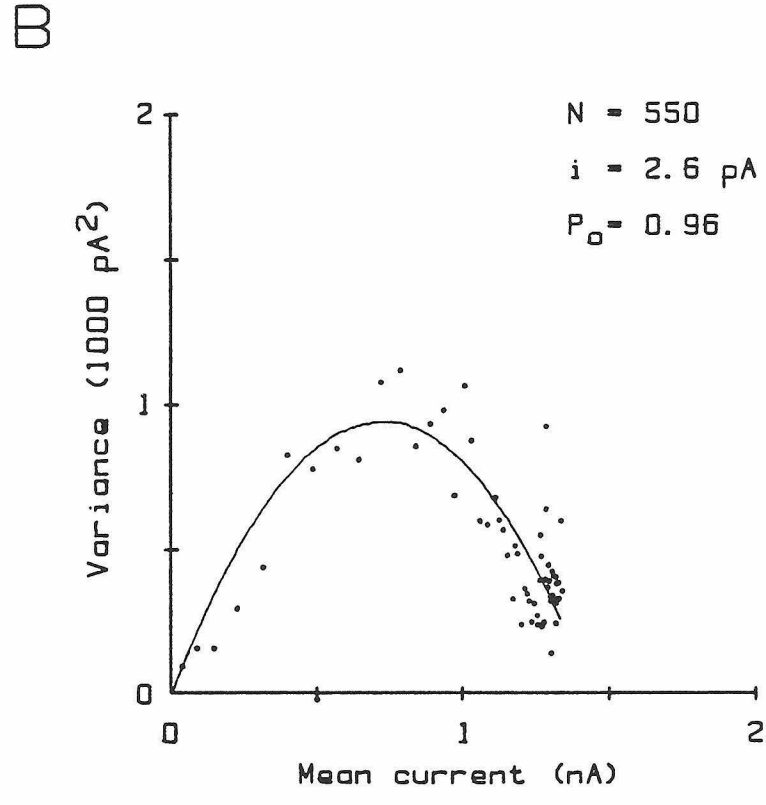
B
N = 550
i = 2.6 pA
Po= 0.96
Variance (1000 pA2)
Mean current (nA)
0
1
2

been caused by a slowly-activating current summing with I_c, since the TEA-subtraction protocol was not used to isolate I_c in these experiments. The slowly-rising variance component was not included in the analysis. The total number of C channels in the cell and the amplitude of the single-channel ("elementary") current underlying the macroscopic current were estimated by fitting a parabola (equation (3)) to a plot of variance vs. mean current (Fig. 13B). In this case, the cell was estimated to have 550 C channels, each producing an elementary current of 2.6 pA at -30 mV. The probability of a C channel being open is simply calculated from the number of channels, the size of the elementary current, and the magnitude of the macroscopic current (equation (1)). The open-state probability for C channels in this cell was 0.96. In six cells tested at -30 mV, the number of C channels was 807 ± 325, the open-state probability in the steady state was 0.88 ± 0.10, and the single-channel current was 1.9 ± 0.4 pA.

Attempts to describe I_c with Model I ("Michaelis-Menten model")

The numerical values of the parameters in model I were adjusted in attempts to simultaneously describe three characteristics of whole-cell I_c: the sigmoidal time course of activation, the rapid exponential decay of the tail current, and the high open-state probability of the C channel at -30 mV. First, m_{inf} and τ_m were varied to fit I_{ca} at the different test voltages as described above; then σ, K_s, and K_d were adjusted to fit I_c produced at -30 mV. In response to each Ca current elicited by a voltage step, internal Ca concentration rises to a plateau level and then returns to zero following the step. Increasing σ, the volume to

which incoming Ca is confined, lowers the internal Ca concentration at all times without changing its time course. Increasing K_s, the rate at which Ca leaves the submembrane compartment, lowers the steady-state level of internal Ca and shortens the time course of Ca concentration change; this in turn lowers the magnitude of I_c while speeding up its activation and tail current decay. Increasing K_d, the dissociation constant of the C channel's hypothetical Ca binding site, slows I_c activation, lowers its steady-state magnitude, and speeds up the decay of the I_c tail current. After adjusting these parameters to obtain the best description of I_c at -30 mV, the model was used to predict C currents at the other voltages. Three subclasses of model I are considered below, in which one, two, or three Ca ions must bind to open the C channel.

One Ca per channel. If binding of one Ca ion is assumed to open the C channel, the model cannot adequately predict, at any voltage, both the long I_c onset latency and its rapid approach to a steady-state level.

Two Ca per channel. With the assumption of two Ca binding sites, the model predicts I_c kinetics fairly well at -30 mV (Fig. 14A), although the predicted onset latency is too short. At lower potentials the model fails to accurately predict the time course or magnitude of I_c. The inability to predict the observed I_c magnitude occurs because of the second-order dependence of I_c on internal Ca concentration; although this helps produce an onset latency, it makes I_c much too Ca-dependent. If the open-state probability at -30 mV is allowed to take values lower than 0.6, the onset latency is better approximated, but the steady-state I_c predictions at lower voltages are still too Ca-dependent.

Three Ca per channel. This variation of model I can adequately predict the time course and magnitude of I_c at -30 mV, but, like the

Figure 14. Attempts to describe the C current with model I ("Michaelis-Menten model"). After the Ca currents evoked by a series of voltage-clamp steps were fitted (Fig. 7), parameters σ, K_s, and K_d were adjusted to provide the best fit to I_c at -30 mV, given the constraint that the C-channel open-state probability at this voltage is 0.7 to 1.0. The model was then used to predict I_c at the other voltages. The I_c and I_{ca} data are from cell 36 (see Figs. 7 and 9). Command voltage in millivolts is indicated to the left of each I_c trace, and the dashed lines indicate the baseline current level. The bottom trace in *A* and *B* shows the time course of the voltage steps. *A*, Model I predictions assuming that two Ca ions must bind to activate the C channel. At voltages more positive than -45 mV, the model predicts too short a latency for I_c activation. More importantly, at voltages negative to -30 mV the predicted amplitude of I_c is significantly smaller than is experimentally observed. Values of I_{ca} activation parameters are listed in Table 2; G_c = 23.4 nS; K_d = 149 μM; σ = .004; K_s = 657 sec^{-1}. *B*, Model I predictions assuming that three Ca ions must bind to activate the C channel. The predicted latencies are better than for the two-Ca model in *A*, but the model still cannot accurately predict I_c amplitude at voltages negative to -30 mV. G_c = 17.5 nS; K_d = 904 μM; σ = .004; K_s = 639 sec^{-1}. The inability of model I to accurately describe I_c responses at a range of potentials probably stems from the assumption that C conductance is at all times in equilibrium with the internal concentration of Ca; this condition will not hold if Ca concentration changes on a fast time scale relative to transition rates of C channels among kinetic states.

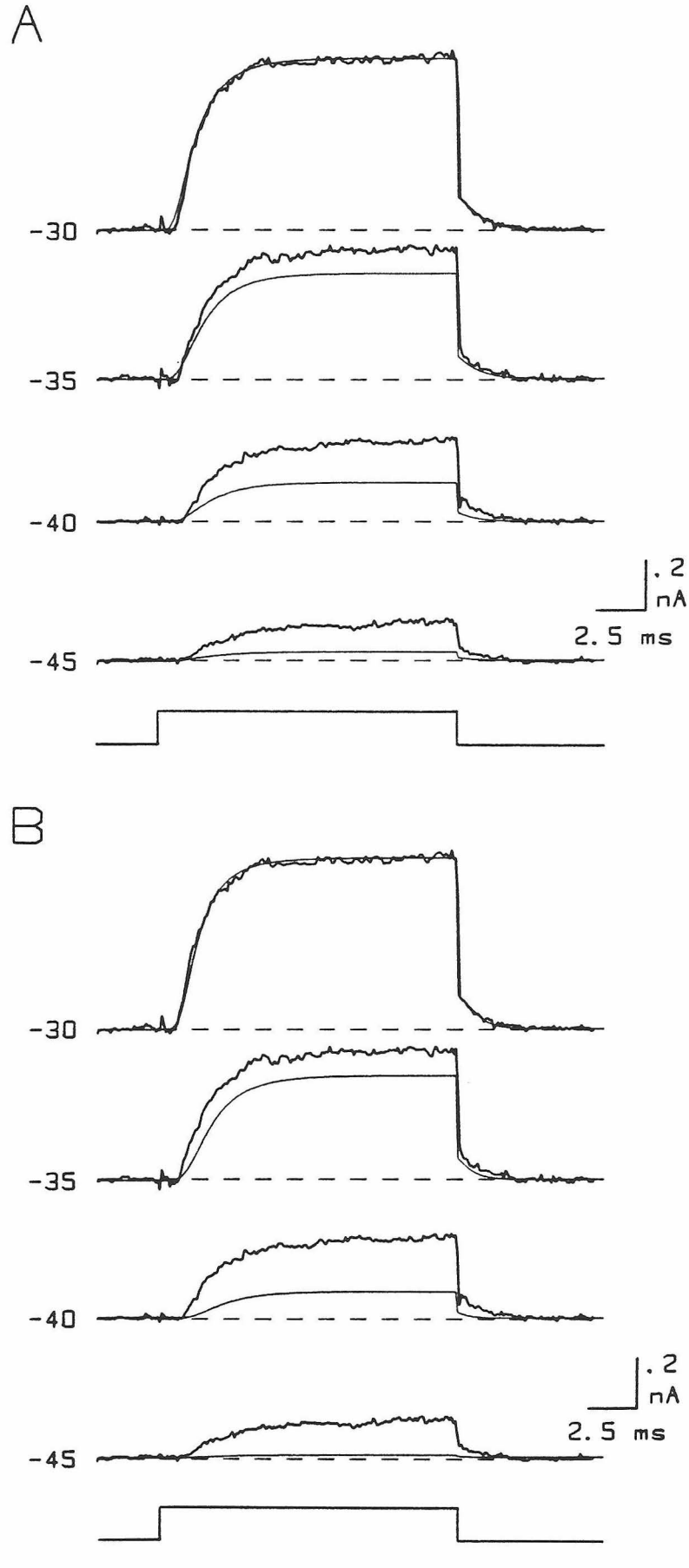
A
-30
-35
-40
-45
.2
nA
2.5 ms
B
-30
-35
-40
-45
.2
nA
2.5 ms

two-Ca model above, predicts too much Ca dependence of steady-state I_c amplitude (Fig. 14B).

Thus, regardless of the assumed number of Ca ions required to open the C channel, model I cannot predict the observed whole-cell C currents in the voltage range studied. The model might be improved by changing its description of Ca regulation. For example, one could introduce a term describing the time necessary for Ca to diffuse from its point of entry (Ca channels) to C channels; this diffusion time would add a delay to the activation of I_c, thereby relaxing some of the restrictions imposed on other parameters by the long observed I_c onset latency. Similarly, one could assume that Ca is removed from the submembrane compartment at a rate proportional to higher powers of Ca concentration, which would allow steady-state Ca levels to increase less than linearly with I_{ca}, improving the model's predictions of steady-state I_c.

However, it seems more likely that the failure of model I to describe whole-cell C current accurately stems from its simplistic description of C-channel activation. The assumption that the C conductance reacts instantaneously to changes in Ca, while being an adequate approximation for cells in which internal Ca concentration and G_c change slowly (Gorman and Thomas, 1980), is clearly unrealistic in light of what is known about C-channel gating kinetics in a number of preparations and in view of the rapid kinetic behavior of I_c, and presumably internal Ca concentration profile, in the hair cell. Recent descriptions of the Ca-activated K channel in rat muscle have indicated kinetic behavior that is slow enough to be rate-limiting on the time scale of I_c activation in the hair cell (Moczydlowski & Latorre, 1983; Magleby & Pallotta, 1983; Methfessel & Boheim, 1982). These studies have also shown the ex-

istence of multiple closed states of the channel. Obligatory passage through these closed states prior to opening could in theory produce onset latencies in whole-cell macroscopic current like those observed for I_c in the hair cell. For these reasons, a second hair-cell model was developed which includes a five-state activation scheme for the C channel. The next section describes experiments on single C channels that support the general form of this scheme and constrain the values of several of its parameters.

Part Two: Single-channel experiments

The original aim of the single-channel experiments was to characterize the kinetic behavior of the hair cell's C channel in terms of a simple gating scheme. A sufficiently detailed description of the channel in excised patches, for which Ca concentration and membrane potential can be controlled, would fix the values of most of the parameters in model II. Unfortunately, several difficulties precluded a quantitative description of this sort in the limited time available for these experiments. First, the great majority of patches contained more than a single C channel, making difficult or impossible the interpretation of closed- and open-state durations. Second, kinetic properties of six C channels in single-channel patches that were analyzed in detail varied with time during recording and with respect to each other, so that consistent quantitative estimates of rate constants in the C-channel gating scheme (S1) could not be made.

Nevertheless, all of the observed C channels shared characteristics on a qualitative level. These common features are described below to lend support to the general form of scheme (S1) and to place rough constraints on the values of several of its parameters.

Identification of C channels in excised patches

Over half of the patches excised from the basolateral membranes of hair cells contained large-conductance, K-selective ionic channels whose activity was modulated by internal Ca and membrane potential. The channel's high prevalence, in addition to its conductance, ionic selectivi-

ty, and Ca-dependence, strongly suggest that it is responsible for the hair cell's macroscopic C current.

The slope conductance of the channel was determined by measuring the amplitude of single-channel currents at different voltages; the results of such a measurement are shown in Fig. 15. The channel in this excised, inside-out patch was activated by 100 μM Ca in contact with the intracellular face of the membrane. The traces show current through the channel in the presence of 122 mM KCl on both sides of the patch at membrane voltages of -50 to +40 mV. A conspicuous kinetic feature of the channel is that openings are interrupted frequently by brief closures, most of which are too rapid to be fully resolved at the bandwidth of this recording (2 kHz). The average size of the single-channel current at each voltage was measured from amplitude histograms of these data as shown in Fig. 16A. This histogram was compiled from current recorded at -30 mV membrane potential; the rightmost peak represents current with the channel closed, while the leftmost peak indicates current through the open channel. The separation between Gaussian curves fitted to the two amplitude distributions indicates the size of the single-channel current, which at this voltage was -6.3 pA. The excess of recorded current values between the two Gaussian curves corresponds to incompletely resolved open-closed transitions in current level. The single-channel currents measured in this way are plotted against voltage in Fig. 16B. The data indicate a slope conductance of 195 pS over the range of -50 to +40 mV. The reversal potential is 1.8 mV, close to a value of 0 mV which would be expected under these symmetrical ionic conditions. The conductance and reversal potential were unaffected by changes in intracellular Ca in the micromolar range. The large single-channel conductance resem-

Figure 15. Single-channel C currents in an excised inside-out patch. The holding potential is given at the right of each trace, and the current levels corresponding to the closed and open channel are indicated by lines marked "C" and "O" on the left. The lines correspond to the peaks in current- amplitude histograms (Fig. 16). Current through the channel was inward at negative potentials and outward at positive potentials, reversing near 0 mV. Channel openings were frequently interrupted by very brief closures, many of them too brief to be fully resolved at this recording bandwidth. Cell 2; filter = 2 kHz Bessel, sampling interval = 100 μsec; internal = KCl + 100 μM Ca; external = KCl saline.

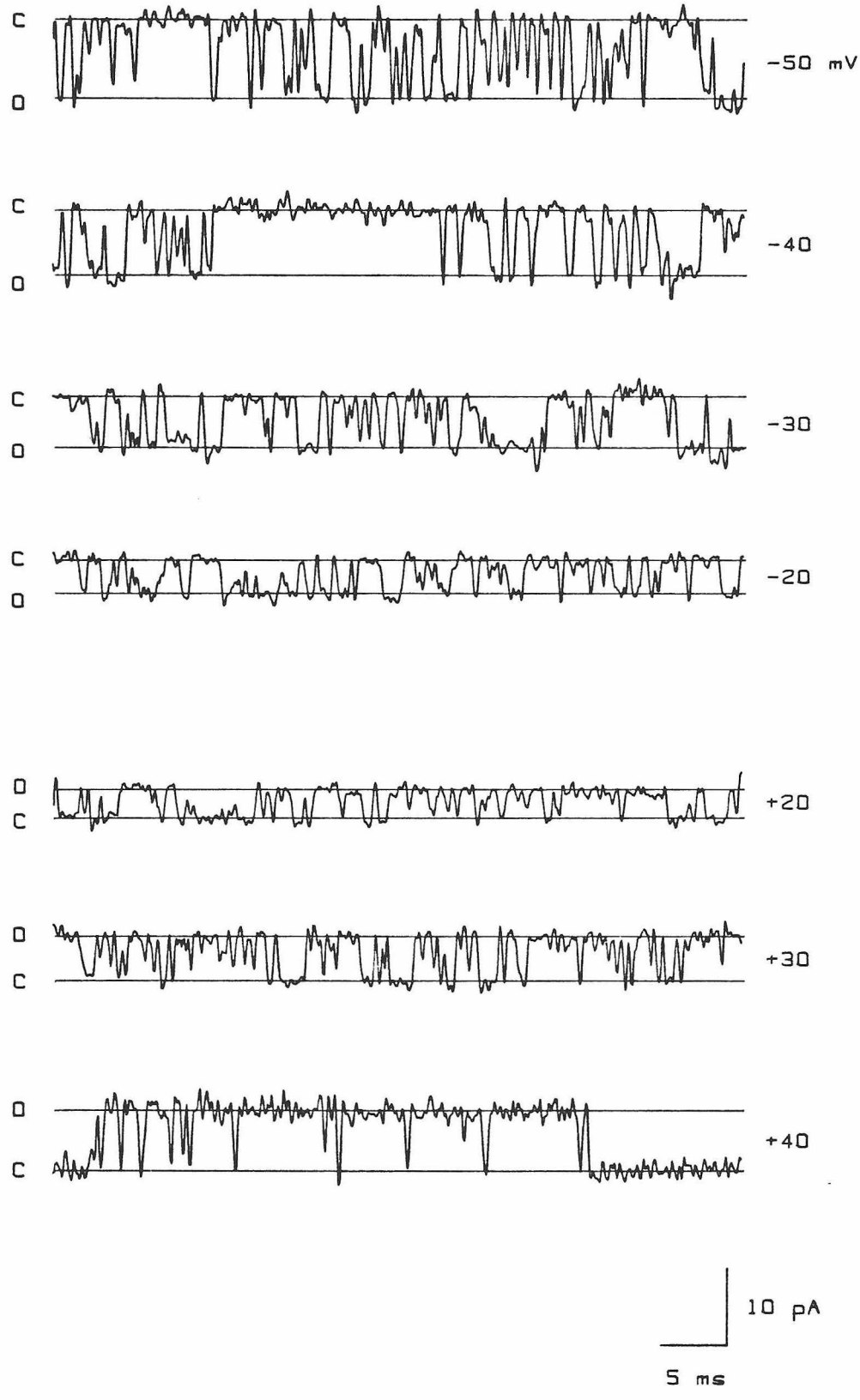
C
O
-50 mV
C
O
-40
C
O
-30
C
O
-20
O
C
+20
O
C
+30
O
C
+40
10 pA
5 ms

Figure 16. Estimating the conductance of the C channel. Experiment of Fig. 15. *A*, Current-amplitude histogram from 3.3 seconds of data recorded at a membrane potential of -30 mV. The current amplitude has a bimodal distribution corresponding to background current when the channel was closed (rightmost peak) and current through the open channel (leftmost peak). Gaussian functions have been fitted to the two distributions by eye; the spacing between them indicates the size of the single-channel current, which was -6.3 pA at this voltage. The excess of current events between the Gaussian curves is due to incompletely resolved channel openings and closings. Bin size = 0.16 pA. *B*, Current-voltage relation of the C channel. At holding potentials of -50 to +40 mV, current-amplitude histograms were compiled and analyzed as described in *A*. A line has been fitted to the data points by linear regression and indicates a slope conductance of 195 pS and a reversal potential of 1.3 mV. Conductance and reversal potential were unaffected by varying internal Ca concentration from 10 μM (△) to 100 μM (□).

A

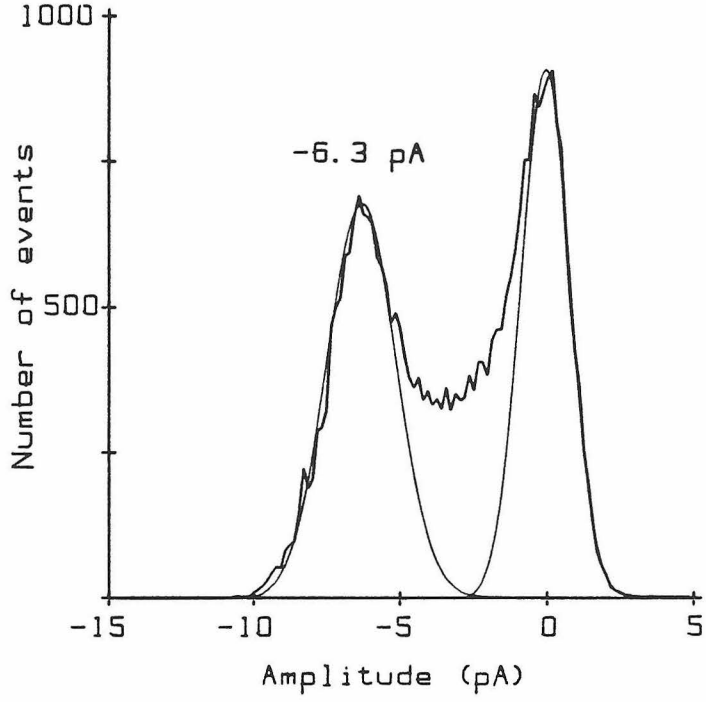
1000
500
Number of events
-6.3 pA
-15
-10
-5
0
5
Amplitude (pA)

B

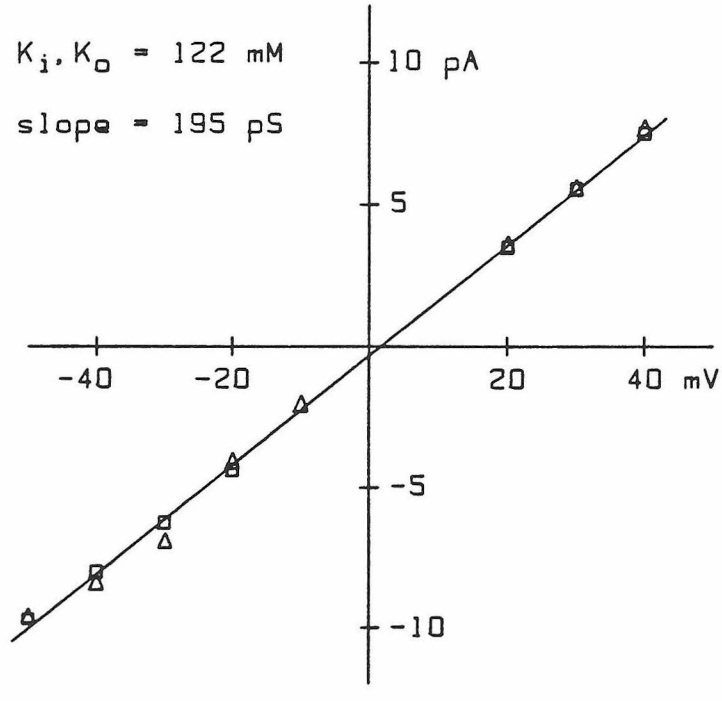
K_i, K_o = 122 mM
slope = 195 pS
10 pA
5
-5
-10
-40
-20
20
40 mV

bles that of "maxi" Ca-activated K channels in a number of preparations (for review, see Latorre & Miller, 1983).

Measurements of the reversal potential for single-channel current under different ionic conditions show that the channel is selectively permeable to K over Cl and Na. With 124 mM KCl outside and 124 mM K aspartate inside, current through the channel reversed at 0.8 mV (±1.2 mV, n=3); this result indicates that the channel is not significantly permeable to Cl, since the Nernst potential for Cl under these conditions is +85 mV. In addition, the channel is highly selective for K over Na (Fig. 17). In this experiment, voltage ramps were applied to the patch in the presence of standard saline (external face) and K aspartate solution with 100 μM Ca (internal face). Two responses are shown in Fig. 17A; in the lower trace, the channel remained closed throughout the duration of the ramp, while in the upper record the channel was open most of the time, producing an outward current. Closed-channel segments of 49 traces were averaged and subtracted point by point from the averages of open-channel segments to construct the open-channel I/V relation of Fig. 17B. There is no clear reversal of current through the channel at even the most negative voltage used here, -73 mV; applying the constant-field equation (Hodgkin & Katz, 1949) under these ionic conditions indicates a permeability ratio P_{Na}/P_K of less than 0.05. The channel's high selectivity for K over Na is similar to that of the C conductance measured in whole cells fromk the reversal potential of C tail current (Lewis & Hudspeth, 1983a). The channel's slope conductance between -40 and 0 mV was 124 pS, significantly lower than the conductance of these channels measured in symmetrical K solutions (see Fig. 16). This could be an effect of low K concentration on the external side of the membrane (for a

Figure 17. Current/voltage relation of the C channel under conditions of asymmetric K concentration. These responses were obtained by the "ramp-clamp" method (Yellen, 1982) in the presence of high internal K and low external K concentrations used in whole-cell I_c recordings. This excised inside-out patch contained a single C channel. *A*, Two responses to a 51-msec voltage ramp from -73 to 27 mV. The lower trace (C) represents leakage and residual capacitive current; the C channel was closed. In the upper trace (O), a single C channel was open most of the time, giving rise to net outward current. *B*, Averaged I/V relation of a single C channel. Open- and closed-channel segments of 49 ramp-clamp responses (including those in *A*) were identified and averaged separately, point for point. The closed-level average was then subtracted from the open-level average to give the net I/V relation shown here. A linear regression fit at voltages between -40 and 0 mV indicates a slope conductance of 124 pS. The current did not reverse in sign up to voltages as negative as -73 mV, demonstrating that the channel, like the whole-cell C conductance, is highly selective for K ions over Na ions. Cell 15; filter = 1 kHz Bessel; repetition interval = 0.8 sec; sampling interval = 0.2 msec; internal = K aspartate + 100 μM Ca; external = standard saline.

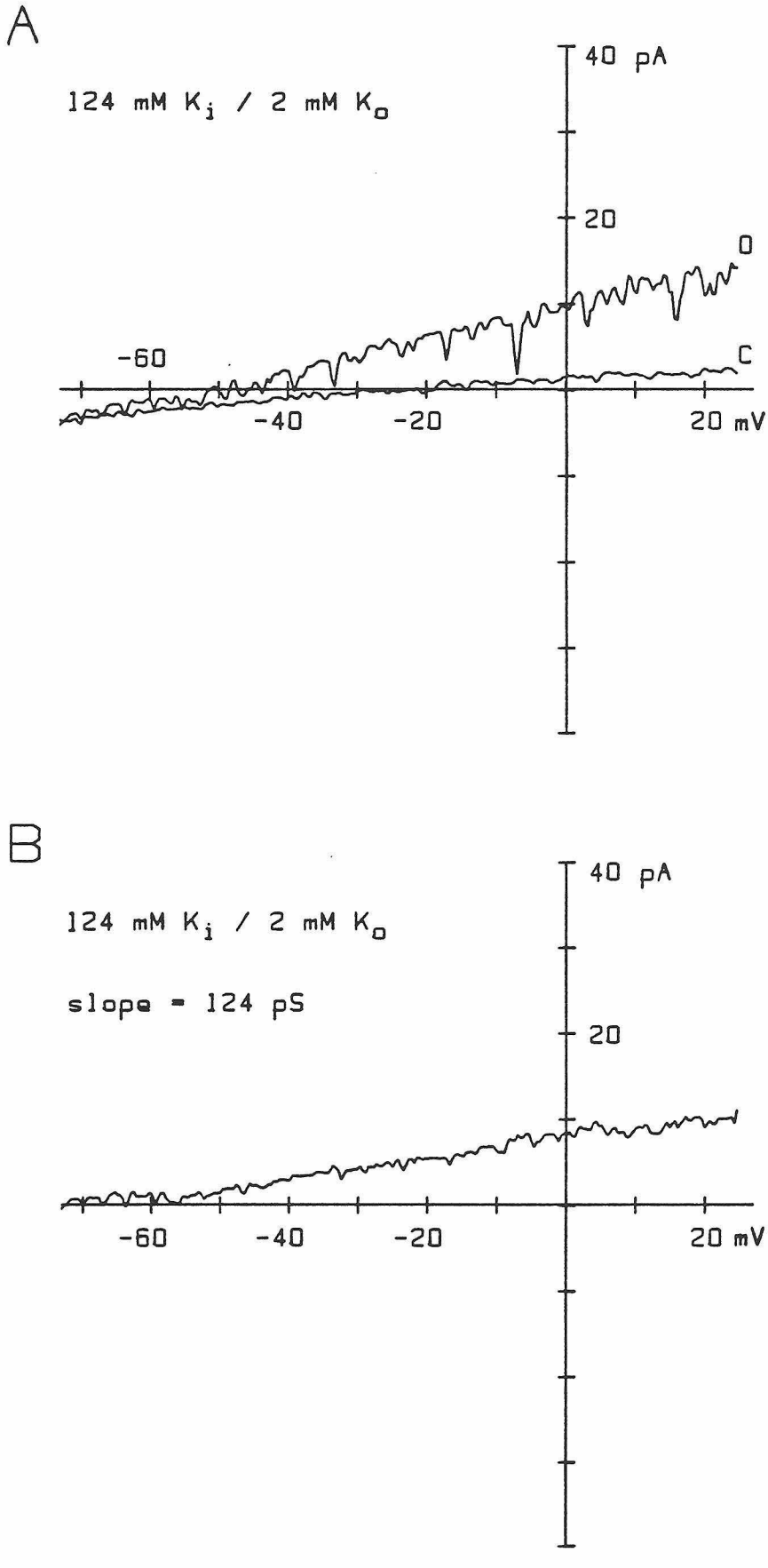
A
124 mM K_i / 2 mM K_o
40 pA
20
O
C
-60
-40
-20
20 mV
B
124 mM K_i / 2 mM K_o
slope = 124 pS
40 pA
20
-60
-40
-20
20 mV

similar effect of K concentration on C-channel conductance, see Wong et al., 1982). The size of the single-channel current at -30 mV was 4.2 pA, which is larger than estimates based on ensemble variance measurements of whole-cell C current under similar ionic conditions (1.9 ± 0.4 pA). This discrepancy could be due to a membrane-potential error in whole-cell recordings caused by a junction potential between the pipette and the cell's interior. Recently, several groups have reported shifts of -10 to -20 mV in the voltage-dependence of the Na current occurring within 10-30 minutes of the start of whole-cell recordings (Marty & Neher, 1983; Fox et al., 1983). To explain this shift, Marty and Neher have proposed that large cellular anions initially establish a Donnan potential across the tip of the pipette, making the membrane voltage more negative than the clamp command voltage, and that this Donnan potential dissipates slowly as the anions equilibrate with the pipette solution. The same potential dissipates much more quickly for excised patches, presumably because of the smaller amount of cytoplasm involved (Fenwick et al., 1982). Thus, the membrane potential in the ensemble variance experiments may have been 10 to 20 mV more negative than assumed. A shift of -10 to -20 mV along the voltage axis in Fig. 17B gives single-channel current values of 1.5 to 2.8 pA, which agree with the range estimated from the ensemble variance experiments.

The dual Ca and voltage dependence of the channel's activity is demonstrated in Fig. 18. At holding potentials of -50 to 40 mV and with 1, 10, and 100 μM internal Ca, 3.3-second stretches of recorded activity were scanned for opening and closing transitions (see Methods). The open-state probability, P_o, was calculated as the fraction of time spent in the open state. As shown here, increases in Ca concentration or depo-

Figure 18. Dual dependence of C-channel activity on internal Ca and membrane potential. Same patch as in Fig. 15. For each concentration of internal Ca, current was recorded at holding potentials of -50 to +40 mV, and the amplitude of the single-channel current was evaluated as in Fig. 16. Data were then analyzed for open and closed events with 50% of the open-channel current level defining the transition between open and closed levels. Open-state probability was calculated as the total fraction of time spent in the open state. An increase in internal Ca concentration or membrane depolarization promoted C-channel activity. At voltages of -50 to -30 mV, encompassing the range of voltage oscillations in the cell under current clamp, a relatively high internal concentration of Ca (around 10 μM) was needed to activate the C channel significantly. Cell 2; filter = 2 kHz Bessel; sampling interval = 0.1 msec; internal = KCl + 1 μM Ca (∇), 10 μM Ca ($\triangle$), or 100 μM Ca ($\square$); external = KCl saline. 3.3 seconds of data were sampled for each point.

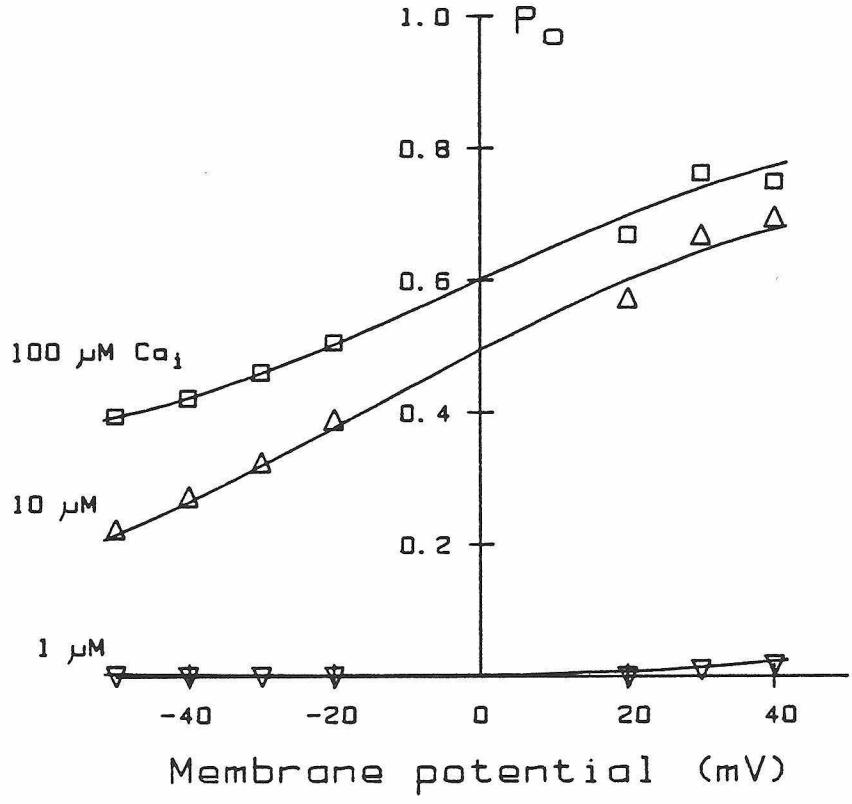
1.0
P_o
0.8
0.6
0.4
0.2
100 μM Ca_i
10 μM
1 μM
-40
-20
0
20
40
Membrane potential (mV)

larization can activate the channel. The dual dependence of activity on Ca and membrane voltage is a characteristic common to C channels from a variety of sources (Barrett et al., 1982; Marty, 1981; Wong et al., 1982; Maruyama et al., 1983). Note that at potentials between -50 and -30 mV, the range used to activate the C conductance in whole-cell experiments, high concentrations of internal Ca are required to activate the channel even moderately in a patch. This rather low Ca sensitivity was consistently observed: in nine other patches, Ca concentrations of 10 to 100 μM were needed to moderately activate the channel at a membrane potential of -40 mV. The absolute sensitivities of C channels in other preparations to internal Ca and membrane potential vary widely; of these, the sensitivities of the C channel in rat myotubes (Barrett et al., 1982) most closely resemble those of the hair cell's C channel.

In summary, the high prevalence, ionic selectivity, and Ca- dependent activation of this "maxi"-K channel strongly suggest that it is the channel responsible for the hair cell's C conductance. If a possible junction-potential error is taken into account, the single-channel current size is also compatible with predictions from fluctuation analysis of whole-cell C currents. For these reasons, I will hereafter refer to this channel as the C channel.

Number of C-channel kinetic states

Histograms of open- and closed-channel lifetimes recorded under conditions of constant membrane voltage and internal Ca concentration can be used to estimate the number of kinetic states that a C channel can assume. In theory, assuming that transitions between states consti-

tute a Markov process, the number of open or closed states should equal the number of exponential distributions in the open- or closed-lifetime histogram (Colquhoun & Hawkes, 1981). However, two or more of the components may have the same time constant, or a time constant may fall outside the bandwidth of the recording apparatus; therefore, in practice, the number of exponential components only indicates a lower limit for the number of states.

In four single-channel patches that were examined, the open lifetime distribution was well described by a single exponential function, with a slight surplus of very brief events (duration less than 100 μsec). The mean open-channel lifetime increased with the level of internal Ca or membrane depolarization. For the patch shown in Fig. 19, raising internal Ca from 10 to 100 μM at 30 mV membrane potential increased the open time from 0.76 to 1.03 msec. The simplest interpretation of these data is that there are two open states of the channel, as in scheme (S1); the channel can open only to the first open state, which can bind a Ca ion to become the second open state. In addition, binding and unbinding of Ca from the open states is much faster than the closing conformational transition. This sort of scheme predicts a single-exponential open-time distribution which is lengthened by increasing Ca concentration (Moczydlowski & Latorre, 1983). In addition, membrane depolarization increases the open-state lifetime; for the patch of Fig. 19 with 10 μM Ca, changing the voltage from -50 to 40 mV increased the mean open lifetime from 0.28 to 0.88 msec.

In all four patches, closed lifetimes of the C channel were distributed as the sum of two exponential distributions, suggesting the existence of at least two closed states (Fig. 20). In several other patches

Figure 19. Ca dependence of the mean open lifetime of the C channel. Same patch and experimental conditions as in Fig. 15. Channel openings were detected using a threshold criterion of 50% of the open-channel current level, and histograms of open-event durations were compiled using a bin width of 0.1 msec. Conditional probability density functions (conditional pdf's) were fitted to the durations data using a maximum likelihood method. Membrane potential was +30 mV. *A*, Open-lifetime distribution in the presence of 10 μM internal Ca. 2483 events were observed; the conditional pdf providing the best description of these data had the form $p(t) = 1/\tau \cdot \exp(-t/\tau)/P(t>t_{min})$, where $p(t)$ is the probability density of an event of duration t given that its duration is greater than the minimum detection limit t_{min}, and $P(t>t_{min})$ is the probability that the event is longer than t_{min}. A curve representing the conditional pdf, scaled by the number of observed events, has been superimposed on the histogram. Although a single exponential pdf was the best description of the data, an excess number of short events was observed; the durations of these events were too close to the detection limit of the recording to permit a meaningful estimate of their mean value. *B*, Increasing internal Ca concentration to 100 μM increases the mean open lifetime. The distribution of 1965 observed openings was best fitted by a conditional pdf of the form given in *A*, with a τ of 1.03 msec. The dependence of open lifetime on Ca concentration implies the existence of multiple open states, and the predominantly single-exponential distribution of open lifetimes therefore suggests that transitions between open states are rapid compared to the closing conformational transition.

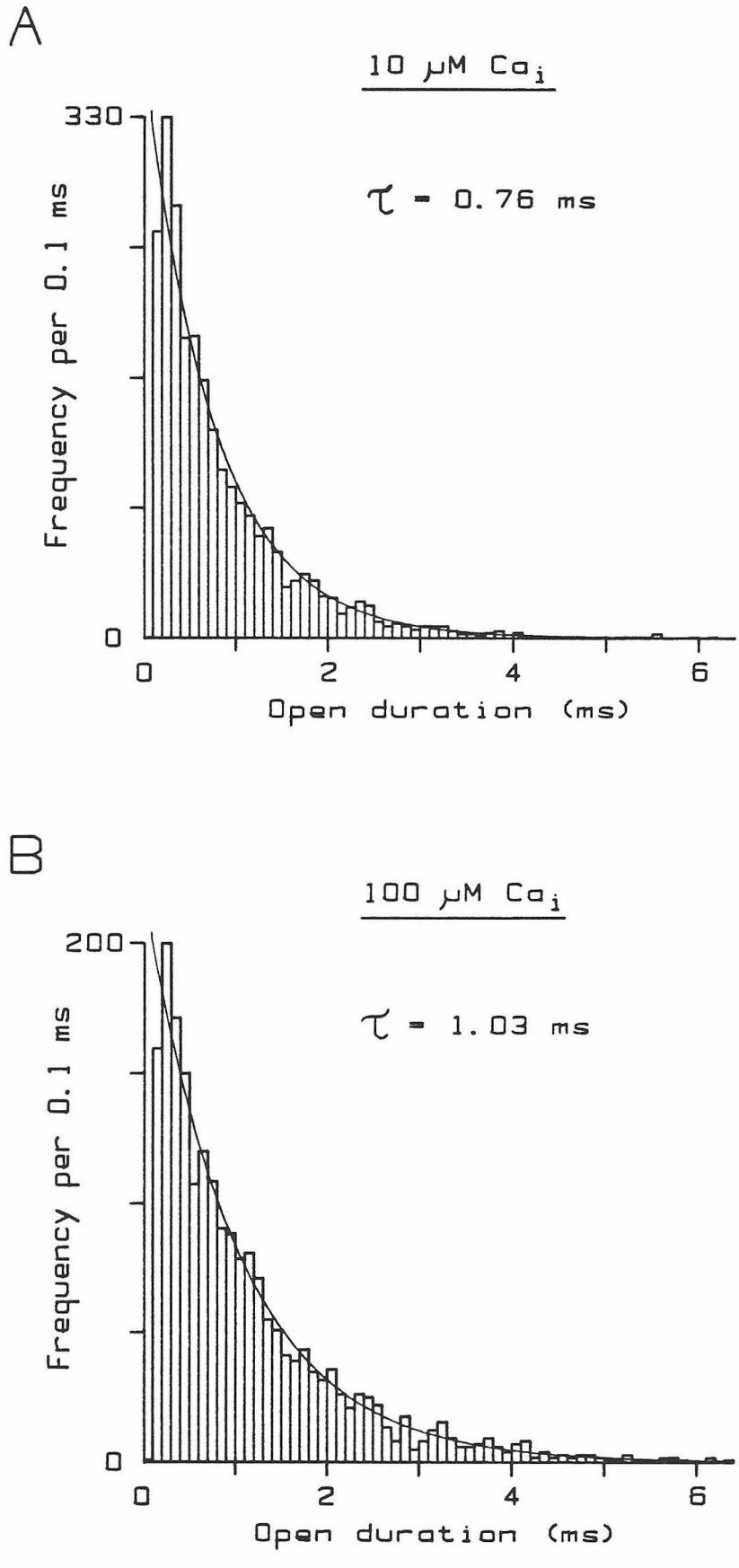
A
10 μM Ca$_i$
τ = 0.76 ms
330
0
Frequency per 0.1 ms
0
2
4
6
Open duration (ms)
B
100 μM Ca$_i$
τ = 1.03 ms
200
0
Frequency per 0.1 ms
0
2
4
6
Open duration (ms)

that were observed over longer periods, closures lasting 100 to 500 msec occurred at moderate levels of activation. These events were too frequent to be a part of the 1-2 msec closed-time distribution, but could be ascribed to the presence of a third closed state. The long events could not be sampled adequately in the short time period used for histogram data collection (3.3 sec), which explains the absence of a corresponding third exponential component in the closed lifetime histogram. To account for these data, three C-channel closed states were assumed in scheme (S1). This proved to be a minimal assumption, since all attempts to fit whole-cell C currents with a model that included only two closed C-channel states were unsuccessful. The average closed-channel lifetime decreases with increasing concentration of internal Ca and depolarization; in Fig. 20, increasing Ca from 10 to 100 μM at a membrane potential of -40 mV lowers the average closed time from 0.96 to 0.59 msec. The dependence of closed lifetime on Ca concentration indicates that Ca binds to one or more closed states to bias the channel towards opening. In the gating scheme (S1) I have assumed that two Ca ions must bind before the channel can open, by analogy to a model proposed recently for the C channel in rat myotubes (Magleby & Pallotta, 1983). Although there is no quantitative evidence for or against this assumption regarding the hair cell's C channel, it is qualitatively consistent with the steep dependence of mean closed lifetime on Ca concentration in a range that produces low levels of C-channel activity (1-10 μM). Depolarization of the membrane also decreases the mean closed lifetime; for this patch with 10 μM Ca, changing voltage from -50 to 40 mV decreased the average closed duration from 1.2 to 0.3 msec.

Figure 20. Ca dependence of the mean closed lifetime of the C channel. Same patch and experimental conditions as in Fig. 15; method of analysis is described in Fig. 19. Membrane potential was -40 mV. *A*, Closed-lifetime distribution in the presence of 10 μM internal Ca. 1807 closed events were observed, and their distribution was best described by a conditional probability density function (conditional pdf) having two exponential components: $p(t) = [a_1/\tau_1 \cdot \exp(-t/\tau_1) + a_2/\tau_2 \cdot \exp(-t/\tau_2)]/P(t>t_{min})$, where $p(t)$ and $P(t>t_{min})$ are as defined in Fig. 19, and a_i and τ_i are the area beneath and time constant of the ith exponential component. Values for a_1, τ_1, a_2, and τ_2 are shown above the histogram. About half of the closings came from a class having a mean duration of 0.39 msec, while the other half were from a class of mean duration 1.56 msec. *B*, Mean closed lifetime is decreased by raising internal Ca concentration to 100 μM. The distribution of 2327 closed events was best described by the conditional pdf shown in *A*, with values of a_1, τ_1, a_2, and τ_2 shown above the histogram. Increasing internal Ca caused more of the closings to fall within the short-duration distribution, leading to a decrease in the average closed lifetime from 0.96 msec (10 μM Ca) to 0.58 msec (100 μM Ca).

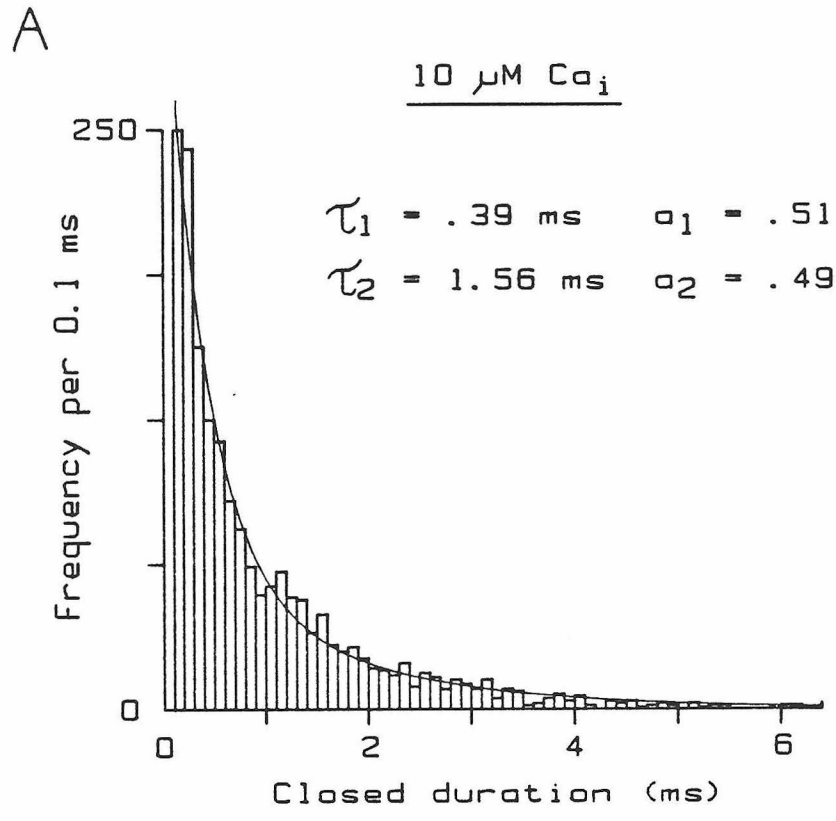
A
10 μM Ca_i
250
0
Frequency per 0.1 ms
τ_1 = .39 ms a_1 = .51
τ_2 = 1.56 ms a_2 = .49
0
2
4
6
Closed duration (ms)

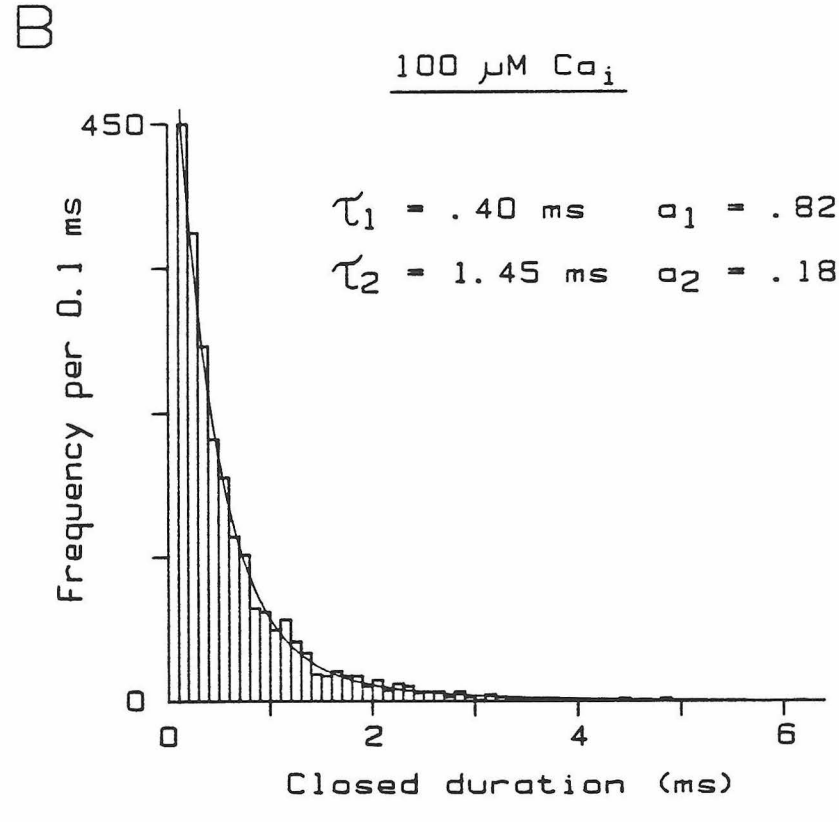
B
100 μM Ca_i
450
0
Frequency per 0.1 ms
τ_1 = .40 ms a_1 = .82
τ_2 = 1.45 ms a_2 = .18
0
2
4
6
Closed duration (ms)

Kinetics of C-channel activation by voltage steps

In studies of chemical reactions, the analysis of steady-state behavior and of responses to perturbations yields overlapping but different sets of information about the rate constants involved in the reaction mechanism. For this reason I sought to supplement the information obtained from the study of steady-state C-channel behavior presented above, by investigating the time course of C-channel activation induced by voltage steps. Fig. 21 shows the results of this type of experiment, in which repetitive depolarizing voltage steps were applied in the presence of 8 μM internal Ca to a patch containing a single C channel. The voltage-dependent activation of the C channel is clearly evident in the individual responses to four depolarizations shown in Fig. 21A; at the holding potential of -93 mV the channel was almost always closed, but depolarization to +87 mV opened the channel, producing a rapidly fluctuating outward current of 12 pA amplitude. Under the conditions of symmetrical K concentration used in this experiment, reversal potential for C current was 0 mV, so that occasional channel openings at -93 mV produce inward current (top trace). The stochastic nature of C-channel gating is revealed by the variations in response from one stimulus presentation to the next; to observe the average activation time course in the presence of this stochastic "noise," the responses to 124 consecutive voltage steps were averaged (Fig. 21B). Both the onset and offset kinetics of the averaged response have important implications for model II. The average current was activated with a time course resembling that of macroscopic I_c recorded in whole cells; in particular, the average single-channel response increased with a sigmoidal time

Figure 21. Activation of the C channel by voltage steps. *A*, Four responses of a single C channel in an excised inside-out patch to a voltage-clamp step from -93 to +87 mV. At the holding potential of -93 mV, with 8 μM internal Ca, the channel was closed well over 99% of the time. Membrane depolarization to +87 mV opened the channel, resulting in a rapidly fluctuating outward current of 12 pA amplitude. At the holding potential of -93 mV, C current was inward (top trace). These responses show the characteristically rapid, stochastic gating of the channel. *B*, Average of an ensemble of 124 responses to the voltage step in *A*. Closed-channel segments of each response were identified, averaged point by point, and subtracted from the mean of all 124 responses to remove the contributions of residual capacitative and leakage currents from the average. The open-state probability of the C channel, measured by dividing the ensemble-average current by the single-channel current amplitude, rose from 0 to 0.26 during the step. The channel was activated with a sigmoidal time course following an apparent lag of 0.5 msec, which implies the existence of multiple closed states of the C channel. The current returned to 0 within 100 μsec of repolarization to -93 mV; this rapid return to baseline places a lower limit on the closing rate constant for the C channel, α_c, of about 10^4 sec^{-1} at this voltage. Cell 136; filter = 2 kHz Bessel; repetition interval = 0.5 sec; sampling interval = 0.1 ms; internal = K aspartate + 8 μM Ca; external = KCl saline.

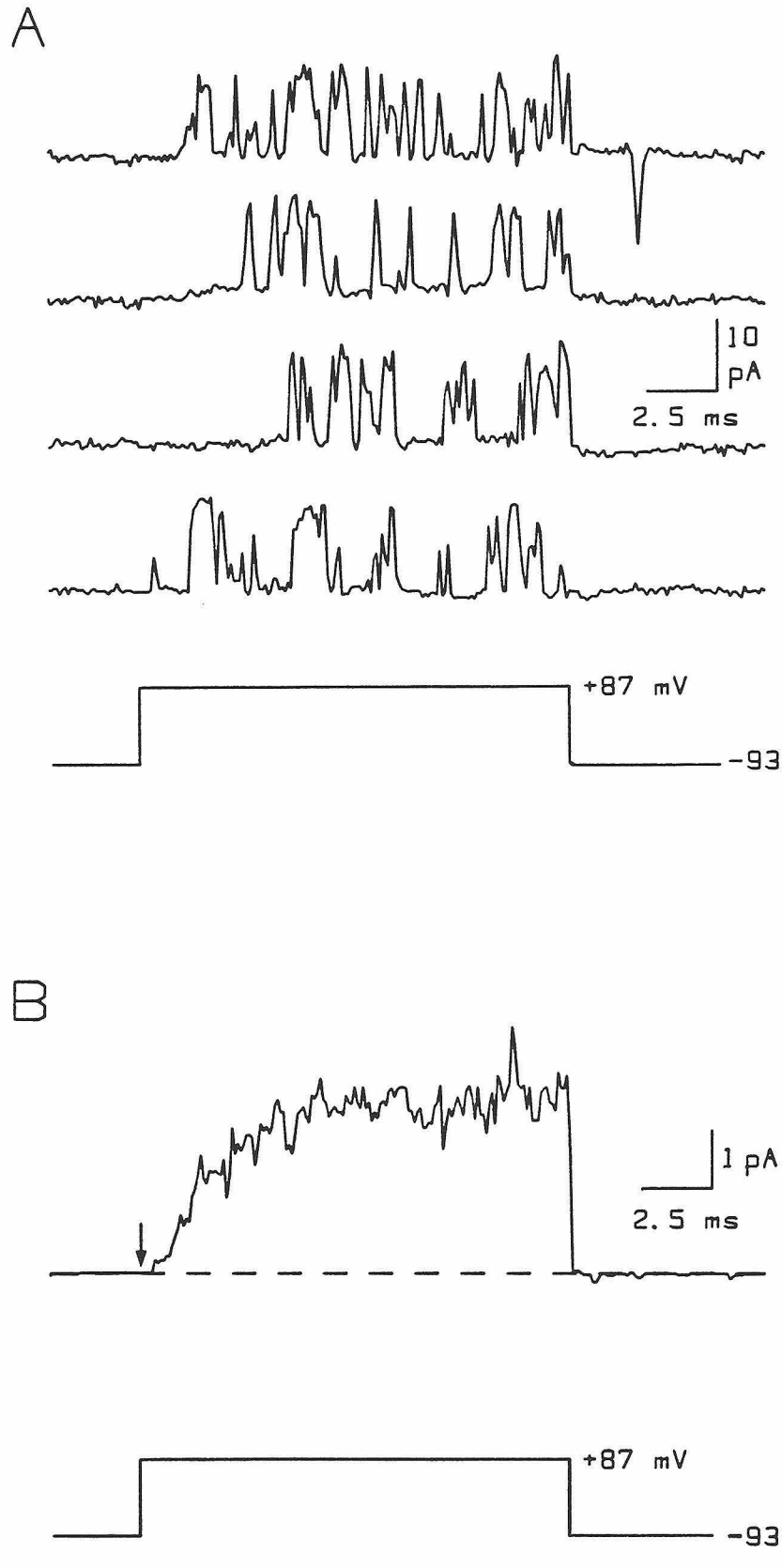
A
10
pA
2.5 ms
+87 mV
-93
B
1 pA
2.5 ms
+87 mV
-93

course, producing the first measurable outward current about 0.5 msec after the start of the voltage step. Because Ca concentration in this experiment was constant, this onset latency must have resulted from time-dependent transitions among multiple closed C-channel states. This result also implies that a substantial part of the I_c onset latency in whole-cell recordings (Fig. 10) can be accounted for by C-channel transition rates, thus supporting the earlier conclusion that the Michaelis-Menten-type description of the C conductance in model I was inadequate. The average C-channel current returned to zero within 100 μsec after the end of the voltage step. In this and other experiments described below, the open C channel closed upon repolarization of the membrane to the holding potential and did not reopen during the period in which the average activity decayed to zero. Therefore, the time course of average current decay after repolarization reflects only transitions leading up to the closing transition and does not include reopenings. In terms of scheme (S1), the overall rate of channel closing depends on k_3[Ca], k_{-3}, and α_c; thus, the observed rate of decline of the ensemble-average current places a lower limit on α_c of 10^4 sec^{-1}. In addition, the rate at which channel activity declined following the voltage step depended on the holding potential, decreasing with depolarization. In another patch the average C-channel activity produced by a depolarizing voltage step declined to zero 0.9 msec after the return to a holding potential of -53 mV. This may reflect voltage-dependence of α_c, or may include possible voltage dependence of k_3 and/or k_{-3} as well.

Part Three: Modeling

Strategy for choosing parameter values in Model II

Model II has a large number of independent parameters for which values must be specified before it can predict the electrical behavior of the hair cell. Most of these parameters are associated with the five-state scheme used to describe C-channel gating; constraints on the values of these parameters and others were provided by the results presented in previous sections and are described below. The final choices of parameter values are listed in Table 2. For convenience, the C-channel gating scheme is restated here:

(S1) $$C \underset{k_{-1}}{\overset{k_1}{\rightleftharpoons}} CaC \underset{k_{-2}}{\overset{k_2}{\rightleftharpoons}} Ca_2C \underset{\alpha_c}{\overset{\beta_c}{\rightleftharpoons}} Ca_2O \underset{k_{-3}}{\overset{k_3}{\rightleftharpoons}} Ca_3O$$

state: 1 2 3 4 5

I. General form of the C-channel gating scheme. The number of closed and open states in the model was supported by the analysis of channel lifetimes presented in Part Two.

II. Estimate of the closing rate constant, α_c. The average activity of C channels opened by depolarizing voltage steps decayed very rapidly to zero upon repolarization to -93 or -53 mV. The rates of decay were used to place lower limits on α_c at the two voltages, and the difference between them was assumed to indicate voltage dependence of α_c. Closing rate was described by the expression

(16) $$\alpha_c = \alpha_c(0) \cdot \exp(-V_m/V_a)$$

where $\alpha_c(0)$ is the closing rate constant at 0 mV membrane potential, V_a

is membrane potential, and V_a is a voltage used to express the voltage dependence of α_c. Values for $\alpha_c(0)$ and V_a were chosen such that α_c was roughly consistent with the decay rates of the averaged C-channel activity at -93 and -53 mV.

III. Relative values of k_{-2} and β_c. C channels that were opened by depolarizing voltage steps closed on repolarization to -93 or -53 mV and rarely reopened during the time the averaged activity decayed to zero. (Fig. 21). Since the probability of reopening is equal to $\beta/(\beta+k_{-2})$, these results suggest that k_{-2} is significantly larger than β_c in the voltage range of -53 to -93 mV.

IV. Estimates of k_3 and k_{-3}. Open C-channel lifetimes followed a single-exponential distribution at voltages of -50 to +40 mV in the presence of high levels of internal Ca (10-100 μM), suggesting that the sum of rate constants for Ca binding to and unbinding from open states (k_3[Ca]+k_{-3}) under these conditions is much larger than the closing rate constant (α_c).

V. Voltage-dependence of C-channel rate constants. The observed voltage-dependence of closed and open lifetimes implies that at least one rate constant in scheme (S1) is voltage-dependent. Aside from α_c, the choice of which constants to make voltage-dependent was arbitrary and based only on the ability of the model to fit whole-cell I_c at a series of voltages.

VI. Estimate of σ, the fractional volume of the submembrane Ca compartment. σ was varied to provide a steady-state internal Ca concentration of about 100 μM in response to the Ca current recorded at -30 mV. This value for Ca concentration was chosen to be broadly consistent with the high open-state probability of the C channel in whole cells at

-30 mV (Fig. 13), given the observed Ca sensitivity of the channel in excised patches at the same voltage (Fig. 18).

VII. Constraints on K_s, the rate at which Ca leaves the submembrane compartment. In response to voltage steps to values more negative than -30 mV, the whole-cell C current reaches a plateau value within several milliseconds. Since the C channel is not fully activated under these conditions, internal Ca concentration must reach a steady level within this time, putting a constraint on the value of K_s. Moreover, the rate of C tail-current decay in whole cells (τ = 1 msec) is much slower than the decay rate of averaged C-channel activity in the presence of constant Ca concentration at comparable holding potentials (τ < 0.3 msec). This difference in channel closing rates implies that the time course of C tail current in whole-cell recordings is largely determined by the rate at which internal Ca concentration returns to its baseline level, rather than by gating kinetics intrinsic to the C channel. The rate at which Ca concentration declines following the voltage step is determined by K_s.

VIII. Leakage conductance (G_L) and reversal potential (E_L). For the cell used in the modeling (cell 36), leakage conductance was measured from the whole-cell current evoked by a voltage-clamp step from -70 to -60 mV; because of quantization errors in A/D conversion at the gain setting that was used, only an upper limit of 1 nS could be established, and this value was included in the model. In 37 cells, G_L ranged from 0.5 nS to 10 nS with a mean of 2.1 nS. The equilibrium potential for G_L was not measured directly. One contribution to "leak" could come from transduction channels that are open at rest, and these would have a reversal potential of 0 mV (Corey & Hudspeth, 1979). In some cells a por-

tion of I_L could be blocked by external TEA, suggesting the possibility that some C channels might be open even in the absence of a Ca current; this contribution to "leak" would have a reversal potential of -80 mV. To reflect the possible contributions of these two sources E_L was set to -30 mV.

IX. Membrane capacitance (C_m). Membrane capacitance was measured from the integral of the capacitive current elicited by a small voltage-clamp step, as described in the Methods.

After I_{Ca} was fitted with a third-order Hodgkin-Huxley scheme for a series of voltage steps (Fig. 7), parameter values in model II were varied within the range constrained by the results discussed above, to provide the best description of I_c recorded at the same voltages. Even with these constraints, model II contained many free parameters. Although this large number of degrees of freedom made fitting the model to I_c at any given voltage easy, it was nonetheless difficult to find a set of parameter values that could predict I_c at all five applied voltages. Finding such a combination of values was complicated by the fact that each parameter affects more than one aspect of the I_c waveform, and to different degrees. For example, lowering either k_{-1} or k_{-3} can decrease the maximum rate of rise in I_c, but the former change also increases the onset latency of I_c, while the latter change slows the decay of tail current. My approach to fitting could be described simply as trial-and-error. One could adopt a more elegant approach, in which an error-minimizing routine could be used to vary all parameter values to generate the best simultaneous fits to all five I_c responses, but the time required for the application of this kind of approach would be prohibitive due to the long (four-minute) time required to compute each

TABLE 2. Values of parameters in model II

Parameter	Value
$\bar{G}_{Ca}$	4.14 nS
E_{Ca}	100 mV
α_0	22800 sec^{-1}
V_0	70 mV
V_A	8.01 mV
K_A	510 sec^{-1}
β_0	0.97 sec^{-1}
V_B	6.17 mV
K_B	940 sec^{-1}
U	0.02
σ	$3.4 \cdot 10^{-5}$
C_{VOL}	1.25 pliter
K_S	2800 sec^{-1}
$\bar{G}_C$	16.8 nS
E_C	-80 mV
$K_1(0)$	6 μM
δ_1	0.2
k_{-1}	300 sec^{-1}
$K_2(0)$	45 μM
δ_2	0
k_{-2}	5000 sec^{-1}
$K_3(0)$	20 μM
δ_3	0.2
k_{-3}	1500 sec^{-1}
$\alpha_C(0)$	450 sec^{-1}
V_a	33 mV
β_C	1000 sec^{-1}
G_L	1 nS
E_L	-30 mV
C_m	15 pF

I_c response.

Model II predictions of whole-cell C current under voltage clamp

The predictions of model II under simulated voltage-clamp conditions are superimposed on a series of whole-cell C currents in Fig. 22. The close correspondence between the data and the predicted responses shows that model II can adequately describe the time course and magnitude of I_c elicited at voltages of -55 to -30 mV. Two minor discrepancies are apparent between model II's predictions and the data; for steps to voltages more positive than -45 mV, the predicted maximum rates of C current increase are somewhat lower than observed, and the predicted tail current amplitudes following these steps are slightly smaller than expected. These discrepancies could not be removed without creating more significant degradation of the overall fits and were therefore allowed to remain.

In principle, any sufficiently complex and flexible model could predict the correct waveform of I_c at each voltage, regardless of its assumptions of whether I_c is activated by Ca, membrane potential, or both. To cite an extreme example, a model that assumes the C conductance is solely voltage dependent, given a large enough number of C-channel states, could probably be fitted to the observed C currents. Such a model would, however, have little predictive value, since it could not account for changes in C conductance brought about by changes in Ca conductance (independent of voltage changes) or Ca regulation processes in the cell. In order to develop as realistic a model as possible, I incorporated both Ca- and voltage-dependence in the C-channel gating scheme.

Figure 22. Model II predictions of whole-cell C current. *A*, Predictions of I_c elicited by 15-msec voltage-clamp steps from -70 mV to the voltages listed to the left in millivolts. The noisy traces are the experimentally observed responses; same data as in Figs. 9 and 14. The dashed lines indicate the baseline current level, and the bottom trace shows the time course of the voltage steps. Superimposed on the data are the predictions from model II, using the parameter values listed in Table 2. *B*, Model simulation of the effect on I_c of lowering external Ca concentration from 4 mM to 0.5 mM. Predicted responses to a 15-ms voltage step from -80 to -30 mV, starting at the time indicated by the arrow. The low-Ca condition was simulated by lowering the maximal Ca conductance, G_{Ca}, to 25% of its value in 4 mM external Ca. The model predicts a decrease in the rate of I_c activation and a 43% decrease in steady-state I_c magnitude. Similar results were observed experimentally under equivalent conditions (see Fig. 11), providing evidence that the relative degrees of Ca- and voltage-dependence in the C-channel gating scheme (S1) are reasonable.

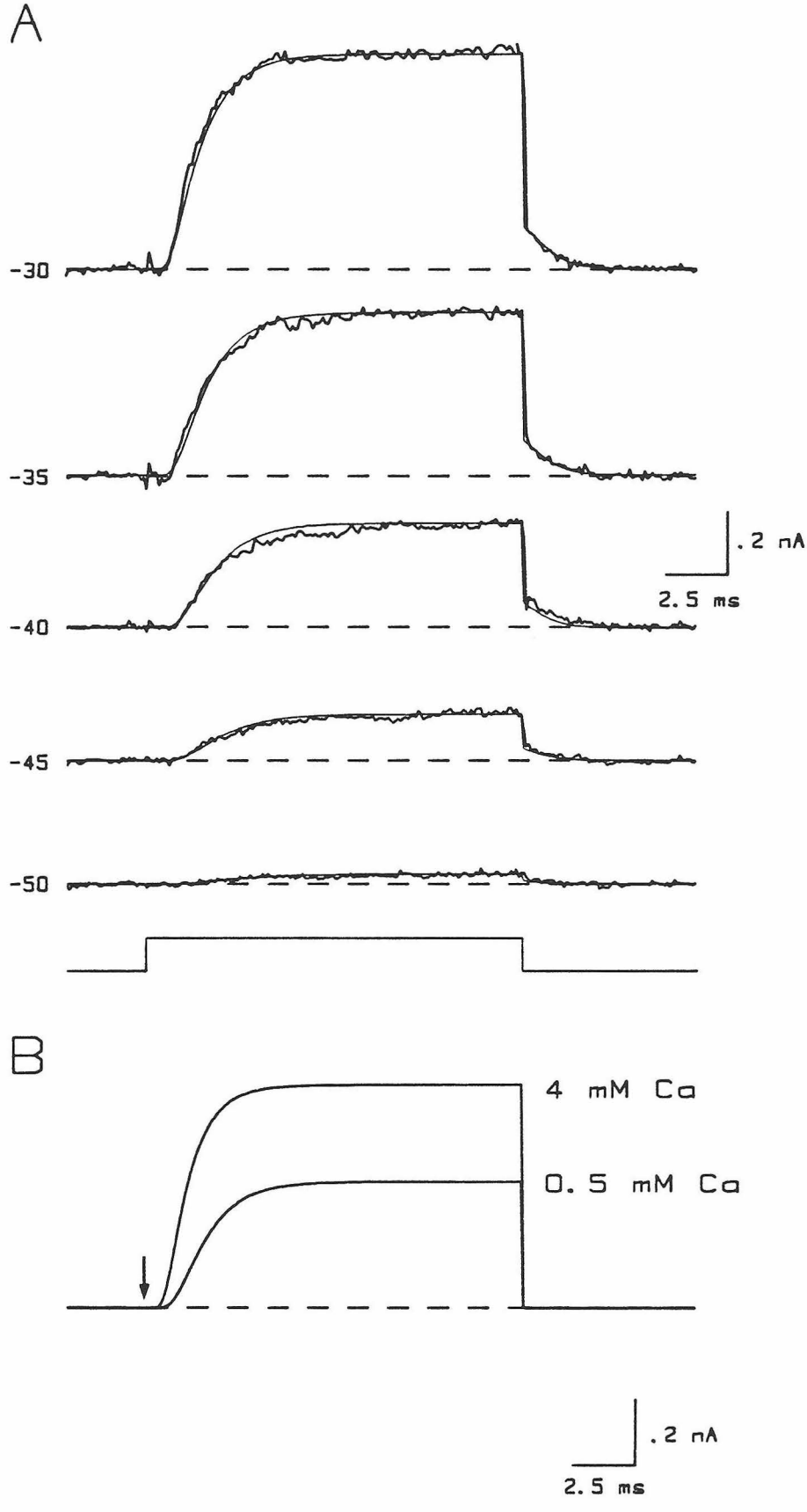
A
-30
-35
-40
-45
-50
.2 nA
2.5 ms
B
4 mM Ca
0.5 mM Ca
.2 nA
2.5 ms

Because quantitative constraints on the channel's sensitivities to both parameters were not available, the model's assumptions of Ca- and voltage-sensitivities of G_c were tested by simulating the effect on I_c of lowering external Ca concentration under voltage clamp conditions. Fig. 22B shows the model's prediction of I_c in response to a voltage step from -80 mV to -30 mV under simulated conditions of 4 mM and 0.5 mM external Ca. Experimentally, the low-Ca condition reduces $I_{c,a}$ under voltage clamp to about 25% of its value in 4 mM Ca; therefore, the low-Ca condition was simulated by setting $G_{c,a}$ to 25% of its normal value. For this condition the model predicts a slower rate of I_c activation (including a longer onset latency), as well as a 43% decrease in steady-state I_c. These results are consistent with the slower I_c kinetics and 37% decrease in steady-state I_c observed experimentally under similar conditions (see Fig. 11). Thus, it appears that the parameter values chosen for model II provide a good description of the relative degrees of Ca and voltage dependence of the C conductance observed in whole cells.

Model II predictions of voltage oscillations under current clamp

Given the evidence presented above that model II provides an accurate description of Ca and C conductances under voltage-clamp conditions, the model can be used to test the sufficiency of these two conductances (plus leakage conductance) in generating electrical resonance properties. This test is shown in Fig. 23, in which experimentally observed hair-cell responses to applied current pulses are compared with the corresponding predictions of the model. Fig. 23A shows the membrane

voltage of a cell in response to three pairs of depolarizing/hyperpolarizing current pulses. Note the pronounced rectification around resting potential (cf. Corey & Hudspeth, 1979), which leads to larger hyperpolarizations than depolarizations in response to current steps of equal but opposite values. The corresponding predictions of model II are shown in Fig. 23B. The similarities between these predictions and the responses in Fig. 23A are striking, especially considering that a different cell from the one of Fig. 23A was used to constrain the parameter values in the model. In particular, the model predicts a resting potential of -50 mV, which is within the range observed for isolated hair cells, and the strong rectification around resting potential. Most significantly, however, the model predicts damped voltage oscillations in response to the onset of depolarizing current pulses and the termination of depolarizing or hyperpolarizing pulses. As is experimentally observed, oscillation frequency increases with depolarization, and the frequency of oscillations following the current pulse is independent of the size of the preceding pulse, thereby indicating the "natural" resonant frequency. *The ability of the model to predict voltage oscillations clearly shows that the Ca, C, and leakage currents interact to produce electrical resonance in the hair cell.*

Two differences are evident between observed and predicted responses in Fig. 23 which may be attributable to differences in the magnitudes of $\bar{G}_{Ca}$, $\bar{G}_{c}$, and G_{L} among cells. First, the predicted membrane resistance and time constant for hyperpolarizations were greater than observed; to produce hyperpolarizations of about the same magnitude, current steps of -17, -34, and -51 pA were used in the model vs. -40, -80, and -120 pA for the cell. These differences could be accounted for

Figure 23. Model II predictions of electrical resonance in the hair cell under current clamp. *A*, Responses of a solitary hair cell to 50-msec current steps of (bottom to top) -120, -80, -40, 40, 80, and 120 pA from 0 pA holding current. The hyperpolarizations (single traces) have been separated from the depolarizations (averages of 2 responses each) for clarity. Note the pronounced rectification around the resting potential (-51 mV). Cell 59; repetition interval = 1 sec; sampling interval = 0.4 msec; internal = K aspartate; external = standard saline. *B*, Model II predictions of the responses to current steps of -51, -34, -17, 17, 34, and 51 pA from 0 holding current. The predictions closely resemble the experimentally observed responses in *A*. Most importantly, the model predicts damped oscillations upon depolarization, or upon the termination of a depolarizing or hyperpolarizing current pulse, indicating that the Ca, C, and leakage conductances can account for the electrical resonance properties of the hair cell.

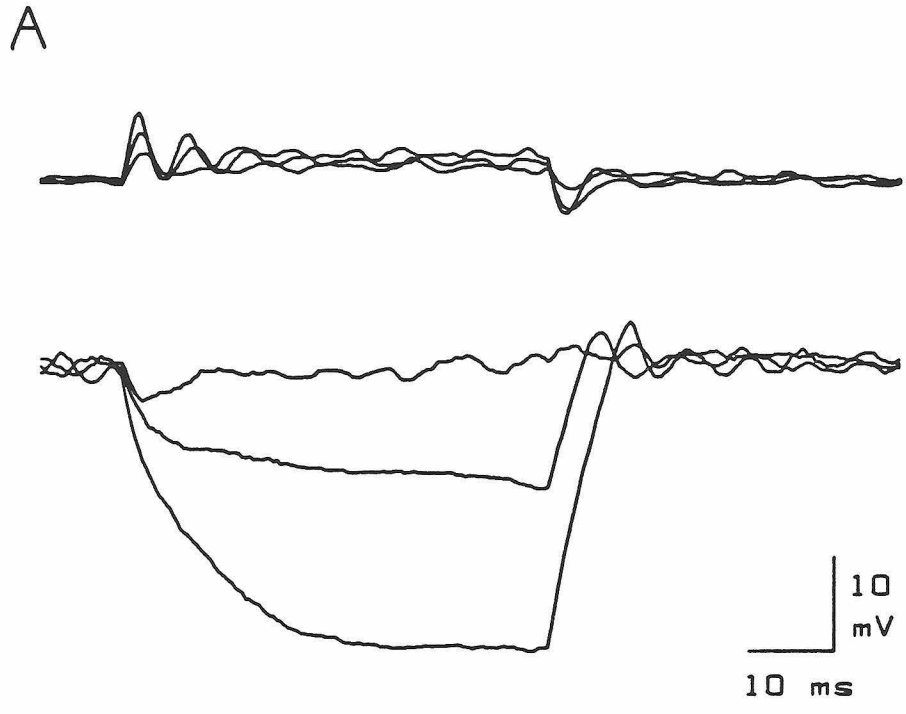
A
10
mV
10 ms

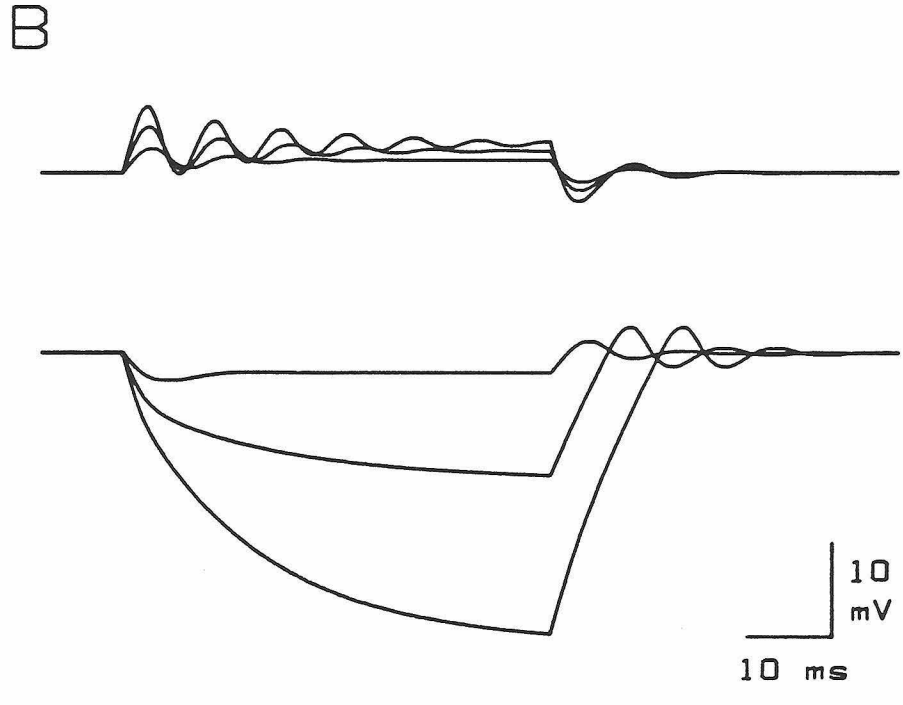
B
10
mV
10 ms

if the leakage conductance in the cell used to constrain the model was lower than that of the cell in Fig. 23A. The second difference is that the oscillation frequencies predicted by the model are somewhat lower than those observed, which may be due to the fact that $\bar{G}_{Ca}$ and particularly $\bar{G}_{C}$ were smaller in the cell used for modeling (cell 36) than in many of the hair cells I have studied. Of six cells from which both I_{Ca} and I_{C} were measured under voltage clamp, I_{Ca} in cell 36 was 92% and I_{C} was 44% of the respective average amplitudes at -30 mV. Increasing $\bar{G}_{Ca}$ and $\bar{G}_{C}$ in the model to compensate for these differences raises the natural resonant frequency to within the experimentally observed range (see Discussion).

Predicting the effects of TEA and lowered external Ca concentration on electrical resonance using model II

Model II's ability to predict voltage oscillations in response to extrinsic current pulses under standard ionic conditions strongly supports the idea that Ca, C, and leakage conductances underlie electrical resonance in the hair cell. A more stringent test of this idea and of assumptions made in the model was afforded by a comparison of electrical resonance characteristics of hair cells exposed to TEA or lowered Ca with the model's predictions under these simulated conditions. Simulated conditions of 1 mM TEA or 0.5 mM Ca were chosen to allow comparisons between the model and experimental results shown in Figs. 4 and 5. Since 1 mM TEA blocks about half of the C current evoked in voltage-clamp experiments, this treatment was simulated by lowering the maximal C conductance, $\bar{G}_{C}$, by half. Similarly, lowering external Ca to 0.5 mM de-

creases I_{ca} under voltage clamp by about 75%; to simulate this condition $\bar{G}_{ca}$ was lowered by the same amount. The model-generated responses to depolarizing current pulses under these two conditions as well as standard conditions (Fig. 24A) showed a number of similarities to the experimental results of Figs. 4 and 5. The model predicted voltage oscillations that were approximately exponentially damped under all three conditions, and predicted a resting potential shift of +2.8 mV in TEA and +5 mV in low Ca, close to the respective +3 mV and +9 mV shifts observed experimentally (see Fig. 4).

For the standard saline condition the model predicted an increase in oscillation frequency with membrane voltage (Fig. 24B). For small depolarizations the frequency rose at a rate of 18 Hz/mV from a value of 88 Hz (the natural resonant frequency) at resting potential. For larger current pulses the frequency approached a limiting value of 145 Hz with the cell depolarized about 6 mV from rest. These predictions of natural resonant frequency, maximum f/V slope, and the asymptotic relation between frequency and voltage, were all within the observed range of experimental results (see Figs. 2, 3, and 5). The predicted frequency range of oscillations was somewhat smaller than was usually observed in hair cells, but can be explained by the comparatively low magnitude of C conductance in the cell used in the modeling; doubling $\bar{G}_c$ in the model increased the limiting frequency to 200 Hz. The model also predicted a peaked relation between tuning sharpness, denoted by Q_e, and membrane voltage; Q_e rose from 1.9 at resting potential to a maximum of 11.7, with the cell depolarized about 5 mV from rest (Fig. 24C). The maximum Q_e values observed in experiments were generally lower and occurred at voltages closer to resting potential; however, both of these differences

Figure 24. Model II predictions of the effects of external TEA or lowered Ca concentration on electrical resonance behavior. Model II parameters are listed in Table 2; to simulate the external conditions of 1 mM TEA or 0.5 mM Ca, G_c was set to 50% of its normal value, or $G_{c,e}$ to 25% of normal, respectively. Responses to 50-msec current pulses of 10 to 190 pA amplitude in 10-pA increments were generated, and responses were analyzed by a method similar to the one described in Fig. 2. *A*, Modeled responses to current pulses of four amlitudes in the presence of standard saline, 1 mM TEA, or 0.5 mM Ca externally. Current-pulse amplitudes are listed at the far right. The oscillatory response to extrinsic current pulses was diminished by both TEA and lowered Ca. In addition, resting potential was shifted from a value of -50.1 mV in standard saline to -47.3 mV in TEA or -45.1 mV in low Ca. These results are similar to the data shown in Fig. 4. *B*, Predicted effects of TEA and lowered external Ca on oscillation frequency. In standard saline, frequency increased with depolarization in an approximately exponential manner; a plot of the function $f = 152-127 \exp(-(V+52)/2.89)$ has been superimposed on the data. TEA lowered the oscillation frequencies by lowering the sensitivity of frequency to voltage; the slope near resting potential was 7.3 Hz/mV, compared with 18.3 Hz/mV in standard saline. Lowered external Ca diminished frequencies with a moderate decrease in the maximum slope to a value of 12.0 Hz/mV. These results, particularly those obtained for depolarizations of less than 5 mV, are comparable to experimental results in Fig. 5A. *C*, Predicted effects of TEA and lowered external Ca on electrical quality factor, Q_e. For standard saline, the model predicted a bell-shaped relation between Q_e and voltage. Both TEA and lowered external Ca decreased the values of Q_e for the range of ap-

plied currents. These model results are partially consistent with experimental results of Fig. 5B; some of the discrepancies may be due to variations in the magnitudes of ionic conductances among cells.

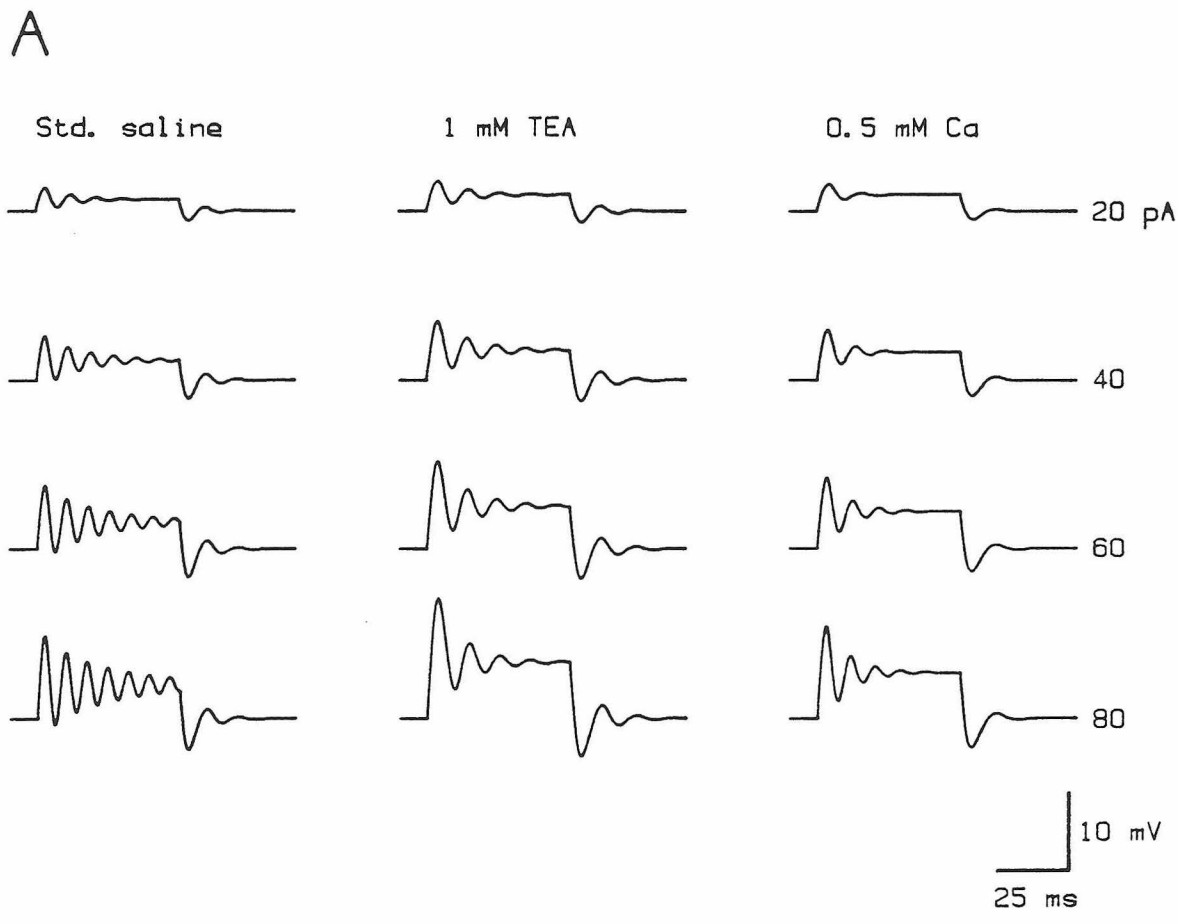
A
Std. saline
1 mM TEA
0.5 mM Ca
20 pA
40
60
80
10 mV
25 ms

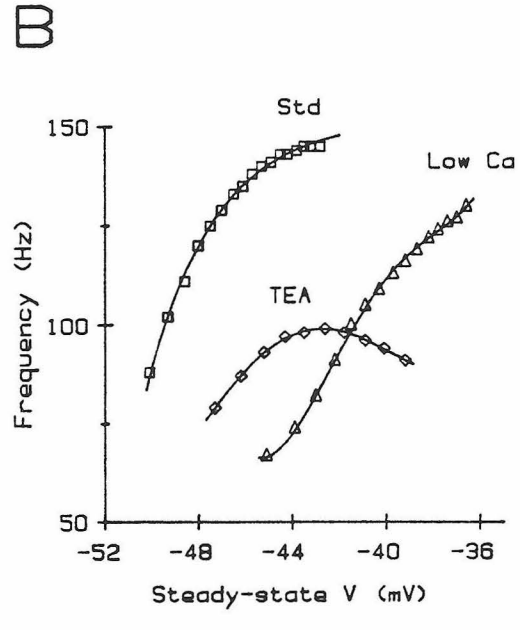
B
Std
Low Ca
TEA
150
100
50
Frequency (Hz)
-52
-48
-44
-40
-36
Steady-state V (mV)

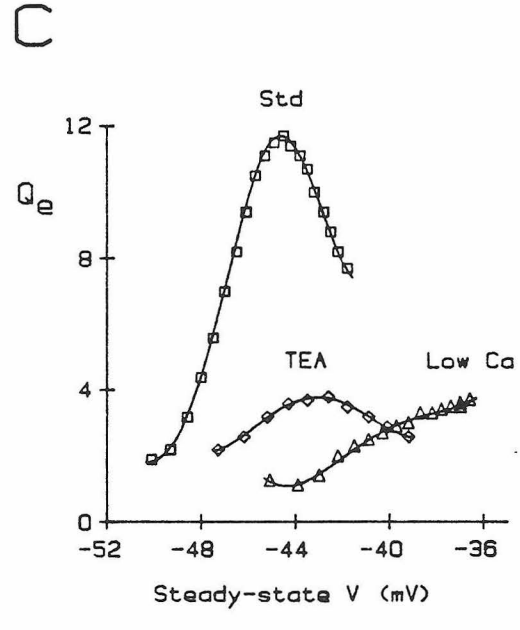
C
Std
12
8
4
0
Q_e
TEA
Low Ca
-52
-48
-44
-40
-36
Steady-state V (mV)

could be removed by doubling G_L in the model.

The model's predictions of TEA effects on oscillation frequency and tuning were also consistent with experimental observations. The simulated TEA treatment lowered the range of evoked oscillation frequencies primarily by decreasing the sensitivity of frequency to voltage (Fig. 24B); the f/V slope near resting potential was 7 Hz/mV, the same value measured in the experiment of Fig. 5B. For depolarizations greater than about 6 mV, the model predicted a decrease in frequency; although this cannot be compared to experimental results, as cells were never depolarized to this extent in the presence of TEA, it may indicate inaccuracy of the model for high levels of applied current. The TEA simulation also lowered Q_e (Fig. 24C) as expected on the basis of experimental results (see Fig. 5B).

The model's predictions of low-Ca effects on resonance were partially consistent with experimental observations. For each value of applied current, the predicted frequency in Fig. 24B was lower than that in standard saline (the same was observed for the cell of Fig. 4). However, the maximum f/V slope was decreased to 12 Hz/mV, in contrast to the slight increase in slope observed in Fig. 5A. Although the model correctly predicted a decrease in Q_e in response to lowered Ca (Fig. 24C), the sensitivity of Q_e to voltage was not as high as that predicted for the standard saline condition; roughly equal sensitivities would have been expected from the data of Fig. 5B. The cause of these minor discrepancies is not known, but might be related to the lower than expected shift in the resting potential predicted by the model under low-Ca conditions.

Emergence of electrical resonance properties from the interaction of ionic currents in the hair cell

The biophysical "source" of electrical resonance in the hair cell may be understood by considering model II's predictions of ionic currents and intracellular Ca concentration during voltage oscillations, shown in Fig. 25. Because the cell is essentially isopotential, no longitudinal current can flow, and therefore at all times the sum of ionic and capacitive currents is equal to the extrinsic current applied through the patch electrode, I_{app} (see equation (22)). When I_{app} is zero, the sum of inward I_{Ca} and I_L is equal and opposite to outward I_c, such that the total ionic current, I_{ion}, is also zero; this condition defines the resting potential. The applied current pulse acts initially to charge up the membrane capacitance and appears as a capacitive current equal to $I_{app}-I_{ion}$. As the membrane depolarizes, voltage-dependent I_{Ca} is further activated, causing a rise in intracellular Ca which, after a short delay, activates an increased level of I_c. Now, because I_c increases at a higher rate than I_{Ca}, it soon exceeds the magnitude of inward I_{Ca}, making I_{ion} positive; in this way, the large magnitude of I_c keeps inward ionic current from increasing regeneratively, thus preventing the occurrence of a Ca action potential. At some point I_{ion} increases to the level of I_{app}, at which time capacitive current, and hence dV_m/dt, is zero, and a voltage peak is attained. Crucial to the mechanism of oscillations is that, due to the delays between voltage change and I_c change, *I_c continues to increase*; I_{ion} therefore becomes more positive than I_{app}, causing the cell to hyperpolarize. As membrane potential becomes more negative, I_{Ca} decreases, and the resulting fall

Figure 25. Description of the biophysical mechanism for electrical resonance in terms of ionic currents. Response of model II to a 100-pA current step, showing the time courses of extrinsic applied current (I_{app}), membrane potential (V_m), Ca, C, and leakage currents (I_{Ca}, I_c, and I_L), the total ionic current ($I_{ion}=I_{Ca}+I_c+I_L$), and intracellular Ca concentration adjacent to the membrane ($[Ca]_i$). Dashed lines indicate zero current and Ca concentration, or resting potential (bottom trace). The current pulse, I_{app}, depolarizes the membrane, activating I_{Ca}, which increases $[Ca]_i$, which in turn activates I_c. When $I_{ion}=I_{app}$, the first peak in V_m is reached; further activation of I_c beyond this time causes I_{ion} to exceed I_{app}, leading to hyperpolarization. Similarly, when I_{ion} subsequently decreases to the level of I_{app}, the first minimum of V_m is reached, but the further decrease in I_c beyond this time causes I_{ion} to fall below I_{app}, and the membrane depolarizes again. Thus, the time lags between changes in membrane voltage and changes in I_c, and to some extent I_{Ca}, activation, are largely responsible for the oscillatory responses characteristic of electrical resonance in the hair cell.

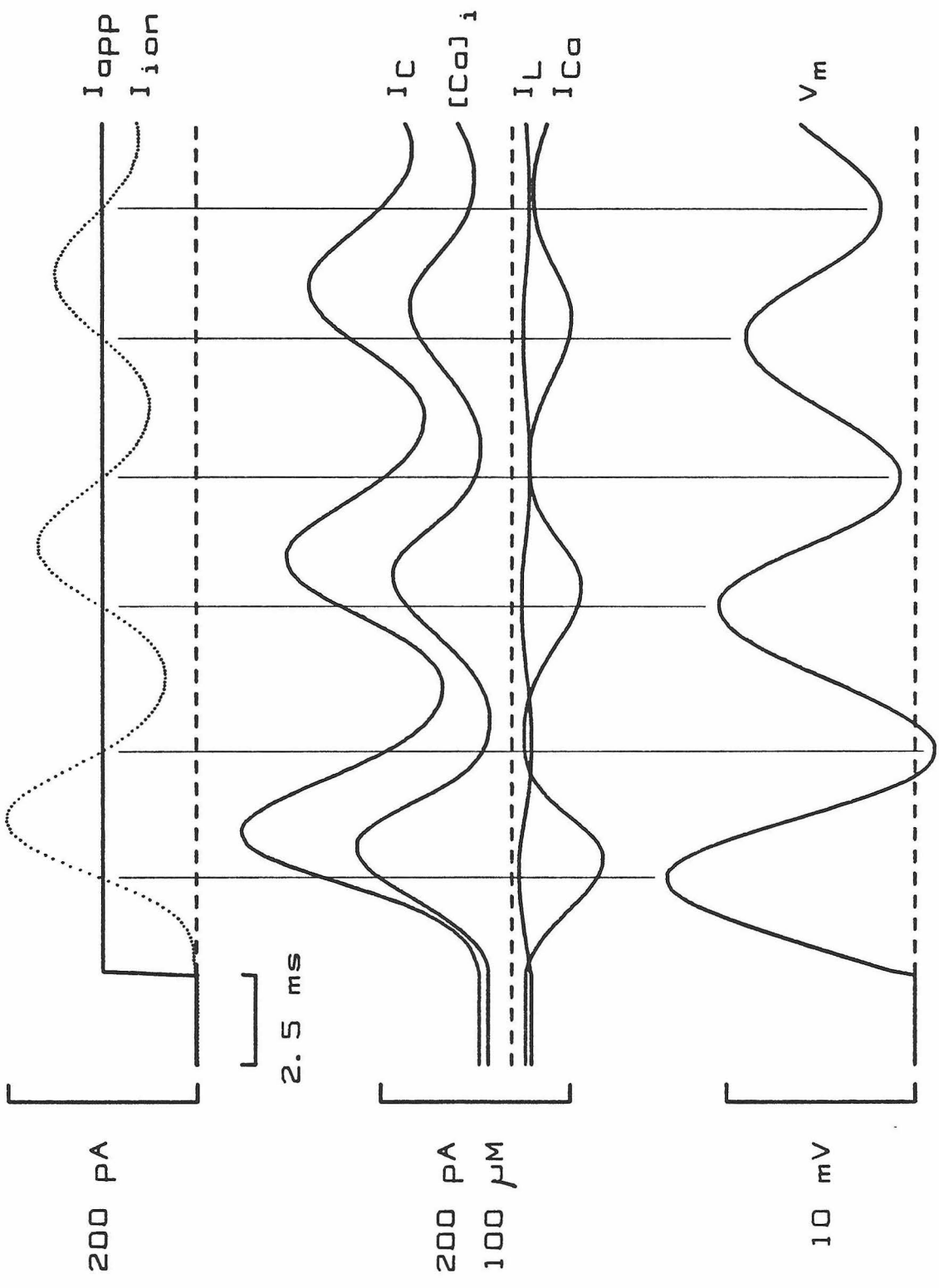
I_{app}
I_{ion}
I_C
$[Ca]_i$
I_L
I_{Ca}
V_m
2.5 ms
200 pA
200 pA
100 μM
10 mV

in intracellular Ca turns off I_c. At a later time I_{ion} falls to the level of I_{app}, at which point membrane potential reaches a minimum. However, *I_c continues to decrease* beyond this point, such that I_{ion} is less than I_{app}, thereby causing the membrane to depolarize again. Changes in membrane voltage are produced by the difference between I_{app} and I_{ion}, and therefore all three ionic currents play a role in producing the oscillations. However, because of its large size relative to I_{Ca} and I_L, I_c tends to dominate the total ionic current; viewed in this way, it appears that the relatively long lag time between changes in voltage and changes in I_c (also see Fig. 10), resulting in part from time-dependent I_{Ca} activation and intracellular Ca regulation processes, is largely responsible for generating electrical resonance in the hair cell.

What properties of the system account for the damping of voltage oscillations? In order for oscillations to persist indefinitely during the application of extrinsic current, I_{Ca}, I_c, I_L, and $[Ca]_i$ must all be at their resting values each time the membrane potential passes through resting potential. Under most conditions, this criterion is not met; in Fig. 25 it is evident that, due to delays in the deactivation of I_c, it cannot decline fully to its resting level before membrane potential ascends through resting potential. The effect is cumulative; because I_c starts at a higher value at the beginning of the second cycle than the first, the membrane potential changes less rapidly, and V_m for the second peak is lower than that for the first.

DISCUSSION

Electrical resonance arises from the interaction of Ca and Ca-activated K currents

The property of electrical resonance is demonstrated in hair cells from the bullfrog's sacculus by the damped voltage oscillations elicited by applied pulses of extrinsic current. Through voltage-clamp experiments on solitary hair cells, three ionic conductances have been identified that are active in the same voltage range in which oscillations occur: a Ca conductance, an A-type K conductance, and a Ca-activated K (or "C") conductance. Degradation of resonance behavior by treatments that inhibit I_{Ca} or I_c, and the lack of effect upon blocking I_A, suggests that only the first two currents are involved in generating electrical resonance. The steady-state inactivation of I_A at resting potential argues further that I_A does not play a significant role in producing voltage oscillations.

Modeling hair cell responses under current- and voltage-clamp conditions shows in addition that the Ca and C conductances are *sufficient* to account for the phenomenon of electrical resonance; after being constrained to fit the observed waveforms of whole-cell I_{Ca} and I_c at a series of voltages, model II correctly predicts the characteristics of voltage oscillations under current clamp, including the dependencies of oscillation frequency and tuning sharpness on membrane potential. Thus, as was concluded earlier from the occurrence of voltage oscillations in cells lacking a hair bundle, there is no need to invoke electromechanical feedback (Weiss, 1982) to account for the hair cell's electrical

resonance. These results do not, however, rule out such a process in hair cells from other organs or species, e.g., in the mammalian cochlea, where an active mechanical process is thought to be part of the tuning mechanism (Kim, 1980; Neely & Kim, 1983).

Is model II an accurate description of the hair cell?

In addition to showing the sufficiency of I_{Ca} and I_c in accounting for electrical resonance, the development of model II has added to an understanding of the resonance mechanism by providing a description of the time courses of processes underlying the oscillations (see Fig. 25). The model can also be used as a predictive tool, to simulate conditions that may be difficult to achieve experimentally, such as increasing the relative numbers of ionic channels in a cell or changing the properties of intracellular Ca regulation. To apply the model in these ways, one must recognize to what extent the model is a realistic description of the hair cell.

Ca current activation was described empirically by model II in terms of a simple third-order Hodgkin-Huxley scheme. This description is adequate for the purposes of modeling I_{Ca} in the voltage range of -70 to -30 mV, but is unlikely for two reasons to provide accurate predictions at voltages outside this range. First, exponential functions were used to describe the dependencies of α_m and β_m on voltage, but both rates must eventually reach maximal values at or below the limiting rate for a protein conformational change. Second, at positive membrane potentials the current-voltage relation of open Ca channels is expected to be highly nonlinear, due to the extreme asymmetry of Ca concentration across

the membrane (Hagiwara & Byerly, 1981). However, both of these potential sources of error are unlikely to be important in the physiologically relevant voltage range. The Ca-current reversal potential, E_{Ca}, was assumed to have a constant value, even though it must decrease as intracellular Ca accumulates. However, the decrease in I_{Ca} due to the accumulation of 100 μM internal Ca, calculated using the constant-field equation (Hodgkin & Katz, 1949), is less than 1% at -30 mV. E_{Ca} was given a constant value to account for the constancy of driving force on Ca in the presence of changing levels of internal Ca.

The equilibrium potential for the leakage conductance, E_L, was not measured directly; it was guessed to be about -30 mV. However, varying the assumed value of E_L between 0 and -60 mV did not significantly affect the characteristics of resonant behavior predicted by the model.

Model II's description of C-channel gating involves more uncertainty than that of the Ca channel, due to the dual dependence of C-channel activity on intracellular Ca concentration and membrane potential, and the fact that Ca concentration next to the inner surface of the membrane cannot be measured directly during voltage clamp steps. Experiments on single C channels were used to develop a five-state gating scheme for the channel, similar in form to one proposed recently for the C channel in rat myotubes (Magleby & Pallotta, 1983). Unfortunately, variations in the kinetic behavior and the Ca- and voltage-sensitivities among C channels and with time for single C channels, coupled with the infrequent occurrence of single-channel patches, precluded consistent quantitative estimates of rate constant values in the scheme. Kinetic heterogeneity and instability appear to be common properties of C channels from rat muscle (Methfessel & Boheim, 1982; Moczydlowski & Latorre, 1983) and

could reflect very slow gating processes, chemical modifications of the channel (De Peyer et al., 1982), or other molecular heterogeneity in the C-channel population. Although the results of single-channel experiments provided rough constraints on parameter values, there remained a large degree of arbitrariness in adjusting the values of the remaining free parameters to fit whole-cell I_c data. Moreover, one of the constraints, pertaining to the transition rates between the two open states, had to be relaxed to obtain good predictions of I_c; the final values for the rates of Ca binding and unbinding from the open states were too low to predict the observed single-exponential distribution of channel open lifetimes. This discrepancy might have been avoided by making one or more of the reverse rate constants (k_{-1}, k_{-2}, or k_{-3}) voltage-dependent, or by introducing a time-dependent term to describe intracellular Ca diffusion (discussed below), but this was not attempted because of the increased number of free parameters such changes would introduce into the model. Clearly more data are needed on the behavior of the hair cell's C channel to specify its gating scheme more precisely. Unfortunately, the rate constants in the gating scheme of Magleby and Pallotta (1983) do not account for the voltage dependence of transition rates, and therefore could not be applied; attempts to predict the observed waveform of I_c using the four-state scheme of Moczydlowski and Latorre (1983), which does include voltage dependence, were unsuccessful,

With the rather large degree of arbitrariness in the choice of parameter values in scheme (S1), it was reassuring that model II can successfully predict the observed changes in I_c brought about by a decrease in extracellular Ca under voltage clamp (see Figs. 11 and 22). This result indicates that the model's description of C-channel gating,

although probably not complete, is nonetheless adequate to account for the relative Ca- and voltage-sensitivities of the channel.

Model II includes a simple description of the regulation of intracellular Ca next to the membrane (see Methods); since the time course of membrane Ca concentration during voltage-clamp pulses could not be measured directly, precise constraints could not be applied to the values of Ca-regulation parameters. Initially, I sought to develop a description of C-channel behavior in excised membrane patches that was sufficiently detailed to allow the estimation of the the time course of intracellular Ca concentration from the whole-cell I_c during a voltage-clamp step. In other words, after "calibrating" the C channel under controlled conditions in excised membrane patches, one could use it as a Ca electrode in the cell. Although this goal was not achieved, ruling out a direct test of the assumptions made about intracellular Ca regulation, a variety of evidence suggests that the model is a reasonable approximation. In order to produce the high levels of internal Ca needed for C-channel activation given the size of I_{Ca}, Ca was assumed to be confined to a small fraction of the cell's total volume. The effective Ca diffusion coefficient in cytoplasm is lowered by the reversible binding of Ca to intracellular buffers (Hodgkin & Keynes, 1957), and this could serve to confine incoming Ca to a small volume near the membrane. In fact, a spatial gradient of Ca has been observed experimentally following Ca influx through Ca channels in molluscan neurons (Smith & Zucker, 1980; Levy et al., 1982) and has also been predicted from a model incorporating many of the known features of intracellular Ca regulation (Smith, 1978; Smith & Zucker, 1980). Additional evidence for the confinement of Ca next to the membrane comes from observations of the C current in hair cells for

which the Ca current was unmeasurably small (see Figs. 11 and 12). I_c in these cells could be blocked by bath-applied Ca-channel blockers, suggesting that Ca entered the cell too slowly to carry an appreciable current, but accumulated to moderate levels next to the membrane to activate I_c. Alternatively, a small influx of Ca might have caused the release of a larger amount of Ca from intracellular storage sites, thereby amplifying the submembrane Ca concentration to a level sufficient to activate I_c. This type of Ca release mechanism has been studied in the sarcoplasmic reticulum of muscle (Ohnishi, 1979). The time necessary for Ca to diffuse from its site of entry, the Ca channel, to its target, the C channel, was not included in the model for reasons of simplicity, although this diffusion time is likely to contribute to the delays between activation of I_{Ca} and I_c (see Fig. 10). The average distance, $\bar{x}$, that Ca diffuses in a time Δt is given by Einstein's diffusion equation, $\bar{x}^2 = 2 \cdot D \cdot \Delta t$, where D is the Ca diffusion coefficient in the cytoplasm (Eisenberg & Crothers, 1979). Given an estimate for D of about $6 \cdot 10^{-7}$ cm^2/sec (Hodgkin & Keynes, 1957), Ca could diffuse an average distance of only 0.3 μm in the time between activation of I_{Ca} and I_c. The onset latency of I_c was considered to be entirely the result of time-dependent transitions among closed states of the C channel; including a term to describe Ca diffusion time would remove some of the restrictions that this assumption imposed on the choice of values for C-channel rate constants. The actual contribution of Ca diffusion time to I_c kinetics cannot be accurately estimated, as it depends on the average distance between Ca channels and C channels, which is not known.

The ideal test of model II as a description of electrical resonance mechanism would have been to use the voltage-clamp data from a cell to

constrain parameter values of the model and reconstruct, using the model, current-clamp data from the same cell. This was not possible because of the short lifetimes of hair cells in the whole-cell clamp configuration (see Methods), which necessitated pooling data that were collected from a number of cells. As already noted in the Results, differences in the Ca, C, and leakage conductances among cells could account for minor discrepancies in oscillation frequency and tuning between predicted and experimentally observed responses. In addition, the ensemble variance estimates of the open-state C-channel probability under whole-cell voltage clamp may have differed from the true value for the cell used in modeling (cell 36), as this cell produced a comparatively small C current. However, inspection of C tail-current amplitudes in cell 36 supported the conclusion that most of the cell's C channels were activated at -30 mV.

To test model II in light of the assumptions discussed above, the predicted effects of TEA and lowered external Ca on electrical resonance behavior were compared with experimental results. Within the limits set by conductance differences among cells, the model generated adequate predictions of the effects of both treatments on the frequency and Q_e of oscillations evoked by small current pulses. These results suggest that, although the model contains a number of simplifying or arbitrary assumptions, it is nevertheless a reasonable description of the resonance mechanism.

Can the model account for electrical resonance properties in other cells of the acousticolateralis system?

There is a growing amount of evidence which suggests that electrical resonance is a widespread phenomenon among receptor cells of the acousticolateralis system in different species. These observations include current-evoked voltage oscillations in hair cells from the turtle cochlea (Crawford & Fettiplace, 1981a) and the sacculus of bullfrog (Lewis & Hudspeth, 1983a) and leopard frog (Ashmore, 1983), extracellular potential oscillations from tuberous electroreceptors (Bennett, 1971), and spontaneous discharge patterns of auditory nerve fibers in the Tokay gecko (Eatock et al., 1981) and the starling (Manley, 1979) which may indirectly reflect oscillatory hair-cell potentials. Because of the homology among the receptor cells of these preparations, one might expect the operation of a common resonance mechanism. Indeed, a variety of experimental observations suggest that a mechanism of the type described here for bullfrog saccular hair cells also produces electrical resonance in these other cells.

Nerve fibers innervating the tuberous electroreceptors of gymnotoid fish respond best to alternating electric fields at frequencies of 50 to 1200 Hz, depending on species (Hopkins, 1976). In *Sternopygus* the electroreceptors produce oscillatory potentials at 70 to 200 Hz in response to a pulse of transepithelial current, and Ca-channel blockers (Co, Mg) or a K channel blocker (TEA), applied to the basal surfaces of these cells, reduce the oscillations *in vitro* (H. Zakon, manuscript in preparation). Both the frequency range and pharmacological sensitivity of the oscillations are similar to those of voltage oscillations in

bullfrog hair cells, and therefore may indicate a common mechanism. Interestingly, the resonant frequency of these electroreceptors can be lowered as much as 60 Hz by systemic injections of androgens; whether this is a direct effect of hormone on the receptors or a secondary one caused by a change in the frequency of electric organ discharge is not yet clear (Meyer & Zakon, 1982).

Electrical resonance properties have also been demonstrated in saccular hair cells from *Rana pipiens* by current-evoked and spontaneous membrane-potential oscillations (Ashmore, 1983). The resonance at resting potential was characterized by frequencies of 11 to 85 Hz and Q_e values of 0.7 to 3, and external addition of 1 mM Co abolished the oscillations. The tuning sharpness and pharmacological sensitivity are both consistent with corresponding observations in the bullfrog, while the upper limit of the frequency range overlaps with the lower frequency limit observed in solitary bullfrog hair cells. These lower frequencies in *R. pipiens* may indicate a species difference in membrane properties, e.g., a lower number of Ca and/or C channels per cell compared to *R. catesbeiana*, but membrane damage from microelectrode impalement can also cause a decrease in resonant frequency (see Appendix).

The resonance characteristics of hair cells from the turtle's cochlea have been studied extensively (Crawford & Fettiplace, 1980, 1981a,b) and show a number of similarities to those of bullfrog saccular hair cells. In response to extrinsic current pulses turtle hair cells exhibit damped voltage oscillations whose frequency increases steeply with membrane depolarization, and which are abolished by TEA applied to the basal membrane surface. The sharpness of electrical tuning and its dependence on membrane voltage are also comparable between the two spe-

cies (peak Q_e's in bullfrog are typically around 8; those in turtle are around 5). However, Q_e for turtle hair cells reaches a maximum at a voltage slightly negative to resting potential, while in bullfrog hair cells it peaks slightly positive to resting potential. Correspondingly, hair-cell resting potential in the turtle is situated in the high-conductance limb of the membrane's I/V relation (R. Fettiplace, personal communication), while bullfrog hair cells rest close to the juncture between low and high conductance regions. These differences may be explained by the different ionic conditions in the two experimental preparations. The turtle experiments were performed on hair cells *in situ*, for which the apical and basal membrane surfaces were respectively contacted by high-K endolymph and an artifical 4 mM-K perilymph; in contrast, both surfaces of the bullfrog hair cells were bathed in a 2 mM-K saline resembling perilymph. If there are any K channels in the apical membrane, the low-K saline will hyperpolarize bullfrog hair cells relative to their resting potential *in vivo*.

The major difference between hair cells of turtle cochlea and bullfrog sacculus concerns the frequency range of electrical tuning. Turtle cochlear hair cells exhibit natural resonant frequencies of less than 100 Hz to greater than 400 Hz (and probably extending to about 1 kHz), while the tuning of bullfrog saccular hair cells at their resting potential is restricted to frequencies of about 80 to 160 Hz. Since the electrical resonance in the two species is similar in most other respects, the question arises as to whether the mechanism producing resonance in the bullfrog's sacculus can be changed simply to produce oscillations in the range of frequencies observed in the turtle's cochlea. For this purpose, I observed the effects of systematic variations of

$\bar{G}_{Ca}$, $\bar{G}_C$, G_L, and C_m in model II on its predictions of natural resonant frequency at a resting potential of -50 mV. Changing G_L had no significant effect on oscillation frequency and was raised only to offset the hyperpolarization of the resting potential caused by increasing $\bar{G}_C$ or $\bar{G}_{Ca}$. Lowering C_m from 15 pF to 10 pF raised the frequency by less than 10%. In contrast, the resonant frequency was increased substantially by elevating $\bar{G}_C$ alone or in combination with $\bar{G}_{Ca}$; multiplying $\bar{G}_C$ by four, or $\bar{G}_C$ and $\bar{G}_{Ca}$ by two, raised the frequency to 200 Hz. Thus, moderate changes in the numbers of C channels and/or Ca channels can account for the full range of natural resonant frequencies observed in bullfrog hair cells, and the lower portion of the frequency range observed for turtle hair cells. However, simple changes in the numbers of channels were inadequate to predict resonance at frequencies much higher than 300 Hz; variations in other parameters, such as the speed of intracellular Ca regulation, would probably extend the predicted frequency range beyond 300 Hz, but this has not been tested.

The surprising role of a Ca-activated K conductance in generating rapid voltage oscillations

Until recently, the sole function of the C conductance in excitable cells was considered to be the slow modulation of electrical activity in response to accumulation of intracellular Ca (for review, see Meech, 1978). This view arose from observations of slow hyperpolarizations following single action potentials in vertebrate neurons (Barrett & Barrett, 1976) and muscle fibers (Barrett et al., 1981) or following bursts of spikes in molluscan neurons (Junge & Stephens, 1973), which were at-

tributed to the activation of a Ca-dependent K conductance by Ca entering the cells during action potentials. In molluscan bursting neurons, interaction of the C conductance with a Ca conductance produces slow voltage oscillations that underlie the bursting pattern; although the ionic mechanism producing resonance in these cells is similar to the one in the hair cell, the resulting resonant frequency is over 1000 times slower. Voltage-clamp studies of these and other preparations have revealed correspondingly slow kinetic behavior of the C current. Indicator dye measurements of intracellular Ca concentration in these cells have shown that I_c activation and tail-current kinetics are limited by the time course of internal Ca concentration (Gorman & Thomas, 1978, 1980; Ahmed & Connor, 1979); consistent with these findings, the time course of C current in molluscan neurons can be successfully described by models in which the C conductance is assumed at all times to be in equilibrium with the concentration of internal Ca (Smith, 1978; Barish & Thompson, 1983). This type of model, represented by model I (see Methods), cannot accurately predict the kinetic behavior of the hair cell's C current at a series of voltages (see Fig. 14), implying that kinetic transitions of the hair cell's C channel occur on a time scale comparable to that of changing internal Ca concentration. This conclusion might also have been expected from the fact that I_c kinetics in the hair cell are several orders of magnitude faster than those in most other preparations (cf. Thompson, 1977; Meech & Standen, 1975).[1]

[1] Recently, a C current with kinetic behavior comparable to the hair cell's I_c has been reported in bullfrog sympathetic neurons, and its response kinetics are fast enough to involve it in terminating the action potential (Adams et al., 1982).

What is the underlying basis for the rapid kinetics of I_c in the hair cell? Although the gating kinetics of the hair cell's C channel may differ from those of other C channels, there are not yet enough data from the hair cell to permit a quantitative comparison. In any case, it seems more likely that the rapid kinetics of the cell's C current is the product of an unusually fast mechanism of intracellular Ca regulation. Indirect evidence supports the idea that Ca concentration in the hair cell is in fact controlled on a very rapid time scale. In the turtle, firing of auditory nerve fibers is phase-locked to cycles of an acoustic tone stimulus up to frequencies of 1 kHz (Crawford & Fettiplace, 1980). If Ca entering the cell during the depolarizing phase of the alternating receptor potential were to accumulate slowly with time, as occurs during bursts of action potentials in molluscan neurons (Gorman & Thomas, 1978), one would expect transmitter release from the hair cell to become more sustained during a long tone presentation, resulting in a time-dependent decrease in phase-locking of the postsynaptic response. Instead, the degree of phase-locking appears constant over time (Crawford & Fettiplace, 1980), supporting the notion that internal Ca in the hair cell is controlled on a rapid time scale.

Given the unusual role of the C conductance in high-frequency voltage oscillations in the hair cell, the question arises as to why such a mechanism might have evolved; i.e., what special properties accrue from a Ca-dependent mechanism that would not result from a purely voltage-dependent one? Ca dependence provides an additional level of control over resonance properties; modifications of the processes that regulate internal Ca, including buffers, pumps, and Ca channels, will affect resonant frequency and tuning of the cell. In addition, this link

to the internal level of Ca gives the system a short-term memory, for gradual accumulation of Ca during long periods of intense activity will raise the level of C conductance, producing a shunt that will temporarily lower tuning sharpness; the resultant decrease in sensitivity to sound or vibration could function as part of an adaptation mechanism. Finally, the Ca dependence of electrical resonance might play a role in the action of efferent input on hair-cell tuning. In the turtle, activation of direct efferent input to the hair cell causes an increase in K conductance of the hair-cell membrane, which hyperpolarizes the cell and quite effectively diminishes its electrical tuning properties (Art et al., 1982). The efferent transmitter is thought to be acetylcholine. Although a direct activation of a K conductance by the efferent transmitter is possible, an interesting alternative is that the transmitter causes release of Ca from large subsynaptic cisternae (observed by electron microscopy of bullfrog saccular hair cells) which then activates C channels in the plasma membrane. This kind of synaptic mechanism has been described recently for cells of rat lacrimal glands, in which application of carbamoylcholine indirectly activates a C conductance (Trautmann & Marty, 1984). This hypothesis for the mechanism of efferent inhibition could be tested by the further application of whole-cell recording techniques to hair cells isolated from the bullfrog's sacculus.

REFERENCES

Adams, P. R., Constanti, A., Brown, D. A. & Clark, R. B. (1982). Intracellular Ca^{2+} activates a fast voltage-sensitive K^+ current in vertebrate sympathetic neurones. Nature 296: 746-749.

Ahmed, Z. & Connor, J. A. (1979). Measurement of calcium influx under voltage clamp in molluscan neurones using the metallochromic dye arsenazo III. J. Physiol. 286: 61-82.

Art, J. J., Crawford, A. C., Fettiplace, R. & Fuchs, P. A. (1982). Efferent regulation of hair cells in the turtle cochlea. Proc. R. Soc. Lond. B 216: 377-384.

Ashmore, J. F. (1983). Frequency tuning in a frog vestibular organ. Nature 304: 536-538.

Atwater, I., Dawson, C. M., Scott, A., Eddlestone, G. & Rojas, E. (1980). The nature of the oscillatory behaviour in electrical activity from pancreatic β-cell. Horm. and Metab. Res. Suppl. Ser. 10: 100-107.

Bader, C. R., Bertrand, D. & Schwartz, E. A. (1982). Voltage-activated and calcium-activated currents studied in solitary rod inner segments from the salamander retina. J. Physiol. 331: 253-284.

Barish, M. E. & Thompson, S. H. (1983). Calcium buffering and slow recovery kinetics of calcium-dependent outward current in molluscan neurones. J. Physiol. 337: 201-219.

Barrett, E. F. & Barrett, J. N. (1976). Separation of two voltage- sensitive potassium currents, and demonstration of a tetrodotoxin- resistant calcium current in frog motoneurones. J. Physiol. 255: 737-774.

Barrett, J. N., Barrett, E. F. & Dribin, L. B. (1981). Calcium-dependent slow potassium conductance in rat skeletal myotubes. Dev. Biol. 82: 258-266.

Barrett, J. N., Magleby, K. L. & Pallotta, B. S. (1982). Properties of single calcium-activated potassium channels in cultured rat muscle. J. Physiol. 331: 211-230.

Bennett, M. V. L. (1971). Electroreception. In Fish Physiology, vol. 5, Hoar, W. S. & Randall, W. J., eds., Academic Press, New York, pp. 493-574.

Bers, D. M. (1982). A simple method for the accurate determination of free [Ca] in Ca-EGTA solutions. Am. J. Physiol. 242: C404-C408.

Blaustein, M. P. (1974). The interrelationship between sodium and calcium fluxes across cell membranes. Rev. Physiol. Biochem. & Pharmacol. 70: 33-82.

Blaustein, M. P., Ratzlaff, R. W. & Schweitzer, E. S. (1978). Calcium buffering in presynaptic nerve terminals. II. Kinetic properties of the nonmitochondrial Ca sequestration mechanism. J. Gen. Physiol. 72: 43-66.

Brinley, F. J., Jr. (1978). Calcium buffering in squid axons. Ann. Rev. Biophys. Bioeng. 7: 363-392.

Brinley, F. J., Jr., Tiffert, T. & Scarpa, A. (1978). Mitochondria and other calcium buffers of squid axon studied in situ. J. Gen. Physiol. 72: 101-127.

Byerly, L. & Hagiwara, S. (1982). Calcium currents in internally perfused nerve cell bodies of *Limnea stagnalis*. J. Physiol. 322: 503-528.

Chay, T. R. & Keizer, J. (1983). Minimal model for membrane oscillations in the pancreatic β-cell. Biophys. J. 42: 181-190.

Clusin, W. T. & Bennett, M. V. L. (1979). The oscillatory responses of skate electroreceptors to small voltage stimuli. J. Gen. Physiol. 73: 685-702.

Cole, K. S. (1941). Rectification and inductance in the squid giant axon. J. Gen. Physiol. 25: 29-51.

Cole, K. S. & Baker, R. F. (1941). Longitudinal impedance of the squid giant axon. J. Gen. Physiol. 24: 771-788.

Cole, K. S. & Curtis, H. J. (1941). Membrane potential of the squid giant axon during current flow. J. Gen. Physiol. 24: 551-563.

Colquhoun, D. & Hawkes, A. G. (1981). On the stochastic properties of single ion channels. Proc. R. Soc. Lond. B 211: 205-235.

Colquhoun, D. & Sigworth, F. J. (1983). Fitting and statistical analysis of single-channel records. In Single-Channel Recording, Sakmann, B. & Neher, E., eds., Plenum Press, New York, pp. 191-263.

Connor, J. A. & Stevens, C. F. (1971a). Voltage clamp studies of a transient outward membrane current in gstropod neural somata. J. Physiol. 213: 21-30.

Connor, J. A. & Stevens, C. F. (1971b). Prediction of repetitive firing behaviour from voltage clamp data on an isolated neurone soma. J. Physiol. 213: 31-53.

Corey, D. P. & Hudspeth, A. J. (1979). Ionic basis of the receptor potential in a vertebrate hair cell. Nature 281: 675-677.

Crawford, A. C. & Fettiplace, R. (1980). The frequency selectivity of auditory nerve fibres and hair cells in the cochlea of the turtle. J. Physiol. 306: 79-125.

Crawford, A. C. & Fettiplace, R. (1981a). An electrical tuning mechanism in turtle cochlear hair cells. J. Physiol. 312: 377-412.

Crawford, A. C. & Fettiplace, R. (1981b). Non-linearities in the responses of turtle hair cells. J. Physiol. 315: 317-338.

Dallos, P., Santos-Sacchi, J. & Flock, A. (1982). Intracellular recordings from cochlear outer hair cells. Science 218: 582-584.

Dallos, P. (1981). Cochlear physiology. A. Rev. Psychol. 32: 153-190.

DePeyer, J. E., Cachelin, A. B., Levitan, I. B. & Reuter, H. (1982). Ca^{2+}-activated K^+ conductance in internally perfused snail neurons is enhanced by protein phosphorylation. Proc. Nat. Acad. Sci. USA 79: 4207-4211.

Detwiler, P. B., Hodgkin, A. L. & McNaughton, P. A. (1980). Temporal and spatial characteristics of the voltage response of rods in the retina of the snapping turtle. J. Physiol. 300: 213-250.

Eatock, R. A., Manley, G. A. & Pawson, L. (1981). Auditory nerve fibre activity in the Tokay gecko. I. Implications for cochlear processing. J. Comp. Physiol. 142: 203-218.

Eckert, R. & Tillotson, D. L. (1981).J. Physiol., Lond. 314, 265-280.

Eisenberg, D. & Crothers, D. (1979). Physical Chemistry with Applications to the Life Sciences, Benjamin/Cummings Publishing Co., Inc., Menlo Park, pp. 707-708.

Evans, E. F. (1972). The frequency response and other properties of single fibres in the guinea-pig cochlea. J. Physiol. 226: 263-287.

Evans, E. F. & Wilson, J. P. (1973). The frequency selectivity of the cochlea. In Basic Mechanisms in Hearing, Moller, A. R., ed., Academic Press, New York, pp. 519-554.

Evans, E. F. & Wilson, J. P. (1975). Cochlear tuning properties: concurrent basilar membrane and single nerve fiber measurements. Science 190: 1218-1221.

Fain, G. L., Quandt, F. N., Bastian, B. L. & Gerschenfeld, H. M. (1978). Contribution of a caesium-sensitive conductance increase to the rod photoresponse. Nature 272: 467-469.

Fenwick, E. M., Marty, A. & Neher, E. (1982). Sodium and calcium channels in bovine chromaffin cells. J. Physiol. 331: 599-635.

Fox, A., Fernandez, J. M. & Krasne, S. (1983). Membrane patches and cell membranes: a comparison. Soc. Neurosci. Abstr. 9: 1188.

Frishkopf, L. S., DeRosier, D. J. & Egelman, E. H. (1982). Motion of basilar papilla and hair cell stereocilia in the excised cochlea of the alligator lizard: relation to frequency analysis. Soc. Neurosci. Abstr. 8: 40.

Furukawa, T. & Matsuura, S. (1978). Adaptive rundown of excitatory post-synaptic potentials at synapses between hair cells and eighth nerve fibres in the goldfish. J. Physiol. 276: 193-209.

Geisler, C. D., Rhode, W. S. & Kennedy, D. T. (1974). Responses to tonal stimuli of single auditory nerve fibers and their relationship to basilar membrane motion in the squirrel monkey. J. Neurophysiol. 37: 1156-1172.

Gorman, A. L. F., Hermann, A. & Thomas, M. V. (1982). The ionic requirements for membrane oscillations and their dependence on calcium concentration in a molluscan pace-maker neurone. J. Physiol. 327: 185-217.

Gorman, A. L. F. & Thomas, M. V. (1978). Changes in the intracellular concentration of free calcium ions in a pace-maker neurone, meas-

ured with the metallochromic indicator dye arsenazo III. J. Physiol. 275: 357-376.

Gorman, A. L. F. & Thomas, M. V. (1980). Potassium conductance and internal calcium accumulation in a molluscan neurone. J. Physiol. 308: 287-313.

Hagiwara, S. & Byerly, L. (1981). Calcium channel. A. Rev. Neurosci. 4: 69-125.

Hamill, O. P., Marty, A., Neher, E., Sakmann, B. & Sigworth, F. J. (1981). Improved patch-clamp techniques for high-resolution current recording from cells and cell-free membrane patches. Pflügers Arch. ges. Physiol. 391: 85-100.

Hermann, A. & Hartung, K. (1982). Properties of a Ca^{2+} activated K^+ conductance in *Helix* neurones investigated by intracellular Ca^{2+} iontophoresis. Pflügers Arch. 393: 248-253.

Hodgkin, A. L. & Huxley, A. F. (1952). A quantitative description of membrane current and its application to conduction and excitation in nerve. J. Physiol. 117: 500-544.

Hodgkin, A. L. & Katz, B. (1949). The effect of sodium ions on the electrical activity of the giant axon of the squid. J. Physiol. 108: 37-77.

Hodgkin, A. L. & Keynes, R. D. (1957). Movements of labelled calcium in squid giant axons. J. Physiol. 138: 253-281.

Holton, T. & Hudspeth, A. J. (1983). A micromechanical contribution to cochlear tuning and tonotopic organization. Science 222: 508-510.

Holton, T. & Weiss, T. F. (1983). Frequency selectivity of hair cells and nerve fibres in the alligator lizard cochlea. J. Physiol. 345: 241-260.

Hopkins, C. D. (1976). Stimulus filtering and electroreception: tuberous electroreceptors in three species of Gymnotoid fish. J. Comp. Physiol. 111: 171-207.

Horn, R. & Brodwick, M. S. (1980). Acetylcholine-induced current in perfused rat myoballs. J. Gen. Physiol. 75: 297-321.

Junge, D. & Stevens, C. L. (1973). Cyclic variation of potassium conductance in a burst-generating neurone in *Aplysia*. J. Physiol. 235: 155-181.

Kemp, D. T. (1978). Stimulated acoustic emissions from within the human auditory system. J. Acoust. Soc. Am. 64: 1386-1391.

Khanna, S. M. & Leonard, D. G. B. (1982). Basilar membrane tuning in the cat cochlea. Science 215: 305-306.

Kim, D. O. (1980). Cochlear mechanics: implications of electrophysiological and acoustical observations. Hearing Res. 2: 297-317.

Latorre, R. & Miller, C. (1983). Conduction and selectivity in potassium channels. J. Membr. Biol. 71: 11-30.

Levy, S., Tillotson, D. & Gorman, A. L. F. (1982). Intracellular Ca^{2+} gradient associated with Ca^{2+} channel activation measured in a nerve cell body. Biophys. J. 37: 182a.

Lewis, E. R., Baird, R. A., Leverenz, E. L. & Koyama, H. (1982). Inner ear: dye injection reveals peripheral origins of specific sensitivities. Science 215: 1641-1643.

Lewis, R. S. (1982). Characterization of voltage- and ion-dependent conductances in vertebrate hair cells. Soc. Neurosci. Abstr. 8: 728.

Lewis, R. S. & Hudspeth, A. J. (1983a). Voltage- and ion-dependent conductances in solitary vertebrate hair cells. Nature 304: 538-541.

Lewis, R. S. & Hudspeth, A. J. (1983b). Frequency tuning and ionic conductances in hair cells of the bullfrog's sacculus. In Hearing - Physiological Bases and Psychophysics, Klinke, R. and Hartmann, R., eds., Springer-Verlag, Berlin, pp. 17-24.

Magleby, K. L. & Pallotta, B. S. (1983). Calcium dependence of open and shut interval distributions from calcium-activated potassium channels in cultured rat muscle. J. Physiol. 344: 585-604.

Manley, G. A. (1979). Preferred intervals in the spontaneous activity of primary auditory neurons. Naturwissenschaften 66: 582-583.

Marty, A. (1981). Ca-dependent K channels with large unitary conductance in chromaffin cell membranes. Nature 291: 497-500.

Marty, A. & Neher, E. (1983). Tight-seal whole-cell recording. In Single-Channel Recording, B. Sakmann & E. Neher, eds., Plenum Press, New York.

Maruyama, Y., Petersen, O. H., Flanagan, P. & Pearson, G. T. (1983). Quantification of Ca^{2+}-activated K^+ channels under hormonal control in pig pancreas acinar cells. Nature 305: 228-232.

Mauro, A., Conti, F., Dodge, F. & Schor, R. (1970). Subthreshold behavior and phenomenological impedance of the squid giant axon. J. Gen. Physiol. 55: 497-523.

McAllister, R. E., Noble, D. & Tsien, R. W. (1975). Reconstruction of the electrical activity of cardiac Purkinje fibers. J. Physiol. 251: 1-59.

Meech, R. W. (1978). Calcium-dependent potassium activation in nervous tissues. A. Rev. Biophys. Bioengng. 7: 1-18.

Meech, R. W. & Standen, N.B. (1975). Potassium activation in *Helix aspersa* neurones under voltage clamp: a component mediated by cal-

cium influx. J. Physiol. 249: 211-239.

Methfessel, C. & Boheim, G. (1982). The gating of single calcium-dependent potassium channels is described by an activation/blockade mechanism. Biophys. Struct. Mech. 9: 35-60.

Meyer, J. H. & Zakon, H. H. (1982). Androgens alter the tuning of electroreceptors. Science 217: 635-637.

Moczydlowski, E. & Latorre, R. (1983). Gating kinetics of Ca^{2+}-activated K^+ channels from rat muscle incorporated into planar lipid bilayers. J. Gen. Physiol. 82: 511-542.

Morris, C. & Lecar, H. (1981). Voltage oscillations in the barnacle giant muscle fiber. Biophys. J. 35: 193-213.

Neely, S. T. & Kim, D. O. (1983). An active cochlear model showing sharp tuning and high sensitivity. Hearing Res. 9: 123-130.

Neher, E. (1971). Two fast transient current components during voltage clamp on snail neurons. J. Gen. Physiol. 58: 36-53.

Ohnishi, S. T. (1979). Calcium-induced calcium release from fragmented sarcoplasmic reticulum. J. Biochem. 86: 1147-1150.

Plant, R. E. (1978). The effects of $calcium^{++}$ on bursting neurons: a modeling study. Biophys. J. 21: 217-237.

Rhode, W. S. (1984). Cochlear mechanics. Ann. Rev. Physiol. 46: 231-246.

Russell, I. J. & Sellick, P. M. (1978). Intracellular studies of hair cells in the mammalian cochlea. J. Physiol. 284: 261-290.

Sand, O., Ozawa, S. & Hagiwara, S. (1975). Electrical and mechanical stimulation of hair cells in the mudpuppy. J. Comp. Physiol. 102: 13-26.

Schatzmann, H. J. (1975). Active calcium transport and Ca^{2+}-activated ATPase in human red cells. Curr. Top. Membr. Transp. 6: 126-168.

Scriven, D. R. L. (1981). Modeling repetitive firing and bursting in a small unmyelinated nerve fiber. Biophys. J. 35: 715-730.

Sellick, P. M., Patuzzi, R. & Johnstone, B. M. (1982). Measurement of basilar membrane motion in the guinea pig using the Mossbauer technique. J. Acoust. Soc. Am. 72: 131-141.

Sigworth, F. J. (1980). The variance of sodium current fluctuations at the node of Ranvier. J. Physiol. 307: 97-129.

Smith, S. J. (1978). The mechanism of bursting pacemaker activity in neurons of the mollusc Tritonia diomedia. Ph.D. Dissertation, University of Washington, Seattle, Washington.

Smith, S. J. & Zucker, R. S. (1980). Aequorin response facilitation and intracellular calcium accumulation in molluscan neurones. J. Physiol. 300: 167-196.

Standen, N. B. & Stanfield, P. R. (1982). A binding-site model for calcium channel inactivation that depends on calcium entry. Proc. R. Soc. Lond. B 217: 101-110.

Thompson, S. H. (1977). Three pharmacologically distinct potassium channels in molluscan neurones. J. Physiol. 265: 465-488.

Thompson, S. (1982). Aminopyridine block of transient potassium current. J. Gen. Physiol. 80: 1-18.

Trautmann, A. & Marty, A. (1984). Activation of Ca-dependent K channels by carbamoylcholine in rat lacrimal glands. Proc. Nat. Acad. Sci. USA 81: 611-615.

von Békésy, G. (1960). Experiments in Hearing. McGraw-Hill, New York, 745 pp.

Weiss, T. F. (1982). Bidirectional transduction in vertebrate hair cells: a mechanism for coupling mechanical and electrical

processes. Hearing Res. 7: 353-360.

Weiss, T. F., Peake, W. T., Ling, A. & Holton, T. (1978). Which structures determine frequency selectivity and tonotopic organization of vertebrate cochlear nerve fibers? Evidence from the alligator lizard. In Evoked Electrical Activity in the Auditory Nervous System, Naunton, R. F. & Fernandez, C., eds., Academic Press, New York, pp. 91-112.

Wong, B. S., Lecar, H. & Adler, M. (1982). Single calcium-dependent potassium channels in clonal anterior pituitary cells. Biophys. J. 39: 313-317.

Woolum, J. C. & Gorman, A. L. F. (1981). Time dependence of the calcium-activated potassium current. Biophys. J. 36: 297-302.

Yellen, G. (1982). Single Ca^{2+}-activated nonselective cation channels in neuroblastoma. Nature 296: 357-359.

Zurek, P. M. (1981). Spontaneous narrowband acoustic signals emitted by human ears. J. Acoust. Soc. Am. 69: 514-523.

APPENDIX

FREQUENCY TUNING AND IONIC CONDUCTANCES IN HAIR CELLS OF THE BULLFROG'S SACCULUS

FREQUENCY TUNING AND IONIC CONDUCTANCES IN HAIR CELLS OF THE BULLFROG'S SACCULUS

R. S. Lewis and A. J. Hudspeth

Division of Biology, California Institute of Technology
Pasadena, California 91125, USA

1. INTRODUCTION

An important function of the peripheral auditory system is the resolution of complex sounds into their constituent frequency components. The responses of individual nerve fibers and hair cells (Russell and Sellick, 1978; Crawford and Fettiplace, 1980) in the auditory organs of several species show extremely sharp selectivity for particular frequencies. There is currently much debate over the mechanisms that determine this selectivity, or tuning, particularly for frequencies close to the characteristic frequency, or CF (Dallos, 1981). In the cochleas of some species it appears that the sharpness of tuning results from processes that maximize mechanical input to the hair cells. In the turtle's cochlea, however, an electrical resonance in the hair cell may supplement the mechanical properties of the organ in conferring sharp frequency selectivity at the CF, by maximizing the cell's response to sound of frequencies near the resonant frequency (Crawford and Fettiplace, 1981).

We present here preliminary evidence that hair cells in the bullfrog's sacculus are also maximally sensitive to particular frequencies of mechanical input, and that the underlying mechanism is, as for the turtle, most likely electrical in nature. Using gigohm-seal-electrode recording techniques on hair cells enzymatically isolated from the sacculus, we have identified three voltage- and ion-dependent conductances that may contribute to the electrical tuning mechanism (Lewis, 1982).

2. METHODS

(a) Microelectrode recordings from hair cells in the excised sacculus. The saccular macula of the bullfrog, *Rana catesbeiana*, was dissected and mounted in an experimental chamber that allows independent superfusion of the two epithelial surfaces. The otolithic membrane was loosened by exposing the upper surface of the preparation for one hour at 25°C to 30 μg/ml subtilopeptidase BPN' in a solution containing (in mM) 110 Na, 2 K, 4 Ca, 118 Cl, 3 D-glucose, and 5 HEPES (pH 7.2). After the otolithic membrane was removed by gentle dissection, the preparation was maintained in an identical saline medium without enzyme. Stimuli were applied to each hair bundle by sucking the bulbous tip of its kinocilium into a heat-polished capillary approximately 1 μm in internal diameter. This probe was moved by a piezoelectric stimulator (Corey and Hudspeth, 1980) whose displacement output was essentially linear and flat with frequency up to 760 Hz. Intracellular recording was conducted at 20-22°C with microelectrodes having resistances greater than 300 megohms; cells impaled with lower-resistance electrodes in general produced oscillations of smaller amplitude, lower frequency, and more phasic character.

(b) Gigohm-seal-electrode recordings from solitary hair cells. Excised sacculi were treated with a solution containing papain and were scraped with a sharpened needle to dissociate individual hair cells, as described in detail elsewhere (Lewis and Hudspeth, 1983). Recordings were made at 20-22°C in a solution containing (in mM) 120 Na, 2 K, 4 Ca, 128 Cl, 3 D-glucose, and 5 HEPES (pH 7.2). In some experiments, tetraethylammonium ion (TEA) or 4-aminopyridine (4-AP) replaced an equal amount of Na, or Mg an equal amount of Ca. Whole-cell recordings were made using heat-polished glass pipettes which contained (in mM) 126 K or Cs, 1 Ca,

In: Hearing - Physiological Bases and Psychophysics, R. Klinke and R. Hartmann, eds., Springer-Verlag, Berlin, 1983, pp. 17-24.

2 Mg, 120 aspartate, 6 Cl, 3 D-glucose, 2 EGTA, and 5 HEPES (pH 7.2), with 10^{-7} M free Ca. Isolated cells formed seals of 1-20 gigohms' shunt resistance with the pipette tips, which had internal diameters of 1-2 μm. Slight suction was applied to rupture the patch of membrane under the tip, and the cells were current- or voltage-clamped through the pipette (Hamill *et al.*, 1981). Data were digitized and averaged with a computer (Fig. 3) or were recorded and reproduced as single traces with an FM tape recorder (other Figures).

3. RESULTS

(a) Frequency selectivity and electrical oscillations in saccular hair cells. Fig. 1A shows the receptor potential of a hair cell in response to constant-amplitude, sinusoidal deflections of the hair bundle, delivered as a linear frequency sweep from 13 to 163 Hz. The cell responded best at 120 Hz, its CF. Because the amplitude of hair-bundle motion was constant, the frequency selectivity observed in this experiment evidently arose from some mechanism other than a mechanical resonance in the sacculus.

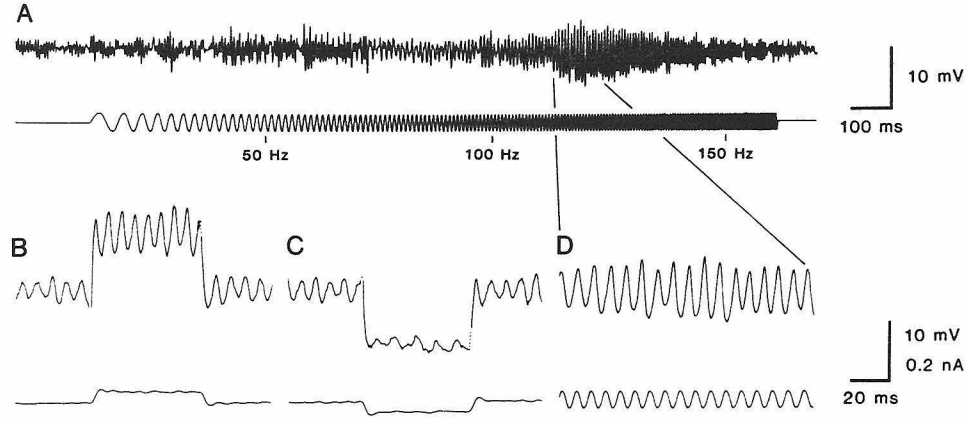

Fig. 1. Recordings from a hair cell in the excised saccular macula, made with a conventional intracellular microelectrode. A, Stimulation of the hair bundle with ±0.03-μm deflections in a frequency sweep (lower trace) evoked a maximal receptor potential (upper trace) at 120 Hz, with a secondary peak at about half that frequency. Note the spontaneous oscillations before and after the frequency sweep. B, Depolarization of the cell by injection of a constant-current pulse (lower trace) increased the frequency of voltage oscillations (upper trace) to 140 Hz from the spontaneous rate of 125 Hz at resting potential (-68 mV). C, Hyperpolarizing current conversely lowered the oscillation frequency to 91 Hz. D, A segment of the cell's response to the frequency sweep near the CF in A, displayed on a faster time scale. Note that the CF of the cell's response to mechanical stimulation is near the frequency of spontaneous oscillation in B and C

It seems likely instead that an electrical resonance in the hair cell forms the basis of the tuning mechanism. The resonance is manifested either as spontaneous voltage fluctuations at the resting potential (Figs. 1B and C) or as voltage oscillations evoked by the injection of small current pulses (Fig. 2B). Because similar oscillatory behavior occurred in cells lacking hair bundles entirely, this phenomenon is not dependent on the transduction process. The oscillation frequency is voltage-dependent, increasing with depolarization. This is shown in Figs. 1B and C, in which pulses of de- or hyperpolarizing current injected into the cell increased or decreased the oscillation frequency. The cell shown in Fig. 1 oscillated spontaneously at 125 Hz at a resting potential of -68 mV. This frequency is close to the CF of the cell measured during mechanical stimulation at the same potential (Fig. 1D), a result that would be expected if the electrical resonance were responsible for the frequency selectivity of the cell's response to mechanical stimuli. Moreover, the CF changed in parallel with the oscillation frequency

when the cell was de- or hyperpolarized by injection of constant current. These observations support the hypothesis that an electrical mechanism determines the frequency selectivity to mechanical stimuli in these cells.

(b) Electrical oscillations in solitary saccular hair cells. The following experiments were designed to investigate the biophysical mechanism of the electrical resonance in hair cells. In order to achieve high temporal resolution in voltage-clamp experiments and to gain relatively unrestricted access of test solutions to the interior and exterior membrane surfaces of the cells, we employed gigohm-seal-electrode recording techniques to study enzymatically dissociated hair cells. A solitary cell is shown in contact with a recording pipette in Fig. 2A. Many of the isolated cells displayed oscillatory responses to current injection (Fig. 2B) similar to those recorded with microelectrodes from cells in the excised sacculus. In 20 cells that clearly showed such behavior, oscillation frequencies ranged from 80 to 160 Hz at resting potentials of -58 to -65 mV. Occasional cells that had lost their hair bundles during the isolation procedure also displayed an ability to oscillate, again demonstrating that an intact transduction apparatus is not necessary to produce this behavior.

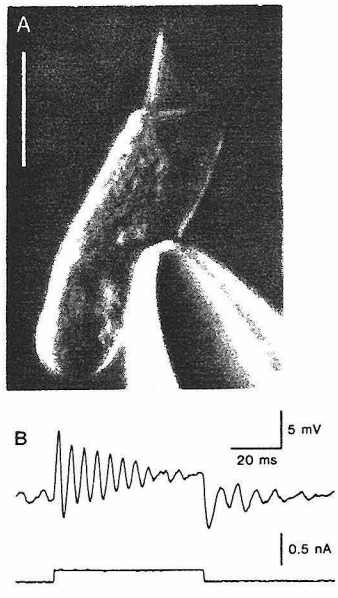

Fig. 2. Voltage oscillations in a solitary hair cell. A, Differential-interference-contrast micrograph of a solitary hair cell from the bullfrog's sacculus, in contact with the tip of a recording pipette. The bar represents 10 μm. B, Injecting a small depolarizing current (lower trace) evoked membrane-potential oscillations in a solitary cell (upper trace). Oscillation frequency increased with depolarization; here it was 195 Hz during the pulse and 137 Hz at the resting potential of -62 mV

(c) Voltage- and ion-dependent conductances in solitary saccular hair cells. Under voltage-clamp conditions, three specific ionic currents could be elicited by depolarization in over 90% of the solitary hair cells that were studied. Each of these conductances was isolated and characterized by its ion and voltage dependences and its pharmacological sensitivity. The three conductance mechanisms are more completely described elsewhere (Lewis and Hudspeth, 1983); here we will emphasize their characteristics relevant to the issue of electrical resonance

I. Calcium current. The substitution of Cs for the cell's internal K blocks outward K currents that are produced by depolarization, leaving a sustained inward current that is activated at potentials more positive than -60 to -55 mV (Fig. 3A). Based on characteristics that it shares with the Ca currents of other preparations (Hagiwara and Byerly, 1981), we have identified this as a Ca current. A significant feature of the current is that it does not inactivate appreciably during prolonged depolarizations. This characteristic, together with its activity at potentials close the the resting potential, suggests that the Ca current functions in the tonic release of transmitter from hair cells onto afferent nerve fibers (Sand *et al.*, 1975).

II. Transient K current (A current). When hair cells are depolarized to potentials more positive than about -50 mV from holding potentials more negative than -60 mV, a transient, outward K current results which is similar in several respects to the A current described in molluscan neurons (Connor and Stevens, 1971). It is the only current we have observed routinely in hair cells that rapidly inactivates as a function of membrane voltage. This characteristic, along with the current's insensitivity to external TEA, can be used to isolate the A current from

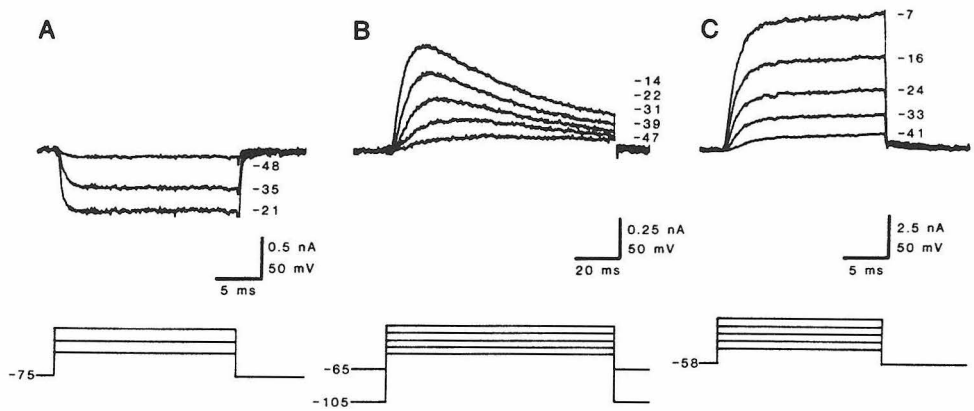

Fig. 3. Voltage-clamp recordings from solitary hair cells, showing the three ionic currents. In each panel the upper set of traces shows membrane current and the lower set represents command voltage. To the right of each current trace is the corresponding command voltage.in millivolts; the holding potential in millivolts is to the left of the voltage command in each panel. A, Ca current, recorded with 126 mM Cs in the pipette to block outward K currents. Averages of five presentations. B, Transient K current (A current). With 20 mM TEA blocking the Ca-activated K current, a series of voltage steps was applied to the cell from holding potentials of -65 or -105 mV. At -65 mV, about 95% of the A current is inactivated at steady-state, and the voltage steps elicited primarily Ca current. At -105 mV the A current's inactivation is removed, and the voltage steps elicited the sum of Ca and A currents. Subtracting the former set of currents from the latter isolated the A current from the Ca current. Averages of four presentations. C, Ca-activated K current. These responses were obtained by subtracting the currents produced by voltage steps in the presence of 20 mM TEA (a fully blocking concentration) from those produced in its absence. Averages of two presentations. Note the different current scale used here

the Ca and Ca-activated K currents (Fig. 3B). The A current is not abolished by divalent cations that block the Ca and Ca-activated K currents, but is blocked by 10 mM 4-AP.

III. Ca-activated K current. The largest current in the hair cell, occurring at potentials more positive than -60 to -45 mV, is an outward K current that is activated by intracellular Ca ions. It can be isolated using its sensitivity to TEA (Fig. 3C), which specifically blocks the Ca-dependent outward current in these cells. The Ca-activated K current is abolished by external agents or conditions that suppress the hair cell's Ca current, suggesting that this K current is dependent on Ca ions that have entered the cell through Ca channels. In addition, lowering external Ca from 4 to 0.5 mM (with Mg substitution) slows the kinetics and lowers the steady-state magnitude of this current.

(d) Effects on oscillatory behavior of conditions that alter the voltage- and ion-dependent currents. If the three currents described above interact to generate electrical resonance, then conditions that change the magnitude or kinetics of the currents should also affect resonant behavior. Fig. 4 shows the effects of several such conditions on the voltage oscillations produced in a solitary hair cell by an applied current step. In normal saline, the cell's voltage oscillated during the step at a frequency of 196 Hz, with a maximum peak-to-peak amplitude of 10 mV (Fig. 4A). External TEA at 1 mM, a level that blocks about half of the Ca-activated K current, partially suppressed the oscillations (Fig. 4B). Lowering external Ca to 0.5 mM, which diminishes the Ca current and slows and reduces the Ca-activated K current, also decreased the amplitude of the oscillations (Fig. 4C). While the low-Ca condition depolarized this cell by 9 mV, similar results were obtained

in cells that were not depolarized by low Ca. In contrast, exposure to 10 mM 4-AP, a treatment that specifically blocks the A current, had little or no effect on oscillations (Fig. 4D). The changes produced by the different treatments were reversible (Fig. 4E).

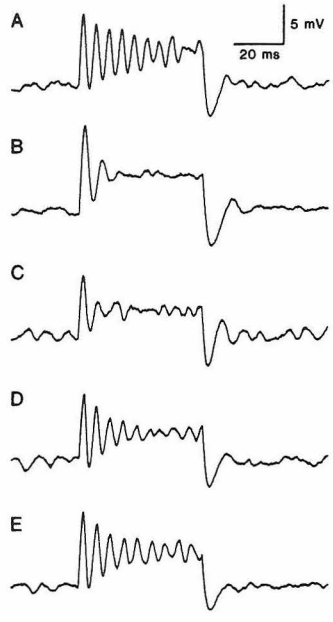

Fig. 4. Effects of various external conditions on voltage oscillations in a solitary hair cell. This cell was stimulated with a 50-ms, 0.17-nA current pulse in different external solutions in the order shown. Resting potentials (RP) are noted in parentheses. A, Control (saline containing 4 mM Ca). The current evoked large voltage oscillations in the cell (RP=-64 mV). B, 1 mM TEA, which blocks about half of the Ca-activated K current, partially suppressed the oscillations (RP=-61 mV). C, Lowering Ca to 0.5 mM, with 3.5 mM Mg added, also reduced oscillatory activity. This condition diminishes both the Ca and Ca-activated K currents (RP=-55 mV). D, 10 mM 4-AP, which blocks the A current, had little or no effect on the oscillations (RP=-62 mV). E, A normal oscillatory response was elicited after returning the cell to control conditions (RP=-64 mV)

4. DISCUSSION

We have shown that hair cells in the excised bullfrog's sacculus are selective for particular frequencies of controlled mechanical input. There are several reasons to suppose that the mechanism involved in this selectivity is electrical in nature. First, tuning was demonstrated by deflecting the hair bundles directly with a suction probe. This stimulation technique bypasses most of the mechanical components of the sacculus that might contribute to mechanical resonance in the system. Second, an electrical resonance tuned to the mechanical CF was observed in these hair cells as manifested by spontaneous or current-induced voltage oscillations at resting potential. This behavior resembles that observed in hair cells of the turtle's cochlea, whose tuning to auditory stimuli results in part from similar electrical properties (Crawford and Fettiplace, 1980, 1981). Third, membrane polarization induced by current injection increased or decreased the CF of cells in parallel with the frequency of electrical oscillations.

Solitary hair cells, which also display oscillatory behavior, possess three voltage- and ion-dependent conductance mechanisms: a noninactivating Ca conductance, an A conductance, and a Ca-activated K conductance. Although the A conductance is largely inactivated at resting potential and therefore may not contribute significantly to generating oscillations, there is evidence that the Ca and Ca-activated K currents play a role. First, they are activated in the same voltage range in which oscillations occur. In addition, their activation becomes more rapid with increasing levels of depolarization, which is consistent with the voltage dependence of oscillation frequency. Finally, conditions which interfere with the Ca and Ca-activated K currents suppress the oscillatory behavior.

Since oscillations occur in hair cells without hair bundles, modulation of the transduction conductance is not necessary to produce oscillatory activity. It remains possible, however, that frequency tuning is enhanced in intact preparations by interactions between the transducer and the electrical resonance mechanism (Weiss, 1982). While an intact efferent innervation is also not required for oscillations to occur in solitary hair cells, postsynaptic conductances associated with the efferent system may contribute to electrical resonance.

Several properties of the hair cell's Ca-activated K current are interesting in view of its probable role in the resonance mechanism. It is activated 10-100 times as rapidly as Ca-activated K currents in other preparations (Meech, 1978), which may permit its participation in oscillatory phenomena usually mediated by

fast, voltage-dependent currents. Furthermore, the hair cell's Ca-activated K channel, like those in other preparations (Barrett *et al.*, 1982), may be sensitive to both voltage and the internal level of free Ca. If so, there are two partially independent means of controlling the current's activity in the cell. Such a dual control mechanism could have important consequences for determining the characteristic frequency of a hair cell and for regulating resonant properties in response to stimulation of the efferent innervation.

Acknowledgments: We thank R. Jacobs for technical assistance and R. A. Eatock and T. Holton for helpful comments on the manuscript. This work was supported by the System Development Foundation and by National Institutes of Health grants NS13154 and GM07737. The authors' present address is: Department of Physiology, University of California School of Medicine, San Francisco, California 94143, USA.

REFERENCES

Barrett, J. N., Magleby, K. L., Pallotta, B. S. (1982). Properties of single calcium-activated potassium channels in cultured rat muscle. *J. Physiol.* 331, 211-230.

Connor, J. A., Stevens, C. F. (1971). Voltage clamp studies of a transient outward membrane current in gastropod neural somata. *J. Physiol.* 213, 21-30.

Corey, D. P., Hudspeth, A. J. (1980). Mechanical stimulation and micromanipulation with piezoelectric bimorph elements. *J. Neurosci. Meth.* 3, 183-202.

Crawford, A. C., Fettiplace, R. (1980). The frequency selectivity of auditory nerve fibres and hair cells in the cochlea of the turtle. *J. Physiol.* 306, 79-125.

Crawford, A. C., Fettiplace, R. (1981). An electrical tuning mechanism in turtle cochlear hair cells. *J. Physiol.* 312, 377-412.

Dallos, P. (1981). Cochlear physiology. *Annu. Rev. Psychol.* 32, 153-190.

Hagiwara, S., Byerly, L. (1981). Calcium channel. *Annu. Rev. Neurosci.* 4, 69-125.

Hamill, O. P., Marty, A., Neher, E., Sakmann, B., Sigworth, F. J. (1981). Improved patch-clamp techniques for high-resolution current recording from cells and cell-free membrane patches. *Pflügers Arch.* 391, 85-100.

Lewis, R. S. (1982). Characterization of voltage- and ion-dependent conductances in vertebrate hair cells. *Soc. Neurosci. Abstr.* 8, 728.

Lewis, R. S., Hudspeth, A. J. (1983). Voltage- and ion-dependent conductances in solitary vertebrate hair cells. Submitted for publication.

Meech, R. W. (1978). Calcium-dependent potassium activation in nervous tissues. *Annu. Rev. Biophys. Bioeng.* 7, 1-18.

Russell, I. J., Sellick, P. M. (1978). Intracellular studies of hair cells in the mammalian cochlea. *J. Physiol.* 284, 261-290.

Sand, O., Ozawa, S., Hagiwara, S. (1975). Electrical and mechanical stimulation of hair cells in the mudpuppy. *J. Comp. Physiol. A* 102, 13-26.

Weiss, T. F. (1982). Bidirectional transduction in vertebrate hair cells: a mechanism for coupling mechanical and electrical processes. *Hearing Res.* 7, 353-360.

GENERAL DISCUSSION

ASHMORE:
Your finding of cells tuned to frequencies around 130 Hz differs from results I have reported in saccular hair cells of R. pipiens (J. Physiol. 336, 24P, 1983). The cells of this preparation show spontaneous oscillations in the range 11-59 Hz at the resting potential and ringing responses characteristic of an electrical resonance. I have also found that best frequencies of the cells are found in this frequency range and match a peak in the amplitude spectrum of the noise.

R.S. LEWIS:
There may not be a significant difference between the tuning properties of saccular hair cells of these two species. We have recorded from bullfrog hair cells that are tuned to mechanical stimuli of about 20 to 150 Hz at resting potential.

However, we cannot say at present whether this range of CFs corresponds to those that would be present in saccular hair cells in vivo, because we commonly found that measured CFs, as well as the frequency of spontaneous or current-evoked oscillations, decreased with time after the start of recordings and were in general lower when lower resistance (<300 Megohm) electrodes were used.

MANLEY:
Your finding of voltage oscillations in sacculus hair cells is interesting. I have reported the presence of preferred intervals in the spontaneous activity in bird cochlear ganglion units of CF below about 900 Hz which may be traceable to such voltage noise in hair cells (Naturwiss. 66, 582, 1979). We subsequently reported similar spontaneous activity patterns in lizard fibres (Eatock et al., J. Comp. Physiol. 142, 203, 1980).

ASHMORE:
Do you have information about whether use of the enzymes papain and subtilopeptidase to prepare the cells affects the membrane channels? It could be that reduction of a channel population enzyme digestion significantly alters the cell's tuning properties.

R.S. LEWIS:
Subtilopeptidase applied to apical and basal surfaces of the saccular macula may decrease the hair cell's Ca^{++} current, as it seems to reduce the occurrence of Ca^{++} action potentials produced under conditions of high external Ca^{++} in these cells. For this reason, and because the Ca^{++} channels are probably localized to the hair-cell basal membrane, we confined this treatment to the apical surface. It is possible that exposure to papain reduces ionic currents in hair cells, since isolated cells did not spontaneously oscillate as frequently as those in excised sacculus. On the other hand, mechanical stresses applied to the cell during the isolation procedure, as well as possible effects of internal perfusion through the gigohm-seal pipette, could produce this result. The important point for this study is that the isolated cells show resonant behaviour similar to that observed in cells in the sacculus and therefore can be used to investigate the biophysical basis of the electrical resonance.

WILSON:
Did I understand you correctly that you can find hair cell tuning under conditions where the possibility of mechanical feedback has been eliminated?

R.S. LEWIS:
Not exactly. Our stimulation technique controls hair bundle motion at the bulb of the kinocilium. If electromechanical feedback acts on the stereocilia to change their mechanical properties (Kim, Hear. Res. 2, 297, 1980; Weiss, Hear. Res. 7, 353, 1982; Flock, this volume) we may not be controlling the mechanical input to the transduction apparatus at a subcellular level. Our results do implicate an electrical resonance in determining the tuning to mechanical stimuli in these cells. However, the question remains as to whether this tuning can be accounted for quantitatively by an electrical resonance in series with the mechanical transduction process, or whether these two systems must also be coupled through electromechanical feedback.

KIM:
I have two questions and a comment. Is the spontaneous oscillation of HC membrane potential affected in any way when the end bulb of the kinocilium was sucked into the stimulating probe? I wonder whether rigidly holding the hair bundle, thereby preventing any possible mechanical oscillation, affects the electrical oscillation. This information should be helpful in evaluating the hypothesis of a bidirectional HC transduction (see comment of Kim on paper by Fuchs et al.). Is there any difference in the spontaneous oscillation behaviour depending upon the location of the HC within the saccule? My comment is that occurrence of spontaneous electrical oscillation in HC without the hair bundle is not evidence against the hypothesis of a bidirectional transduction. This is because an electrical oscillation signal, even if generated by an exclusively electrical mechanism, may still be reverse transduced in to a mechanical oscillation of the hair bundle in a normal HC.

R.S. LEWIS:
Although we have not analyzed this in detail, attaching the stimulating probe to the hair bundle has no obvious effect on spontaneous voltage oscillations. An example of this can be seen by comparing the oscillations occurring before the frequency sweep in Fig. 1A (probe attached) with those occurring in the same cell before current injection in Fig. 1B (probe removed). As I mentioned in the talk, the observation of the electrical oscillations in cells lacking hair bundles does not absolutely rule out operation of a "bidirectional transduction" mechanism (Weiss, 1982) in intact saccular hair cells. However, it does show that spontaneous, sustained oscillations can result from an independent electrical resonance mechanism in the cell, and are not necessarily dependent on the interaction of voltage- and mechano-sensitive systems as suggested by Weiss. Furthermore, spontaneous oscillations in one cell lacking a hair bundle were among the largest we have seen in any cell (12 mV peak-to-peak), which argues against significant enhancement of oscillations by these proposed interactions in saccular hair cells.
I cannot give a complete answer to your second question since in this report we have studied only hair cells in the distal margin of the saccular macula, directly opposite the side of nerve insertion, or isolated hair cells whose original location in the macula was unknown, due to the dissociation procedure.